CDF-6909
July 12, 2004

WW Production in the Dilepton Channel with 200 pb^{-1}

S. Cabrera [i], S. Carron [i], S. Chuang [ii], J. Deng [i], A. Goshaw [i], Y. Huang [i], M. Kruse [i], D. McGivern [iii], D. Waters [iii]

[i] Duke University
[ii] University of Wisconsin
[iii] University College London

Abstract

W pair production in the dilepton channel $W^+W^- \rightarrow l^+l^-\nu\bar{\nu}$ ($l = e$ or μ) has been studied using approximately 200 pb^{-1} of Tevatron Run 2 data collected by the CDF detector. This note represents a comprehensive update of our previous results (CDF-6323 and CDF-6611), which were blessed in summer 2003, and includes an extension of the lepton acceptance, better optimization of the analysis cuts, and several studies and checks of kinematic requirements, acceptances, and background estimates. We find 17 candidate events against an expected $WW \rightarrow \ell\ell\nu\nu$ signal of 10.2 ± 1.1 events and a background of 5.8 ± 0.9 events in a Run 2 data sample with a luminosity for WW events of approximately 184 pb^{-1}. This results in a measured cross-section of:

$$\sigma(p\bar{p} \rightarrow W^+W^-X) = 13.6^{+5.8}_{-5.1}(\mathrm{stat}) \pm 1.7(\mathrm{syst}) \pm 0.8(\mathrm{lum})\mathrm{pb}$$

which is in agreement with a NLO (Next-to-Leading-Order) theoretical prediction of $\sigma^{WW}_{NLO} = 12.4 \pm 0.8$ pb.

Contents

1 Introduction

The study of WW production in the dilepton channel $W^+W^- \to l^+l^-\nu\bar{\nu}$ ($l = e$ or μ) with Run 2 data will improve the measurement of the WW cross-section and the limits on anomalous WWZ and $WW\gamma$ couplings. This note presents a measurement of the WW cross-section using the dilepton channel, with the analysis of anomalous couplings still in progress.

This analysis is a first step towards an optimal understanding of anomalous couplings. Although heavy diboson production can be used in principle to place limits on all four anomalous $WW\gamma, Z$ couplings that are usually considered $(\Delta\kappa_\gamma, \Delta\kappa_Z, \lambda_\gamma, \lambda_Z)$, separating the $WW\gamma$ component from the WWZ component is not easy and it is usually necessary to make further simplifying assumptions such as $\Delta\kappa_\gamma = \Delta\kappa_z$, $\lambda_\gamma = \lambda_z$. The situation is quite different in the analysis of $W\gamma$ events where there is no contribution from the WWZ coupling. Clearly, then, the analysis of heavy diboson production is complementary to the analysis of $W\gamma$ production and comparing the two will help to disentangle the source of any observed non-Standard Model contribution. The best final limits on anomalous couplings will be obtained by combining the results from the two sets of measurements, and we are working with the $W\gamma$ people toward this goal.

The WW cross-section is estimated at NLO to be 12.4 ± 0.8 pb (see section 10.3). We use the Standard Model value for BR($W \to l\nu$) of 0.108 in order to calculate event yields in the dilepton channel.

In Run 1, CDF found 5 candidate $W^+W^- \to l^+l^-\nu\bar{\nu}$ events in a 108 pb^{-1} data sample against an expected background of 1.2 ± 0.3 events to give a measured cross-section :

$$\sigma(p\bar{p} \to W^+W^-) = 10.2^{+6.3}_{-5.1}(\text{stat}) \pm 1.6(\text{syst})\ \text{pb}.$$

that is compatible with the Standard Model prediction at $\sqrt{s} = 1.8\,\text{TeV}$ [1].

In this note we describe the analysis using $\sim$ 200 pb^{-1} of Run 2 data. Although the analysis cuts being used here were based on the Run 1 selection and the Run 2 top dilepton analysis for which WW production is an important background, there have been some important changes which will be discussed in detail below.

We also include a preliminary list of questions from the godparents (D. Stuart (chair), J. Proudfoot, M. Tecchio) and some studies towards answers to those questions. The web page

`http://www-cdf.fnal.gov/internal/physics/WW/`

contains all current documentation, godparent requests, godparent meeting minutes, and links to talks.

2 Executive Summary of Changes since last version

2.1 March 14 2004

- PHX is now treated in the following way: require $|\eta| < 2.0$, and require OS. This replaces going out to $|\eta|$ of 2.5, and not requiring OS. The tightening of this category does little to the signal acceptance but greatly reduces fakes and $W\gamma$, and to a lesser extent DY, in addition to avoiding large uncertainties in the fake and $W\gamma$ estimates.

- Inclusion of a background contribution from $W\gamma$. Determined from MC, and shown not to overlap significantly with the fake background, this source turns out to be more significant than we imagined. A lot of work went into understanding this background, and although we don't fully understand the overlap with fakes, we have shown that it is small, and so we treat it as a completely separate source.

- Further studies of the $\not\!\!E_T$ difference in DY MC versus data resulted in a reevaluation of the 1.85 scaling factor we used on ee DY.

- Reevaluation of all background contributions and final cross-section.

- We saw in the data (after we settled the event selection !), the number of candidates go from 20 to 17.

- Reevaluation of the W/Z cross-checks for PHX.

2.2 July 12 2004

- The most substantial effort has been reevaluating the fakes. The final number did not change much, but was reevaluated by dropping the $\not\!\!E_T$ requirement on the QCD samples to calculate the fake *ratio*, and to subtract off the estimated W contamination that results. In addition the new estimate has been calculated as a function of E_T, which although making little difference (as the spectrum for denominator objects is similar to that for fakeable objects), settles any questions arising because of E_T dependence. We keep the old fake section for comparison, but the latest numbers are in section 7.7.

- An oversight we recently realized is that since we now regain most of the WW acceptance inside the Z window using the $\not\!\!E_T^{sig}$ requirement, we need to re-evaluate a potential background from ZZ production. Previously this was estimated to be negligible but now, mainly through the decay $ZZ \to l^+l^-\nu\bar{\nu}$, contributes roughly 0.7 events to our total background.

- We have rewritten sections 7.3 to 7.5 to make our Drell-Yan background estimate and systematic uncertainty estimates clearer. The data-based cross-check has been substantially revised.

3 Event Selection

3.1 Lepton identification

We select events with 2 high-P_T leptons (electrons or muons) satisfying the criteria listed below. We follow the standard baseline cuts as recommended in the top and electroweak physics groups.

Although mentioned in more detail later we stress here two important features of our event selection for leptons:

- We require both leptons in the event to be isolated (for central electrons and all muons we require both track and calorimeter isolation, and for Phoenix electrons calorimeter isolation only). Due to our requirement that there be no jet activity in the event, this has little effect on the acceptance (compared to requiring only one leg be isolated), about 5% , and simplifies and significantly reduces our fake background calculations. The effect of requiring track isolation in addition to calorimeter isolation (this is an added requirement from winter 2003) reduces the acceptance by about 3% and reduces the fake rate by about 20% (in section 5.5 we give fake rate numbers both with and without track isolation for comparison).

- We veto events with 3 leptons. This approximately halves our WZ background while having almost no effect on the WW signal acceptance.

The identification of **electrons** in the **central part** of the detector is based on the cuts listed in table 1 and is basically unchanged from the summer 2003 analysis. The electrons are required not to be part of a conversion.

EM E_T	> 20 GeV
E_{HAD}/E_{EM}	$< \ 0.055 + 0.00045 \cdot \mathrm{E}$
L_{shr}	< 0.2
Track P_T	>10 GeV/c (if EM E_T ≤100 GeV) >50 GeV/c (if EM E_T >100 GeV)
$\frac{E}{p}$	< 2 (if EM E_T ≤100 GeV)
$\mathrm{q_{track}} \cdot \Delta x$	[-3.0 cm, 1.5 cm]
$\|\Delta z\|$	< 3 cm
χ^2	< 10
track $\|z_0\|$	< 60 cm
Track quality	3 axial and 3 stereo SL with at least 7 out of 12 in each SL
Fiducial	*fidele*=1 (Ces $\|X\|$ <21 cm, 9< Ces $\|Z\|$ <230 cm Tower 9 excluded, most of tower next to chimney included)

Table 1: Baseline cuts for central isolated electrons (CEM) [4].

For the identification of **electrons** in the **plug region** of the detector the silicon tracks considered are reconstructed with the *Phoenix* algorithm [5]. If the plug electron passes all requirements described in table 2, it is classified as PHX.

EM E_T	> 20 GeV
E_{HAD}/E_{EM}	$< \ 0.05 + 0.026 \cdot \ln(\frac{E_{EM}}{100})$ (if E_{EM} >100 GeV) $< \ 0.05$ (if $E_{EM} \leq$100 GeV)
PEM 3×3 Fit tower	$\neq$0
PEM 3×3 Fit χ^2	<10
PES 5×9 U and V	>0.65
Fiducial	PES based $1.2 < \|\eta\| < 2.0$
Silicon track Number of Silicon Hits Track $\|z_0\|$ $\Delta_R(\text{Track}, \text{PES})$	2D Phoenix track $\geq$3 $<$ 60 cm <3

Table 2: Baseline cuts for plug isolated electrons (PHX) [4].

All central electrons are required to be isolated thus:

- $I_{cal} < 0.1$: the ratio of calorimeter energy, excluding the electron EM energy, in a cone of 0.4 around the electron, to the electron tower energy be less than 0.1.

- $I_{trk} < 0.1$: the ratio of the sum of the transverse momenta for all tracks in a cone of 0.4 around the lepton in the $\eta - \phi$ plane, excluding the lepton track, to the the P_T of the lepton be less than 0.1.

A muon is a minimum ionizing high-P_T track passing the baseline **muon** cuts (see table 3). All these tracks must be *calorimeter isolated* and *track isolated* following the same definitions as for electron above.

In addition we require in the data: a cosmic ray veto, the standard curvature correction applied for the beam position, and for CMX the triggering CMX leg is required to have a COT exit radius $> 140\,\text{cm}$.

This minimum ionizing high-P_T isolated track will be classified as:

- A **CMUP** muon, if there are stubs in both the CMU and CMP detectors, with $|\Delta X|_{\text{CMU}} < 3\,\text{cm}$ and $|\Delta X|_{\text{CMP}} < 5\,\text{cm}$ respectively.

- A **CMX** muon, if there is one stub in the CMX detector, with $|\Delta X|_{\text{CMX}} < 6\,\text{cm}$.

- A **non-triggering muon**: this can be 3 different sub-categories, the information for which we will maintain for detailed studies of candidates, and internal consumption, etc., but which for presentation purposes we lump into this one category for simplicity. A non-triggering muon can only be the second leg in a dilepton event, and can appear in the following ways:

Track P_T	>20 GeV/c
Track $\|z_0\|$	< 60 cm
E_{EM}	< 2+Max(0,0.0115(P-100)) GeV
E_{HAD}	< 6+Max(0,0.028(P-100)) GeV
Track $\|d_0\|$	0.2 cm (if no silicon hits attached by OI) 0.02 cm (if silicon hits attached by OI)
Track quality	3 axial and 3 stereo SL with at least 7 out of 12 in each SL

Table 3: Baseline cuts for minimum ionizing isolated tracks [6]. After passing these cuts the muon is then classified as **CMUP**, **CMX** or **non-triggering** according to the definitions in the text.

1. **CMU-only** (**CMP-only**) with a stub in the CMU (CMP) detector and non fiducial in the CMP (CMU) detector according to the muon fiduciality checking tool.
2. If there are no muon detector stubs, the minimum ionizing high P_t isolated track will be classified as a **CMIO**. In the $e\mu$ dilepton channel, where we are not vetoing Z's, we additionally require the track to be fiducial in the calorimeter in order to avoid Z contamination (*fidele=4*).

3.2 Dilepton categories

We build a dilepton event with two baseline isolated leptons according to the categorizations in table 4.

The treatment of trileptons in this analysis is simple: events with three isolated leptons are classified as trileptons and rejected (although we do keep track of them).

3.3 Kinematic Selection

The event selection can be summarized as follows:

- Find two baseline oppositely charged leptons, both isolated.
- Veto events where the same flavor lepton-lepton mass is inside the Z mass window and the $\not\!\!E_T$ significance ($\not\!\!E_T^{sig} = \frac{\not E_T}{\sqrt{\sum E_T}}$) is less than 3.0. A detailed description of $\not\!\!E_T$ significance and its optimization for this analysis is given in reference [7].
- Require a large $\not\!\!E_T$ not near any jet or lepton activity.
- Veto events with at least 1 jet with $E_T^{cor} > 15\,\text{GeV}$.

The corresponding cuts to this selection are summarized in table 5.

The jet veto is applied to tight jets : reclustered jets with the JetClu 0.4 algorithm using the primary vertex and excluding towers from TCE and PHX isolated electrons, with

ee		$\mu\mu$		$e\mu$	
1st leg	2nd leg	1st leg	2nd leg	1st leg	2nd leg
TCE	TCE	**CMUP**	CMUP	**TCE**	CMUP
	PHX		CMX		CMX
			CMU		CMU
			CMP		CMP
			CMIO		CMIO
		CMX	CMX	**CMUP**	PHX
			CMU	**CMX**	PHX
			CMP		
			CMIO		
PHX	PHX			**PHX**	CMU
					CMP
					CMIO

Table 4: Dilepton categories included in the current analysis. The first leg is a triggerable lepton in the data samples studied. The one exception to this is the PHX categories (see section 6). Both lepton legs are required to be isolated.

	Event Selection (Winter 2004)
1	2 20 GeV isolated leptons
2	remove if $76 < M_{ee,\mu\mu} < 106$ and $\not\!\!E_T^{sig} < 3$
3	$\not\!\!E_T > 25$ GeV
4	$\Delta\phi(\not\!\!E_T, \text{nearest } l \text{ or } j) > 20^\circ$ if $\not\!\!E_T < 50$ GeV
5	No jets with $E_T^{\text{corr}} > 15$ GeV, $\mid \eta_{\text{detector}} \mid < 2.5$
6	opposite charge requirement

Table 5: WW dilepton event selection cuts for the Winter 2004 analysis.

corrected $E_T > 15$ GeV and $|\eta| < 2.5$. We correct jets using level 5 corrections. The $\not\!\!E_T$ is corrected for the primary vertex position and for the isolated muons identified in the dilepton category. The $\not\!\!E_T$ is also corrected for the jet corrections affecting the tight jets, although in the end our jet veto ensures that we are not sensitive to this correction to the overall $\not\!\!E_T$.

4 Signal Acceptances

The signal acceptance was evaluated using a PYTHIA MC sample. The sample used (wtop0f, cdfptop) consisted of 828,000 WW events where both W bosons were forced to decay leptonically : $W \to l\nu$; $l = e, \mu, \tau$. The equivalent WW sample size before any decay requirements is 7.9 million events. Using the best theoretical value for the cross-section $\sigma_{NLO}^{WW} = 12.4 \pm 0.8$ pb (see section 10.3), the luminosity of the sample is estimated to be 636 fb^{-1}.

The signal acceptance has been increased since the previous analysis by the simplification of the lepton classification (see section 2.1), the inclusion of the MET_PEM trigger data, and the recovery of WW events in the Z window by using a new Drell-Yan rejection cut. Table 6 summarizes the signal efficiencies including these increases in the acceptance. The final WW expectation in $184\,\mathrm{pb}^{-1}$ is given in the summary table 44.

	WW					
	ee		$\mu\mu$		$e\mu$	
Cut		%		%		%
Lepton ID	23800.00	0.00 ± 0.00	22665.00	0.00 ± 0.00	44486.00	0.00 ± 0.00
Isolation	21407.00	89.95 ± 0.19	20858.00	92.03 ± 0.18	40574.00	91.21 ± 0.13
Conv+Cosmic	21003.00	98.11 ± 0.09	20858.00	100.00 ± 0.00	40169.00	99.00 ± 0.05
Z-veto	18531.00	88.23 ± 0.22	18221.00	87.36 ± 0.23	40169.00	100.00 ± 0.00
$\not\!\!E_T$ >25 GeV :	14478.00	78.13 ± 0.30	14161.00	77.72 ± 0.31	29077.00	72.39 ± 0.22
$\Delta\Phi > 20^\circ$ if $\not\!\!E_T$ <50	13986.00	96.60 ± 0.15	13644.00	96.35 ± 0.16	27970.00	96.19 ± 0.11
0 jets	11214.00	80.18 ± 0.34	10930.00	80.11 ± 0.34	22604.00	80.82 ± 0.24
Opposite Sign	10334.51	92.16 ± 0.25	10930.00	100.00 ± 0.00	21725.03	96.11 ± 0.13

Table 6: PYTHIA WW events passing the WW analysis cuts for each dilepton category and the associated selection efficiencies. Errors are statistical only.

The previous analysis used a veto on any same flavor dilepton event falling in the Z mass window ($76 < M_{ll} < 106$ GeV) to remove the Drell-Yan background. This resulted in a large loss in acceptance (about 30% in the ee and $\mu\mu$ channels). The new Drell-Yan rejection, described in detail in [7], uses a $\not\!\!E_T^{sig}$ cut at 3.0 in combination with the existing WW selection to recover $80.2 \pm 3.2\%$ of the WW events that were otherwise lost due to the Z veto, whilst at the same time continuing to reject a large fraction of the DY background.

Additional acceptance has also been added due to the simplification of muon categories. In the $e\mu$ channel this results in a large increase in the Drell Yan background due to ee events where one electron falls in a crack and fakes a CMIO. To compensate, any non-trigger CMIO in $e\mu$ events is required to have either a stub or be fiducial in the calorimeter. The final result of this reclassification is a 10% increase in the $\mu\mu$ acceptance giving a 3% increase in the overall acceptance.

The inclusion of the MET_PEM trigger allows additional acceptance by including new dilepton categories (PHX-μ and PHX-PHX) giving an increase in acceptance in the ee channel of 10% and in the $e\mu$ channel of 13%.

We have tightened up the PHX requirements by restricting the η coverage (now out to 2.0 instead of 2.5), and require OS. This reduces the signal acceptance by about 8% compared with extended η coverage and no OS requirement for PHX categories, but reduces the total background by about 25%, and makes the fakes somewhat easier to deal with.

The final change in the analysis that affects the acceptance is the inclusion of the track isolation requirement, used to reduce the fake background. This additional cut reduces the overall acceptance by about 3%, but eliminates any $b\bar{b}$ contribution (see later), and reduces the fake background by about 25% from that with calorimeter isolation alone on both legs.

The final acceptance numbers after all these changes is summarized in table 7.

	A_{ee}	$A_{\mu\mu}$	$A_{e\mu}$	$A_{ee+\mu\mu+e\mu}$
A_{abs}	(0.131 $\pm$ 0.001) %	(0.139 $\pm$ 0.001) %	(0.275 $\pm$ 0.002) %	(0.545 $\pm$ 0.003) %
A_{rel}	24.0 %	25.4 %	50.5 %	100.0 %
$A_{abs}(SF)$	(0.114 $\pm$ 0.001) %	(0.109 $\pm$ 0.001) %	(0.224 $\pm$ 0.002) %	(0.447 $\pm$ 0.002) %
$A_{rel}(SF)$	25.6 %	24.3 %	50.1 %	100.0 %

Table 7: The absolute and relative acceptances in the ee, $\mu\mu$ and $e\mu$ channels. These numbers use a BR($W \to l\nu$) of 0.108. The first set of numbers are the raw acceptances, and the second set are after the application of the various scale factors (see section 5) and proper luminosity weighting.

5 Scale Factors

Data/MC scale factors used in the acceptance and MC background calculations and their sources are listed in table 8. We have separately computed scale factors for Phoenix tracking, which are in good agreement with those found elsewhere and listed in table 8. We describe here our calculation of the MET-PEM trigger and Phoenix charge mis-identification scale factors used in this analysis. The lepton ID scale factors in table 8 do not include the extra track isolation requirement we impose. We separately measured this scale factor for all the lepton categories, and saw no systematic deviation from 1.0, so we assigned an additional systematic error of 4% on the acceptance from the maximum deviation observed from 1.0 (see section 10), although this will soon be improved.

5.1 MET-PEM Trigger Scale Factor

We collect PHX-lepton events on the MET-PEM trigger. Certain categories (where the second leg is another PHX or non-triggering muon) can only be collected on this trigger path. We follow closely the calculation of the MET-PEM trigger efficiency for the $W \to e\nu$ plug electron analysis described in [17]. There are two main sources of inefficiency for this trigger :

- L1_MET15. The efficiency of this trigger requirement estimated in [17] is very close to 100%. Moreover the WW analysis described here has a $\not\!\!E_T$ cut at 25 GeV rather

Scale Factor	Value	Reference
Trigger Efficiency		
F_{TCE}	0.961	[11]
F_{CMUP}	0.887	[12]
F_{CMX}	0.954	[12]
$F_{MET-PEM}$(PHX − electron)	0.961	this note
$F_{MET-PEM}$(PHX − muon)	0.942	this note
Data/MC Reconstruction Efficiency		
F_{TCE}	0.965	[13]
F_{PHX}	0.927	[14]
F_{CMU}	0.890	[12]
F_{CMP}	0.943	[12]
F_{CMUP}	0.887	[12]
F_{CMX}	1.008	[12]
F_{CMIO}	1.000	[15]
Data/MC $\|z0\| < 60$ cm Efficiency		
F_{z0}	0.977	[16]

Table 8: The scale factors applied to Monte Carlo expectations for the trigger efficiencies and the lepton ID efficiencies.

than 20 GeV, so the trigger inefficiency should be even smaller. Comparing the $\not\!\!E_T$ distributions in $W \to e\nu$ and $WW \to l\nu l\nu$ Monte Carlo samples indicates that the L1_MET15 requirement is 100% efficient for PHX-electron categories. However for PHX-muon events, the offline cut on the muon corrected-$\not\!\!E_T$ is less well correlated with the online cut on the raw-$\not\!\!E_T$. Monte Carlo studies indicate a residual 2% trigger inefficiency for events in these categories, due to event topologies that result in much smaller raw- compared to corrected-$\not\!\!E_T$.

- L2_PEM20. The efficiency of this trigger requirement is estimated to be 0.966 in [17]. Although the plug electron E_T distributions are not identical for single W and W-pair production, applying the trigger turn-on curve parametrized in [17] indicates that the overall difference in L2_PEM20 efficiencies for these two processes is only around 0.5%.

Other sources of inefficiency such as L3_MET15 are negligible after the above trigger requirements and offline analysis cuts have been made. The resulting trigger efficiencies are therefore :

$$\epsilon_{\mathrm{MET-PEM}}(\mathrm{PHX-electron}) = \epsilon_{\mathrm{L1}} \times \epsilon_{\mathrm{L2}} = 1.00 \times 0.961 = 0.961$$
$$\epsilon_{\mathrm{MET-PEM}}(\mathrm{PHX-muon}) = \epsilon_{\mathrm{L1}} \times \epsilon_{\mathrm{L2}} = 0.98 \times 0.961 = 0.942$$

The systematic uncertainty on the MET-PEM trigger efficiency estimated in [17] is approximately 2%. A similar uncertainty could arise from differences between single W and W-pair production kinematics that may not have been taken completely into account using the above Monte Carlo based cross-checks. We therefore take 3% as an estimate of the overall uncertainty on the MET-PEM trigger efficiency.

5.2 PHX Charge Mis-identification Scale Factor

An η dependent scale factor is calculated to compensate for the discrepancy between the charge fake rate of PHX electrons in the Monte Carlo compared to the charge fake rate in data. This scale factor is applied to the Monte Carlo acceptances to account for the overestimate. The charge ID rate is calculated in central-plug $Z \to ee$ events in both Monte Carlo and data, where the charge ID is defined as the number of opposite sign events divided by all sign events $(OS/(SS+OS))$. This distribution is shown in figure 2 and the resulting scale factor is shown in figure 3.

Since there is a significant difference between the η distributions of plug electrons in WW and Drell-Yan events (see figure 1), the scale factor cannot be applied as an average, so is instead applied as a function of η. A linear fit is applied to each side of the scale factor distribution and these functions (shown in table 9) are used to correct the Monte Carlo estimates.

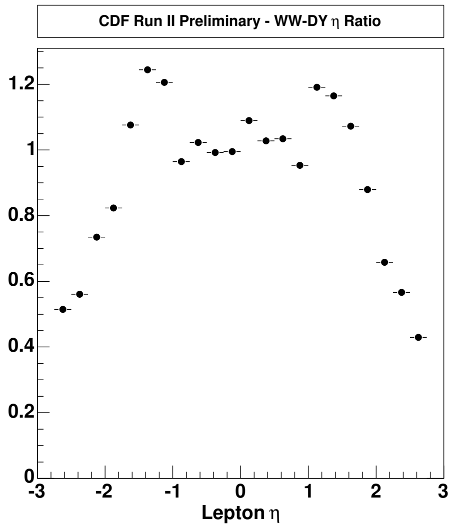

Figure 1: The ratio of the η distributions for WW and DY MC.

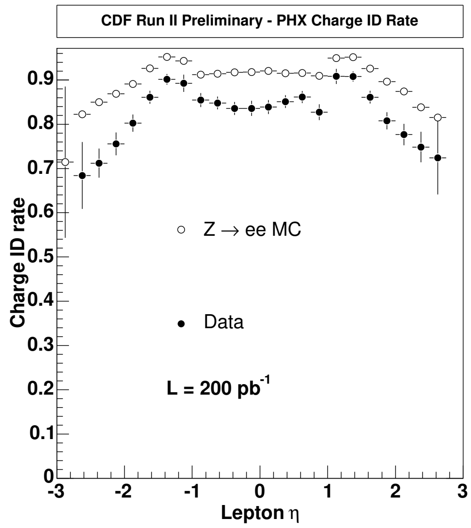

Figure 2: The PHX charge ID rate as a function of η for both $Z \to ee$ MC and data.

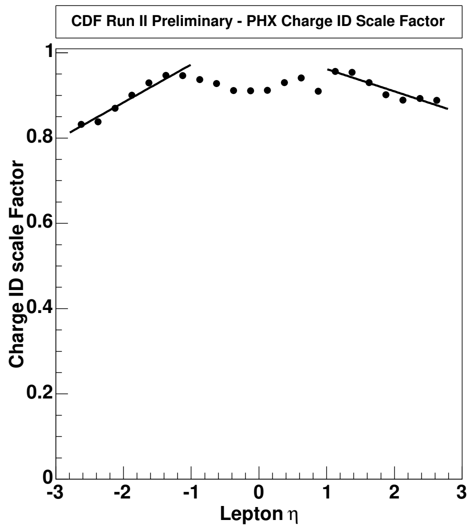

Figure 3: Result of the fit to the MC/data PHX charge scale factor ratio, used to determine the η dependent scale factor for PHX electrons.

	a	b
$+\eta$	1.049	-0.0071
$-\eta$	1.069	0.0093

Table 9: The values of the fit, $a + b\eta$ of the Phoenix charge ID MC/data scale factor

6 Data analysis

6.1 Data samples and luminosity

We use the inclusive high-P_T lepton samples `bhel08`, `bhel09`, `bhmu08`, `bhmu09` (4.8.4 Production) remade with 4.11.1 production. The plug electron samples we use are `bpel08` and `bpel09`, also remade with 4.11.1 production.

Version 4 of the good run list of the Top, EWK and Exotics groups is applied [1], however we note the following:

- In the ee channel we apply the good run list without muon requirements.
- We have applied the good run list without silicon checks to the events that do not contain a PHX in the dilepton category.
- For dilepton events with a PHX (TCE-PHX, PHX-PHX, CMUP-PHX, CMX-PHX, PHX-CMU, PHX-CMP, PHX-CMIO) the good run list with silicon checks has been applied.

	Offline	+1.9% correction and 6% error
No Silicon (ee only)	199.93	203.7 ± 12.2
Good Silicon (ee only)	166.42	169.6 ± 10.2
No Silicon ($e\mu$ and $\mu\mu$)	189.92	193.5 ± 11.6
Good Silicon ($e\mu$ and $\mu\mu$) :	158.56	161.6 ± 9.7
No Silicon with CMX ($e\mu$ and $\mu\mu$):	172.03	175.3 ± 10.5
Good Silicon with CMX ($e\mu$ and $\mu\mu$):	147.03	149.8 ± 8.9

Table 10: Luminosities used in the WW dilepton analysis.

.

[1] http://www-cdf.fnal.gov/internal/dqm/goodrun/v4/goodv4.html

The luminosities relevant for our dilepton categories are summarized in table 10. These luminosities, together with the relative acceptances in the WW dilepton categories, gives us an average luminosity for our WW cross-section measurement of:

$$\mathcal{L}_{WW} = (184 \pm 11)\,\mathrm{pb}^{-1}$$

6.2 Energy Scale factors for Plug electrons.

The transverse energy of the plug electrons is corrected using the result of the plug energy calibration from the combined $WW/WZ/ZZ$ cross-section analysis [9]. The corrections are done separately for the east and west plug calorimeters. The scale factors we use from the aforementioned reference are given in table 11. These come from calibrations against CEM-Plug Z events.

Run Range	Plug, $\eta > 0$	Plug, $\eta < 0$
141544 $\rightarrow$ 159600	1.069	1.057
159600 $\rightarrow$ 163600	1.097	1.084
163600 $\rightarrow$ 168890	1.089	1.077

Table 11: Energy scale factors applied to plug EM clusters in data events.

6.3 Dilepton table

The result of the event selection described in Section 2 on the datasets described above is shown in table 12. We find 16 $WW \rightarrow$ *dilepton* candidates; 8 ee, 6 $\mu\mu$ and 6 $e\mu$. We also observe a trilepton candidate which we do not include in our analysis, but list this category for interest (recall we veto trilepton events as it significantly reduces the WZ background and has almost no effect on the WW acceptance).

6.4 List of candidates

The list of candidate events (17 of them) are as follows in the order in which they came in. Some event pictures and candidate details are given in section 11.2.

Category	ID	ISO	Conv+Cosm	Z veto	$\not{E}_T > 25$ GeV	$\Delta\phi$	0j	OS
TCE-TCE	4227	3620	3455	402	15	7	4	4
TCE-PHX	4015	3585	3487	275	7	6	4	2
PHX-PHX	43	36	36	9	6	4	0	0
$e-e$	8285	7241	6978	686	28	17	8	**6**
TCE-CMUP	30	19	17	17	4	3	1	1
TCE-CMU	7	4	4	4	1	1	0	0
TCE-CMP	11	4	4	4	2	2	1	1
TCE-CMX	24	12	11	11	6	6	2	2
TCE-CMIO	46	16	16	16	3	2	0	0
PHX-CMUP	11	10	10	10	4	4	1	0
PHX-CMU	1	1	1	1	0	0	0	0
PHX-CMP	5	2	2	2	1	1	1	1
PHX-CMX	9	8	8	8	2	1	0	0
PHX-CMIO	15	3	3	3	0	0	0	0
$e-\mu$	159	79	76	76	23	20	6	**5**
CMUP-CMUP	1014	948	948	121	2	2	1	1
CMUP-CMU	429	405	405	41	1	0	0	0
CMUP-CMP	566	517	517	59	5	5	1	1
CMUP-CMX	1151	1079	1079	114	4	3	1	1
CMUP-CMIO	2076	1939	1939	218	4	4	2	2
CMX-CMX	404	363	363	36	1	1	0	0
CMX-CMU	259	249	249	26	0	0	0	0
CMX-CMP	263	243	243	32	0	0	0	0
CMX-CMIO	911	834	834	78	3	1	1	1
$\mu-\mu$	7073	6577	6577	725	20	16	6	**6**
TRILEPTON	7	7	7	3	0	0	0	0

Table 12: WW dilepton channel analysis results in $184\,\mathrm{pb}^{-1}$ for each of the dilepton categories. Also shown is the trilepton category not included in this analysis. The OS requirement is *not* made for categories involving PHX electrons.

	Run/Event	Dilepton subcategory	Dilepton category
1.	154860/2090959	CEM-CEM	ee
2.	155364/3494901	CEM-CMX	$e\mu$
3.	155895/3356769	CMUP-CMIO	$\mu\mu$
4.	160151/842563	CMUP-CMUP	$\mu\mu$
5.	161441/222977	CEM-PHX	ee
6.	161678/5620107	CEM-CEM	ee
7.	161722/330583	CMX-CMIO	$\mu\mu$
8.	162175/1550545	CEM-CMX	$e\mu$
9.	162838/627050	CEM-CEM	ee
10.	163113/3247975	PHX-CMP	$e\mu$
11.	165906/1741744	CEM-PHX	ee
12.	166038/4460001	CMUP-CMIO	$\mu\mu$
13.	166662/8232100	CMUP-CMP	$\mu\mu$
14.	166715/1690893	CMUP-CMX	$\mu\mu$
15.	167053/12891960	CEM-CEM	ee
16.	167849/566726	CEM-CMUP	$e\mu$
17.	168640/4871589	CEM-CMP	$e\mu$

7 Background Estimates

The backgrounds due to $t\bar{t}$, WZ, ZZ, Drell-Yan e^+e^-, $\mu^+\mu^-$ and $\tau^+\tau^-$ are evaluated in the same way as described in [2]. We repeat the salient points for those estimates here, and give the new values for $\sim 184\,\mathrm{pb}^{-1}$, properly weighted for the different CMX and SVX luminosities (which is slightly different from background to background as the relative efficiencies in the subcategories vary slightly).

The resulting background estimates are shown in the tables of this section. Scale factors are not applied in these tables, except for the PHX Charge mis-ID scale factor for the OS cut (see section 5). However in going from the numbers in these tables to the final background estimates in table 44 all the relevant scale factors are applied.

The fake background has been re-evaluated since our previous notes, and below we give a more detailed account of its estimate and the various cross-checks we have performed.

7.1 $t\bar{t}$ background

A contribution to our dilepton signal from $t\bar{t}$ can occur when $t\bar{t}$ decays via the dilepton channel and all jets in the event are missed (either fiducially or by failing the E_T cut). The sample used to determine the $t\bar{t}$ background rejection consisted of 349933 PYTHIA $t\bar{t}$ events (ttopei,cdfptop). Using the theoretical value of $\sigma(t\bar{t}) = 7$ pb, the luminosity of the sample is 50 fb^{-1}. Table 13 shows the $t\bar{t}$ rejection after every analysis cut. The jet veto is mainly responsible for rejecting $t\bar{t}$ events. The expected $t\bar{t}$ background numbers in $184\,\mathrm{pb}^{-1}$ are given at the end of this section in the summary table 44.

	$t\bar{t}$					
	ee		$\mu\mu$		$e\mu$	
Cut		%		%		%
Lepton ID	1278.00	0.00 ± 0.00	1532.00	0.00 ± 0.00	2837.00	0.00 ± 0.00
Isolation	907.00	70.97 ± 1.27	1081.00	70.56 ± 1.16	2057.00	72.51 ± 0.84
Conv+Cosmic	884.00	97.46 ± 0.52	1081.00	100.00 ± 0.00	2021.00	98.25 ± 0.29
Z-veto	813.00	91.97 ± 0.91	997.00	92.23 ± 0.81	2021.00	100.00 ± 0.00
$\not{E}_T$ >25 GeV :	739.00	90.90 ± 1.01	900.00	90.27 ± 0.94	1762.00	87.18 ± 0.74
$\Delta\Phi > 20°$ if $\not{E}_T$ <50	688.00	93.10 ± 0.93	829.00	92.11 ± 0.90	1612.00	91.49 ± 0.66
0 jets	6.00	0.87 ± 0.35	4.00	0.48 ± 0.24	15.00	0.93 ± 0.24
Opposite Sign	5.91	98.57 ± 4.84	4.00	100.00 ± 0.00	14.67	97.82 ± 3.77

Table 13: $t\bar{t}$ events from the PYTHIA sample described in the text passing dilepton cuts for each dilepton category, and the associated efficiencies of each cut (after all previous cuts have been applied). Errors are statistical only.

7.2 WZ background

The contribution due to WZ production predominantly occurs when both bosons decay leptonically and one of the leptons is not detected. The sample used to determine the WZ background consisted of 80430 WZ PYTHIA events (wtop0q, cdfptop). For this sample we did not force the leptonic decays at the generator level but rather we applied a dilepton filter after the generation and prior to simulation that demanded two leptons (e,μ or τ) with $P_T > 10$ GeV and $|\eta| < 2$. (this was so we would include the (very) small contribution from the case when both leptons come from the Z.)

The efficiency of the filter is 5.80±0.01%. With a sample of 80430 analyzed events and a cross-section $\sigma^{WZ}_{NLO} = 3.96 \pm 0.06$ pb [3], the luminosity of the sample was estimated to be about 350 fb^{-1}. The cut efficiencies for WZ are given in table 14 and the expected number of WZ background events is reported in table 44. The requirement that the event have exactly 2 leptons approximately halves this background. The jet veto gets rid of most of the remaining WZ→$q\bar{q}'$ ll contribution. Of the remaining dilepton events from WZ→$\ell\nu$ $\ell^+\ell^-$, approximately 70% of them are opposite sign. In the grand summary table we assign a systematic error the same as that for WW since the processes are somewhat similar.

7.3 Drell-Yan background

The Drell-Yan background is estimated by running over large PYTHIA generated Monte Carlo samples (ztop0e, ztop0m, ztop2t). These samples have 2.85M DY → ee events, 2.89M DY → $\mu\mu$ events, and 422k DY → $\tau\tau$ events, and a dilepton mass cut of 30 GeV. These results are summarized in tables 15 and 16. Drell-Yan $\tau^+\tau^-$ production constitutes a back-

	WZ					
	ee		$\mu\mu$		$e\mu$	
Cut		%		%		%
Lepton ID	10789.00	0.00 ± 0.00	9238.00	0.00 ± 0.00	2480.00	0.00 ± 0.00
Isolation	9221.00	85.47 ± 0.34	8073.00	87.39 ± 0.35	1980.00	79.84 ± 0.81
Conv+Cosmic	9054.00	98.19 ± 0.14	8073.00	100.00 ± 0.00	1962.00	99.09 ± 0.21
Z-veto with $\not{E}_T^{sig}$	2551.00	28.18 ± 0.47	2275.00	28.18 ± 0.50	1962.00	100.00 ± 0.00
$\not{E}_T$ >25 GeV :	2072.00	81.22 ± 0.77	1820.00	80.00 ± 0.84	1512.00	77.06 ± 0.95
$\Delta\Phi > 20°$ if $\not{E}_T$ <50	1909.00	92.13 ± 0.59	1697.00	93.24 ± 0.59	1366.00	90.34 ± 0.76
0 jets	739.00	38.71 ± 1.11	960.00	56.57 ± 1.20	699.00	51.17 ± 1.35
Opposite Sign	591.96	80.10 ± 1.47	739.00	76.98 ± 1.36	328.28	46.96 ± 1.89

Table 14: PYTHIA WZ events passing dilepton cuts for each dilepton category, and the associated efficiencies of each cut (after all previous cuts have been applied). Errors are statistical only.

ground in all three measurement channels, as is summarized in table 17. The final background numbers in 184 pb^{-1} are given in table 44, and are scaled from the numbers in the results tables using $\sigma(p\bar{p} \to Z/\gamma^* \to l^+l^- = 236 \times 1.4$ pb, where 236 pb is the PYTHIA leading order cross-section for a mass cut of 30 GeV and 1.4 is the NNLO/LO k-factor [8].

7.4 Data cross check of Drell-Yan background estimate

Monte Carlo may not model the $\not{E}_T$ distribution of Drell-Yan events very well and since this distribution is the primary variable used to reject Drell-Yan events in this analysis it is possible that our Monte Carlo based estimate of this background is wrong. One possible solution is to try to use the data itself to estimate the Drell-Yan background.

We assume that the number of events passing all cuts can be estimated by first applying all of the WW selection cuts to the data but with the "Drell-Yan rejection" cuts reversed. This gives a data sample that looks like WW in most respects but is dominated by Drell-Yan. We then need a way of predicting how many of these "Drell-Yan rich, WW-like" events could have fluctuated into our event sample by passing the Drell-Yan rejection cuts. To calculate this we return to a pure Drell-Yan data sample and, applying no other cuts, calculate the ratio of the number of events that pass these rejection cuts to the number of events that fail. Applying this ratio to the number of events in the "Drell-Yan rich, WW-like" sample gives us an estimate of the number of Drell-Yan events that fall inside our WW event selection, i.e. the Drell-Yan background. Schematically, this method can be represented by the equation :

$$N(c_1 \wedge c_2 \wedge ... \wedge c_{n-1} \wedge c_n) \;=\; N(c_1 \wedge c_2 \wedge ... \wedge c_{n-1} \wedge \neg c_n) \times \frac{N(c_n)}{N(\neg c_{c_n})},$$

Cut	Drell-Yan e^+e^-					
	ee		$\mu\mu$		$e\mu$	
		%		%		%
Lepton ID	519583.00	0.00 ± 0.00	0.00	0.00 ± 0.00	1084.00	0.00 ± 0.00
Isolation	479025.00	92.19 ± 0.04	0.00	0.00 ± 0.00	805.00	74.26 ± 1.33
Conv+Cosmic	471119.00	98.35 ± 0.02	0.00	0.00 ± 0.00	801.00	99.50 ± 0.25
Z-veto with $\not\!\!E_T^{sig}$	44211.00	9.38 ± 0.04	0.00	0.00 ± 0.00	801.00	100.00 ± 0.00
$\not\!\!E_T$ >25 GeV :	304.00	0.69 ± 0.04	0.00	0.00 ± 0.00	20.00	2.50 ± 0.55
$\Delta\Phi > 20°$ if $\not\!\!E_T$ <50	92.00	30.26 ± 2.63	0.00	0.00 ± 0.00	7.00	35.00 ± 10.67
0 jets	30.00	32.61 ± 4.89	0.00	0.00 ± 0.00	2.00	28.57 ± 17.07
Opposite Sign	28.53	95.11 ± 3.94	0.00	0.00 ± 0.00	2.00	100.00 ± 0.00

Table 15: Effect of WW analysis cuts on Drell-Yan e^+e^- PYTHIA events. Errors are statistical only. Scale factors are not applied here except for the PHX Charge mis-ID scale factor for the OS cut (see section 5).

Cut	Drell-Yan $\mu^+\mu^-$					
	ee		$\mu\mu$		$e\mu$	
		%		%		%
Lepton ID	0.00	0.00 ± 0.00	365037.00	0.00 ± 0.00	1160.00	0.00 ± 0.00
Isolation	0.00	0.00 ± 0.00	344920.00	94.49 ± 0.04	581.00	50.09 ± 1.47
Conv+Cosmic	0.00	0.00 ± 0.00	344920.00	100.00 ± 0.00	542.00	93.29 ± 1.04
Z-veto with $\not\!\!E_T^{sig}$	0.00	0.00 ± 0.00	34110.00	9.89 ± 0.05	542.00	100.00 ± 0.00
$\not\!\!E_T$ >25 GeV :	0.00	0.00 ± 0.00	269.00	0.79 ± 0.05	80.00	14.76 ± 1.52
$\Delta\Phi > 20°$ if $\not\!\!E_T$ <50	0.00	0.00 ± 0.00	106.00	39.41 ± 2.98	39.00	48.75 ± 5.59
0 jets	0.00	0.00 ± 0.00	36.00	33.96 ± 4.60	28.00	71.79 ± 7.21
Opposite Sign	0.00	0.00 ± 0.00	36.00	100.00 ± 0.00	17.09	61.03 ± 9.22

Table 16: Effect of WW analysis cuts on Drell-Yan $\mu^+\mu^-$ PYTHIA events. Errors are statistical only.

where c_i are the cuts used in the WW analysis, c_n being the cut(s) specifically designed to reject Drell-Yan events ($\wedge$ indicates Boolean AND and $\neg$ Boolean NOT).

There are several difficulties in doing this calculation. The first is that the Drell-Yan rejection cuts vary as a function of dilepton mass. Inside the Z window we use a combination of $\not\!\!E_T$ and $\not\!\!E_T^{sig}$ cuts to reject Drell-Yan events but outside the Z window only the $\not\!\!E_T$ cut is applied. So we must split the data estimate into two sections and do the calculation separately for each mass region. Secondly, both terms on the right hand side of the above expression can receive corrections due to contamination from physics sources other than Drell-Yan that we must evaluate using Monte Carlo. Finally, the above expression assumes that the power of the Drell-Yan rejection cuts is uncorrelated with other selection cuts in the WW analysis. The extent to which this is true must also be evaluated using Monte Carlo.

7.4.1 Outside the Z window

The simplest of the two mass regions is that outside the Z window ($M_{ll} < 76$ or $M_{ll} > 106$ GeV). Here the Drell-Yan rejection cut is simply the requirement that we are away from the Z peak. We then apply the methodology described above to yield :

$$N_{\mathrm{DY}}(M_{ll} < 76 \text{ or } > 106 \text{ GeV}) \;=\; n^{in}_{WW} \times R_{\frac{out}{in}},$$

where n^{in}_{WW}, the size of the "Drell-Yan rich, WW-like" sample, is the number of data events that fall inside the Z window but pass all of the WW cuts that would be applied outside the Z window. $R_{\frac{out}{in}}$ is the ratio of the number of Drell-Yan events that fall outside the Z window to those that fall inside.

Here we encounter some of the problems mentioned above. When forming the "Drell-Yan rich, WW-Like" sample we find that even in the Z window there are very few events that survive after applying the $\not\!\!E_T$ cut. With such small numbers of events we can no longer consider n^{in}_{WW} to be dominated by Drell-Yan since we know there are significant contributions from other physics processes. To account for this we estimate the contamination from these other processes (WW, WZ, ZZ, $W\gamma$, fakes, $Z \to \tau\tau$, $t\bar{t}$) using Monte Carlo, and then subtract these estimates from n^{in}_{ww}. The contamination estimates, n^{in}_{other}, and the raw values of n^{in}_{WW} for the ee and $\mu\mu$ channels are shown in tables 19 and 20.

The second difficulty is in the calculation of $R_{\frac{out}{in}}$. When applying this ratio to the event count in the "Drell-Yan rich, WW-like" sample, we are applying it to events that have high $\not\!\!E_T$. Since high $\not\!\!E_T$ will likely be due to mis-measured leptons it implies that these events are more likely to have a lower reconstructed Z mass and hence a different value of $R_{\frac{out}{in}}$ than the pure, well reconstructed Drell-Yan sample. In a pure Drell-Yan data sample we find the ratio is 0.1, but in Drell-Yan MC with a $\not\!\!E_T > 25$ GeV cut we find the ratio is closer to 0.5 when averaged over the dilepton categories (see table 18). We use the MC ratio, resulting in the background estimates from Drell-Yan outside the Z window shown in table 21.

7.4.2 Inside the Z window

The contribution from inside the window is more difficult to calculate in the data because there are two, correlated, cuts used to reject the Drell-Yan events inside the window, $\not\!\!E_T$ and $\not\!\!E_T^{sig}$. Using the method described above, we write :

$$N_{\mathrm{DY}}(76 < M_{ll} < 106 \text{ GeV}) \;=\; \hat{n}_{WW}^{in} \times R_{\frac{\hat{DY}}{DY}},$$

where $\hat{n}_{WW}^{in}$ is the size of the "Drell-Yan rich, WW-like" sample, in this case those events in the Z window that pass all WW cuts but fail *either* the $\not\!\!E_T$ or the $\not\!\!E_T^{sig}$ cut (see table 24). $R_{\frac{\hat{DY}}{DY}}$ is the ratio of the number of Drell-Yan events that pass *both* the $\not\!\!E_T$ and $\not\!\!E_T^{sig}$ cuts to the number that fail *either* the $\not\!\!E_T$ or the $\not\!\!E_T^{sig}$ cut. The numerator of $R_{\frac{\hat{DY}}{DY}}$ is heavily contaminated with non Drell-Yan events, again estimated using Monte Carlo (see tables 22 and 23). The final estimate of the Drell-Yan background inside the Z window is given in table 25.

7.4.3 Total Estimate from Data

Our data-based estimate for the total Drell-Yan background is the sum of the above two contributions :

$$N_{DY}^{tot} = n_{WW}^{in} \times R_{\frac{out}{in}} + \hat{n}_{WW}^{in} \times R_{\frac{\hat{DY}}{DY}}$$

To recapitulate, the terms in this expression are :

- n_{WW}^{in} : the number of data events that have 2 opposite sign baseline leptons in the Z window with $\not\!\!E_T > 25$ GeV, $\Delta\phi(\not\!\!E_T, \text{nearest} - l/j) > 20$ and 0-jets, minus the expected contamination from other physics processes.
- $R_{\frac{out}{in}}$ is the ratio of the number of Drell-Yan events outside the Z mass window to the number inside the Z mass window, calculated using Drell-Yan Monte Carlo with a cut $\not\!\!E_T > 25$ GeV.
- $\hat{n}_{WW}^{in}$ is the number of data events with 2 opposite sign baseline leptons in the Z window with 0-jets, $\Delta\phi(\not\!\!E_T, \text{nearest} - l/j) > 20$, and ($\not\!\!E_T < 25 \vee \not\!\!E_T^{sig} < 3$).
- $R_{\frac{\hat{DY}}{DY}}$ is calculated from data events that have 2 baseline leptons by counting the number of events that have $\not\!\!E_T > 25 \wedge \not\!\!E_T^{sig} > 3$, subtracting the contamination estimated by applying the same cuts to the MC samples for the other physics processes in this region ($\hat{n}_{other}^{in}$), and then dividing by the number of data events that have ($\not\!\!E_T < 25 \vee \not\!\!E_T^{sig} < 3$). That is :

$$R_{\frac{\hat{DY}}{DY}} = \frac{n(\not\!\!E_T > 25 \wedge \not\!\!E_T^{sig} > 3)^{data} - \hat{n}_{other}^{in}}{n(\not\!\!E_T < 25 \vee \not\!\!E_T^{sig} < 3)^{data}}$$

The calculation is performed separately for ee and $\mu\mu$ channels. The totals are summarized in table 26, where negative sub-contributions have been set to zero for the best possible overall data based estimate.

7.4.4 Conclusion

The lack of statistics prohibits too meaningful a cross check, but does suggest we are probably not catastrophically off in our Monte Carlo estimate. This cross check will prove more useful after a lot more luminosity. It also doesn't make much sense to use these data driven values to derive a systematic uncertainty on the DY background. We do this in the next subsection based on $\not{E}_T$ distribution comparisons of Drell-Yan data and MC.

7.5 Systematic Uncertainty on the Drell-Yan Background

The dominant source of systematic uncertainty on the Drell-Yan background derives from the Monte Carlo modeling of the $\not{E}_T$ distribution. The ΣE_T distribution for Drell-Yan data is well described by Monte Carlo, so we believe that discrepancies in the numerator of the $\not{E}_T^{sig}$ also dominate the systematic uncertainty on the Drell-Yan background inside the Z-mass window.

Initial studies were performed in [2] and have been updated here with higher statistics and new Monte Carlo samples. Figure 4 shows the $\not{E}_T$ distribution for Drell-Yan data and Monte Carlo in both e^+e^- and $\mu^+\mu^-$ channels. The left set of plots are before the $\Delta\phi$ cut applied in the WW analysis and the right set of plots are after this cut. It can be seen that the agreement between e^+e^- data and Monte Carlo in particular is substantially improved after this cut. This suggests that a major source of discrepancy between data and Monte Carlo is modeling of electron energy mis-measurements, which is much reduced by the $\Delta\phi$ cut in our analysis and also explains the smaller discrepancy that is seen in the muon channel.

Despite the improvement after the $\Delta\Phi$ cut, there is still some evidence for a harder $\not{E}_T$ distribution in e^+e^- data compared to Monte Carlo. There is no clear evidence for a discrepancy in the muon data, as can be seen in figure 5. To estimate the potential effect on the Drell-Yan background estimated using Monte Carlo, we apply an additional Gaussian smearing directly to the Monte Carlo $\not{E}_T$ distribution. The width of the Gaussian is given by $A \times \sqrt{\Sigma E_T}$, where A is a constant that is varied until the χ^2 between the data and the smeared MC $\not{E}_T$ distributions, calculated in the range 10 to 20 GeV, is minimized. The χ^2 distribution as a function of A is shown in figure 6. A polynomial fit is applied to this χ^2 function to obtain the minimum, and thereby the optimum amount of smearing, which is found to be at $A = 0.18$. The resulting $\not{E}_T$ distribution is is shown in figure 7 where it is compared to the data and the unsmeared Monte Carlo. Applying this optimized additional smearing gives rise to 28% larger Monte Carlo background estimates above the cut of 25 GeV (0.95 events in the smeared MC compared to 0.74 in the unsmeared MC histogram). We apply this scaling factor to our Monte Carlo based estimate of the e^+e^- background. Note that we do not directly compare distributions in the tails due to potentially large signal and other non-DY contamination.

Varying A by 3 units of χ^2 (3 is approximately equal to χ^2_{min}) corresponds to a change in the calculated scale factor of approximately 13%. Changing the form of the smearing from $\sqrt{\Sigma E_T}$ to $\sqrt{\not{E}_T}$ changes the scale factor by around 2% and changing the range over which the χ^2 is calculated gives about a 7% change in the scale factor.

Cut	Drell-Yan $\tau^+\tau^-$					
	ee		$\mu\mu$		$e\mu$	
		%		%		%
Lepton ID	20623.00	0.00 ± 0.00	19406.00	0.00 ± 0.00	36650.00	0.00 ± 0.00
Isolation	18597.00	90.18 ± 0.21	17789.00	91.67 ± 0.20	33181.00	90.53 ± 0.15
Conv+Cosmic	18336.00	98.60 ± 0.09	17789.00	100.00 ± 0.00	32912.00	99.19 ± 0.05
Z-veto with $\not{E}_T^{sig}$	17161.00	93.59 ± 0.18	16749.00	94.15 ± 0.18	32912.00	100.00 ± 0.00
$\not{E}_T$ >25 GeV :	787.00	4.59 ± 0.16	816.00	4.87 ± 0.17	1590.00	4.83 ± 0.12
$\Delta\Phi > 20°$ if $\not{E}_T$ <50	293.00	37.23 ± 1.72	324.00	39.71 ± 1.71	576.00	36.23 ± 1.21
0 jets	42.00	14.33 ± 2.05	44.00	13.58 ± 1.90	89.00	15.45 ± 1.51
Opposite Sign	38.40	91.43 ± 4.32	44.00	100.00 ± 0.00	87.52	98.34 ± 1.35

Table 17: Effect of WW analysis cuts on Drell-Yan $\tau^+\tau^-$ PYTHIA events. Errors are statistical only.

	ee		$\mu\mu$	
	Data	MC ($\not{E}_T > 25GeV$)	Data	MC ($\not{E}_T > 25GeV$)
Outside Window	577	242	604	219
Inside window	5459	471	4934	385
$R_{\frac{out}{in}}$	0.106 ± 0.001	0.51 ± 0.02	0.122 ± 0.001	0.57 ± 0.01

Table 18: Numbers of Drell-Yan events inside and outside the Z-mass window ($76 < M_{ll} <$ 106 GeV), used in the data-based estimate of the Drell-Yan background outside the Z window.

	WW	$t\bar{t}$	WZ	Fake	$Z \to \tau\tau$	ZZ	$W\gamma$	Total (n_{other}^{in})
ee	0.70	0.007	0.28	0.114	0.012	0.38	0.06	1.55
$\mu\mu$	0.65	0.0	0.28	0.086	0.007	0.39	0.0	1.41

Table 19: Event counts in the Z window with all out-of-window WW selection cuts applied, used to decontaminate the outside window "Drell-Yan rich, WW-like" event sample.

	ee	$\mu\mu$
n_{ww}^{in}	2	1

Table 20: Event counts in the outside window "Drell-Yan rich, WW-like" data sample.

Background Estimate	ee	$\mu\mu$
n_{ww}^{in}	2	1
$(n_{ww}^{in} - n_{other}^{in})$	$(2 - 1.55)$	$(1 - 1.41)$
$(n_{ww}^{in} - n_{other}^{in}) \times R_{\frac{out}{in}}$	$(2 - 1.55) \times 0.51$ $= 0.23 \pm 0.61$	$(1 - 1.41) \times 0.57$ $= -0.23 \pm 0.68$

Table 21: Estimated amount of Drell-Yan background originating outside the Z window. Errors are statistical only

	WW	$t\bar{t}$	WZ	Fake	$Z \to \tau\tau$	ZZ	$W\gamma$	Total $hatn_{other}^{in}$
ee	0.74	0.56	0.59	0.09	0.06	0.47	0.23	2.75
$\mu\mu$	0.65	0.51	0.53	0.06	0.05	0.47	0.0	2.26

Table 22: Event counts from MC in the Z window with $\not{E}_T > 25$ and $\not{E}_T^{sig} > 3$ used to decontaminate the numerator of $R_{\frac{\hat{DY}}{DY}}$.

	ee	$\mu\mu$
Numerator Denominator	3 5456	3 4931
$R_{\frac{\hat{DY}}{DY}} = \frac{Numerator - \hat{n}_{other}^{in}}{Denominator}$	$\frac{3-2.75}{5456}$ $= 4.55 \times 10^{-5} \pm 0.0003$	$\frac{3-2.26}{4931}$ $= 0.00015 \pm 0.00035$

Table 23: The Monte Carlo corrected data estimate of Drell-Yan events passing $\not{E}_T$ and $\not{E}_T^{sig}$ cuts (numerator), and those failing (denominator), together with the resulting ratios.

	ee	$\mu\mu$
$\hat{n}_{ww}^{in}$	3160	3107

Table 24: Event counts in the inside window "Drell-Yan rich, WW-like" event sample.

Background Estimate	ee	$\mu\mu$
$\hat{n}_{ww}^{in}$	3160	3107
$\hat{n}_{ww}^{in} \times R_{\frac{\hat{DY}}{DY}}$	$3160 \times (4.55 \times 10^{-05})$	3107×0.00015
	$= 0.14 \pm 1.00$	0.46 ± 1.09

Table 25: Estimate of amount of Drell-Yan background originating inside the Z window.

Channel	Inside	Outside	Total
ee	0.14 ± 1.00	0.23 ± 0.61	0.37 ± 1.18
$\mu\mu$	0.46 ± 1.09	-0.23 ± 0.68	0.46 ± 1.28

Table 26: Data based estimate of DY background inside and outside the Z window.

The uncertainty on the $\mu^+\mu^-$ background is estimated in the same way. We observe much better agreement between data and MC in the muon case, which is born out by the much shallower χ^2 curve shown in figure 8. We conclude that there is no clear need for additional smearing in the muon case. However a wide range of smearing parameters are also not excluded, and these can change the predicted number of events above the $\not\!\!E_T$ cut of 25 GeV by as much as 40%.

We conservatively use 40% as the systematic uncertainty on the Drell-Yan background in all categories.

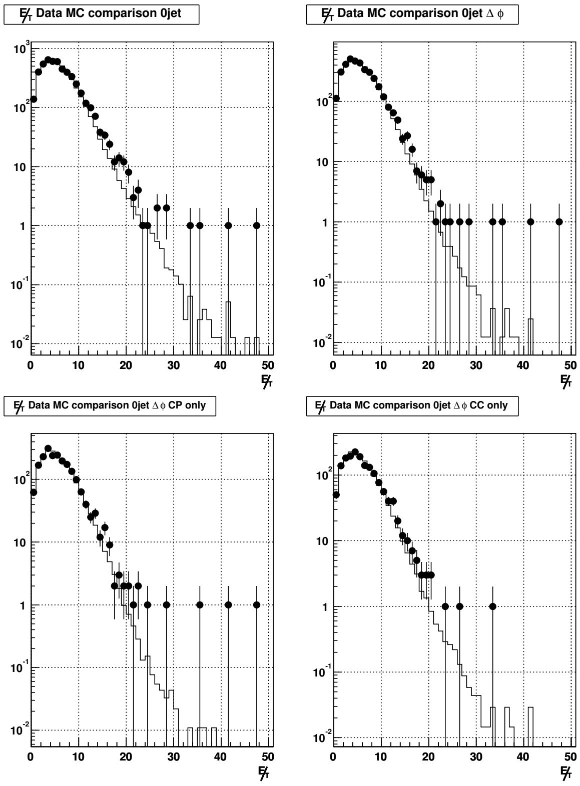

Figure 4: Comparison of the $\not\!\!E_T$ distribution in DY ee MC and data, both with and without a $\Delta\phi$ cut.

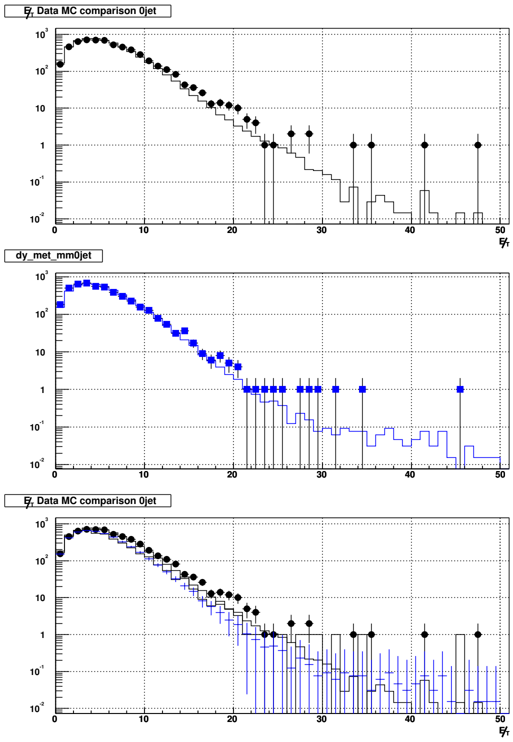

Figure 5: Comparison of the $\not\!\!E_T$ distribution in DY ee (top) and $\mu\mu$ (middle) MC and data. The bottom plot overlays ee and $\mu\mu$.

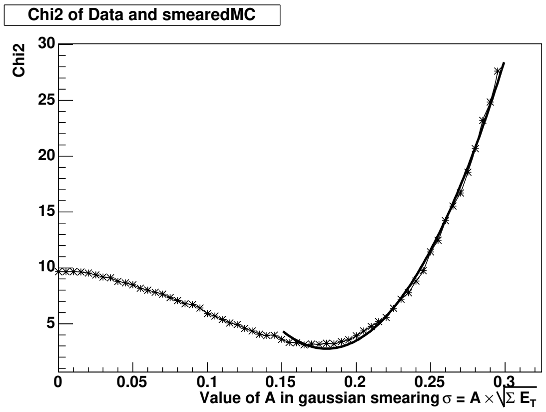

Figure 6: χ^2 between data and smeared Drell-Yan e^+e^- Monte Carlo $\not\!\!E_T$ distributions, as a function of the amount of smearing. See text for details.

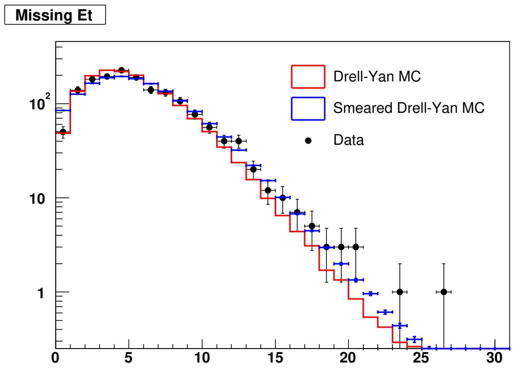

Figure 7: Comparison of the $\not\!\!E_T$ distribution of Drell-Yan e^+e^- events in the data, Monte Carlo and the optimally smeared Monte Carlo.

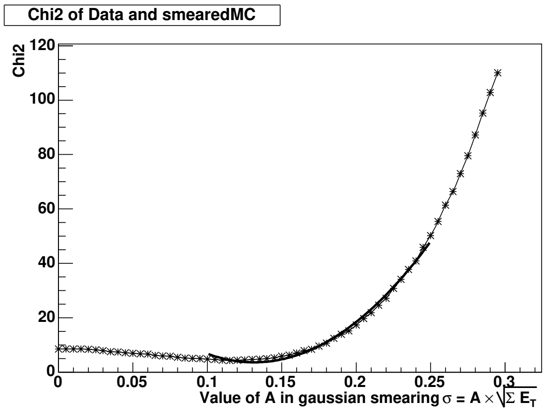

Figure 8: χ^2 between data and smeared Drell-Yan μ^+mu^- Monte Carlo $\not\!\!E_T$ distributions, as a function of the amount of smearing. See text for details.

7.6 Fake Background

The results from this subsection are now superseded by those in the next subsection 7.7, however we keep this subsection intact both for comparison and because a lot of the explanatory information is still relevant.

The origin of the fake background is $W + jets$ events where one jet is misidentified as a lepton. To estimate the fake background, we first obtain a fake *ratio* for each lepton category from QCD samples (Jet-20/50/70/100). These fake ratios are then applied to fakeable jets in the signal sample ($W + jets$) to obtain our fake *rates*. We have performed many cross-checks both across samples, and by changing the fake ratio definition, from which we obtain a systematic error for this background estimate. The details are provided below.

7.6.1 The Fake Ratio calculation

The fake ratios are obtained from the Jet-20, 50, 70, and 100 samples. They are calculated for each lepton category separately. The numerator is the number of isolated baseline e or μ (TCE, PHX, CMUP, CMU, CMP, CMX, CMIO) after removing the real lepton contribution from W's and Z's. The cuts to remove real leptons are $\not{E}_T < 10\,\mathrm{GeV}$ to remove leptons from W's, and a Z mass veto. In addition, we apply conversion removal for electrons, and cosmic-ray removal for muons. The remaining baseline leptons are assumed to be faked by jets (although we do test this assumption in one of our checks below). The trigger jet in each event is excluded from the fake ratio calculation to reduce trigger bias.

The denominators of the fake ratios are jet based for electrons and track based for muons. In principle, if the jets in the QCD sample were "like" the jets in the $W + jets$ sample, the fake ratio should be independent of the definition of the denominator, as long as one used the same definition of "fakeable jet" in the $W + jets$ sample. We performed some studies which did show some variation in the fake rates as we changed the denominator definition, and we added an additional systematic error accordingly (see below).

The electron fake ratios (R_{TCE}, R_{PHX}) are defined per jet thus:

$$R_{TCE} = \frac{\text{Number of isolated TCE}}{\text{Number of jets with raw } \mathrm{E_T} > 20\mathrm{GeV} \text{ and } |\eta| < 1.1}$$

$$R_{PHX} = \frac{\text{Number of isolated PHX}}{\text{Number of jets with raw } \mathrm{E_T} > 20\mathrm{GeV} \text{ and } 1.2 < |\eta| < 2.5}$$

Muon fake ratios (R_{CMUP}, R_{CMU}, R_{CMP}, R_{CMX}, R_{CMIO}, $R_{CMIO-fidele}$) are defined per high-P_T track. The numerator is the number of isolated baseline muons (CMUP, CMU, CMP, CMX, CMIO) after removing real leptons contributed by W's and Z's. Baseline CMIO muons in $R_{CMIO-fidele}$ must be tracks fiducial in the calorimeter (fideleTrk=4) (see Section 2.1). The denominators are tracks that are consistent with Minimum Ionizing Particles. They are required to pass the following selection:

- Corrected track $P_T > 20\,\mathrm{GeV}$
- $E/P < 1.0$
- track $|z_0| < 60.0\,\mathrm{cm}$
- track $|d_0| < 0.2\,\mathrm{cm}$, 0.02 if track has silicon hits
- non-cosmic

The E/P cut was suggested in reference [20] to make the denominator more "muon-like" and reduce those tracks associated with large EM energy (electrons and conversions) that will never fake a muon. In the fake rate checks below we do however try different values of this cut and observe the change in fake rates.

These denominator high-P_T tracks are classified as CMUP, CMU, CMP, or CMX tracks according to the muon fiducial tool. All of them are included in the ratio R_{CMIO}, and those that are also fiducial in the calorimeter are used in the ratio $R_{CMIO-fidele}$.

Table 27 gives the fake ratios obtained from all the QCD samples. The ratios are consistent across the QCD samples within the somewhat large uncertainties, so to obtained the final fake ratio we average the 4 values for a given lepton category and use as the statistical error half the range of ratio values.

7.6.2 Fake Background Estimate

To apply the fake ratios, we search in the inclusive e and μ samples for fakeable events. The fakeable events have one baseline lepton and at least one denominator object, which are the jets or tracks as defined for the fake ratio calculations. Treating denominator objects as baseline leptons, the fakeable events are required to pass the selection criteria as for the WW analysis. The opposite sign requirement is applied to events where the denominator object is a track, assuming it fakes a muon with the same charge. If the denominator object is a jet, it fakes a positive or negative electron with equal probability. The fake estimate is obtained by applying the average fake ratios from the previous subsection to the denominator objects of the fakeable events.

Table 28 summarizes the fake estimates according to the faked object in the events. Below we also add in systematic uncertainties due to other comparisons.

7.6.3 Fake Background cross checks and additional systematics

We have performed the studies and cross checks as outlined below.

- We have checked the effect of adding the track isolation requirement to baseline leptons. The effect is illustrated in table 29. The end result is a reduction in our total fake rate by about 25%.

Sample	Lepton	Fake Ratio
JET-20	CEM	$3.38\ 10^{-5} \pm 1.28\ 10^{-5}$
JET-50	CEM	$8.71\ 10^{-5} \pm 1.59\ 10^{-5}$
JET-70	CEM	$2.35\ 10^{-5} \pm 1.18\ 10^{-5}$
JET1-100	CEM	$2.80\ 10^{-5} \pm 1.25\ 10^{-5}$
AVERAGE	CEM	$(4.3 \pm 3.2) \times 10^{-5}$
JET-20	PHX	$2.73\ 10^{-4} \pm 3.83\ 10^{-5}$
JET-50	PHX	$3.46\ 10^{-4} \pm 4.36\ 10^{-5}$
JET-70	PHX	$6.66\ 10^{-4} \pm 9.51\ 10^{-5}$
JET-100	PHX	$4.26\ 10^{-4} \pm 8.51\ 10^{-5}$
AVERAGE	PHX	$(4.3 \pm 2.0) \times 10^{-4}$
JET-20	CMUP	$2.00\ 10^{-3} \pm 1.00\ 10^{-3}$
JET-50	CMUP	0.00 ± 0.00
JET-70	CMUP	$3.24\ 10^{-4} \pm 3.24\ 10^{-4}$
JET-100	CMUP	0.00 ± 0.00
AVERAGE	CMUP	$(5.8 \pm 10.0) \times 10^{-4}$
JET-20	CMU	0.00 ± 0.00
JET-50	CMU	$7.37\ 10^{-4} \pm 7.37\ 10^{-4}$
JET-70	CMU	0.00 ± 0.00
JET-100	CMU	0.00 ± 0.00
AVERAGE	CMU	$(1.8 \pm 3.7) \times 10^{-4}$
JET-20	CMP	$2.67\ 10^{-3} \pm 1.89\ 10^{-3}$
JET-50	CMP	$5.04\ 10^{-4} \pm 5.04\ 10^{-4}$
JET-70	CMP	$7.51\ 10^{-4} \pm 7.51\ 10^{-4}$
JET-100	CMP	$5.82\ 10^{-4} \pm 5.82\ 10^{-4}$
AVERAGE	CMP	$(1.1 \pm 1.1) \times 10^{-3}$
JET-20	CMX	0.00 ± 0.00
JET-50	CMX	0.00 ± 0.00
JET-70	CMX	0.00 ± 0.00
JET-100	CMX	0.00 ± 0.00
AVERAGE	CMX	0.0 ± 0.0
JET-20	CMIO	$3.06\ 10^{-3} \pm 6.85\ 10^{-4}$
JET-50	CMIO	$2.92\ 10^{-4} \pm 1.31\ 10^{-4}$
JET-70	CMIO	$1.23\ 10^{-3} \pm 3.42\ 10^{-4}$
JET-100	CMIO	$2.38\ 10^{-3} \pm 4.21\ 10^{-4}$
AVERAGE	CMIO	$(1.7 \pm 1.4) \times 10^{-3}$
JET-20	CMIO-FIDELE	$2.18\ 10^{-3} \pm 7.18\ 10^{-4}$
JET-50	CMIO-FIDELE	$1.85\ 10^{-4} \pm 1.31\ 10^{-4}$
JET-70	CMIO-FIDELE	$1.37\ 10^{-3} \pm 4.55\ 10^{-4}$
JET-100	CMIO-FIDELE	$1.81\ 10^{-3} \pm 4.54\ 10^{-4}$
AVERAGE	CMIO-FIDELE	$(1.4 \pm 1.0) \times 10^{-5}$

Table 27: Fake *ratios* calculated from the QCD data for all the lepton categories. The average ratios are used to calculate the final fake rates.

Lepton	Fake Rate (events per 200 pb^{-1})
CEM	$0.17 \pm 0.06 \pm 0.18$
PHX	$0.37 \pm 0.09 \pm 0.27$
CMUP	$0.033 \pm 0.032 \pm 0.129$
CMU	$0.003 \pm 0.004 \pm 0.041$
CMP	$0.033 \pm 0.018 \pm 0.128$
CMX	$0.00 \pm 0.00 \pm 0.00$
CMIO	$0.29 \pm 0.17 \pm 0.38$

Table 28: Fake *rates* for the WW analysis, requiring $\not{E}_T < 10\,\mathrm{GeV}$ in the jet samples. The first error is statistical from the spread in QCD samples and the second is systematic from the studies discussed the following subsections.. These fake rates correspond to the total dilepton contributions where the lepton type listed is the fakeable leg.

Lepton	Fake Rate (events per 200 pb^{-1})	
	WITH TRK-ISO	WITHOUT TRK-ISO
CEM	$0.155 \pm 0.024 \pm 0.035$	$0.239 \pm 0.030 \pm 0.027$
PHX	$0.282 \pm 0.018 \pm 0.053$	$0.282 \pm 0.018 \pm 0.053$
CMUP	$0.122 \pm 0.032 \pm 0.059$	$0.163 \pm 0.039 \pm 0.074$
CMU	$0.000 \pm 0.000 \pm 0.004$	$0.048 \pm 0.024 \pm 0.026$
CMP	$0.104 \pm 0.035 \pm 0.045$	$0.129 \pm 0.040 \pm 0.054$
CMX	$0.029 \pm 0.020 \pm 0.017$	$0.029 \pm 0.020 \pm 0.017$
CMIO	$0.395 \pm 0.053 \pm 0.069$	$0.551 \pm 0.066 \pm 0.145$

Table 29: Fake *rates* for the WW analysis, both with and without the track isolation requirement, and requiring $\not{E}_T < 15\,\mathrm{GeV}$ in the jet samples. The first error is statistical, the second is systematic from the QCD comparison only. These fake rates correspond to the total dilepton contributions where the lepton type listed is the fakeable leg.

- Real leptons coming from W's and Z's in the jet samples that get through the rejection cuts: $\not\!\!E_T < 10\,\text{GeV}$ and $76 < M_{\ell\ell} < 106$ GeV/c^2, could contaminate our fake ratios. These effects could be important for the small statistics in the numerator used in the fake ratios. We have studied how the fake ratio varies as a function of these cuts using the fake ratio definition described at the beginning of this section.

  1. We have varied the $\not\!\!E_T$ cut using four values $\not\!\!E_T <$ 10,15,20 and 25 GeV, (see table 30).
  2. For the Z mass cut, we have loosened the second leg following the loose CEM, PHX and muon definitions from the $W/Z+\gamma$ analysis [30], and we have opened the window from 76-106 to 66-116 and 56-126. We do not observe any significant effect in the jet samples.

  From table 30 we notice little effect from the $\not\!\!E_T$ cut value for those highly prescaled samples where the amount of W's and Z's and is drastically reduced by the prescale, but we do notice a trend higher in fake ratios with $\not\!\!E_T$ value in the Jet-50 and, in particular, the Jet-100 samples. We believe this result nicely shows how we are affected by real leptons from W's. As a result we choose the $\not\!\!E_T < 10$ cut for our final fake rate calculations, and we do not place a systematic error due to this effect.

- The effect of the denominator definition in the final fake estimate has been studied. This could have an effect if the jets in the QCD samples were in some way different than those in the lepton + jets samples. For electrons we have looked at cuts on the jet fraction of electromagnetic energy to the denominator: $f_{EM} > 0.5$, $f_{EM} > 0.8$, and for muons, cuts of $E/P < 0.5$ and $E/P < 1.0$. The effect should be small if jets in the QCD samples are "like" the jets in the lepton + jets samples. The results are shown in table 31. We notice no significant effect for electrons, but due to an observed effect to the muon fake rates from an E/P cut, we use a cut value of $E/P < 0.1$ and apply a 50% systematic to the resulting fake rates.

- Finally, the effect of applying an appropriate scale factor to account for using jet energy rather than EM energy for a denominator object has been studied. We simply define the number of denominator events based on the jet electromagnetic energy, computed as the product of the uncorrected jet energy and the jet electromagnetic fraction. The test has been applied to the choice of denominator cuts $f_{EM} > 0.8$ and $E/P < 1$. (see table 32). We apply a 20% systematic error to electron fake rates due to the observed discrepancy.

7.6.4 Fake Background summary

After adding in the observed variations in the above studies to the systematic uncertainties (which we assume are uncorrelated), we obtain the fake background estimates in $200\,\text{pb}^{-1}$ summarized in table 33. With the $\not\!\!E_T < 10$ cut discussed above, we find no CMX numerator

CEM	$\not\!\!E_T < 10$	$\not\!\!E_T < 15$	$\not\!\!E_T < 20$	$\not\!\!E_T < 25$
JET20	$3.38\ 10^{-5} \pm 1.28\ 10^{-5}$	$3.97\ 10^{-5} \pm 1.20\ 10^{-5}$	$4.26\ 10^{-5} \pm 1.18\ 10^{-5}$	$4.44\ 10^{-5} \pm 1.19\ 10^{-5}$
JET50	$8.71\ 10^{-5} \pm 1.59\ 10^{-5}$	$6.94\ 10^{-5} \pm 1.13\ 10^{-5}$	$6.66\ 10^{-5} \pm 9.93\ 10^{-6}$	$6.34\ 10^{-5} \pm 9.24\ 10^{-6}$
JET70	$2.35\ 10^{-5} \pm 1.18\ 10^{-5}$	$4.25\ 10^{-5} \pm 1.23\ 10^{-5}$	$4.39\ 10^{-5} \pm 1.10\ 10^{-5}$	$4.08\ 10^{-5} \pm 9.89\ 10^{-6}$
JET100	$2.80\ 10^{-5} \pm 1.25\ 10^{-5}$	$4.84\ 10^{-5} \pm 1.25\ 10^{-5}$	$6.42\ 10^{-5} \pm 1.23\ 10^{-5}$	$5.94\ 10^{-5} \pm 1.08\ 10^{-5}$
PHX	$\not\!\!E_T < 10$	$\not\!\!E_T < 15$	$\not\!\!E_T < 20$	$\not\!\!E_T < 25$
JET20	2.73e-04 $\pm 3.83\ 10^{-5}$	3.22e-04 $\pm 3.70\ 10^{-5}$	3.21e-04 $\pm 3.57\ 10^{-5}$	3.19e-04 $\pm 3.52\ 10^{-5}$
JET50	3.46e-04 $\pm 4.36\ 10^{-5}$	3.67e-04 $\pm 3.64\ 10^{-5}$	4.33e-04 $\pm 3.61\ 10^{-5}$	4.67e-04 $\pm 3.61\ 10^{-5}$
JET70	6.66e-04 $\pm 9.51\ 10^{-5}$	5.67e-04 $\pm 6.93\ 10^{-5}$	6.14e-04 $\pm 6.44\ 10^{-5}$	6.53e-04 $\pm 6.28\ 10^{-5}$
JET100	4.26e-04 $\pm 8.51\ 10^{-5}$	4.85e-04 $\pm 6.99\ 10^{-5}$	5.43e-04 $\pm 6.44\ 10^{-5}$	5.99e-04 $\pm 6.25\ 10^{-5}$
CMIOS	$\not\!\!E_T < 10$	$\not\!\!E_T < 15$	$\not\!\!E_T < 20$	$\not\!\!E_T < 25$
JET20	$3.06\ 10^{-3} \pm 6.85\ 10^{-4}$	$2.43\ 10^{-3} \pm 5.07\ 10^{-4}$	$2.16\ 10^{-3} \pm 4.42\ 10^{-4}$	$2.17\ 10^{-3} \pm 4.26\ 10^{-4}$
JET50	$2.92\ 10^{-4} \pm 1.31\ 10^{-4}$	$7.15\ 10^{-4} \pm 1.60\ 10^{-4}$	$9.05\ 10^{-4} \pm 1.60\ 10^{-4}$	$1.00\ 10^{-3} \pm 1.59\ 10^{-4}$
JET70	$1.23\ 10^{-3} \pm 3.42\ 10^{-4}$	$1.57\ 10^{-3} \pm 2.96\ 10^{-4}$	$1.68\ 10^{-3} \pm 2.66\ 10^{-4}$	$2.07\ 10^{-3} \pm 2.72\ 10^{-4}$
JET100	$2.38\ 10^{-3} \pm 4.21\ 10^{-4}$	$2.47\ 10^{-3} \pm 3.22\ 10^{-4}$	$2.98\ 10^{-3} \pm 3.00\ 10^{-4}$	$3.41\ 10^{-3} \pm 2.90\ 10^{-4}$
CMIOS FIDELE	$\not\!\!E_T < 10$	$\not\!\!E_T < 15$	$\not\!\!E_T < 20$	$\not\!\!E_T < 25$
JET20	$2.18\ 10^{-3} \pm 7.28\ 10^{-4}$	$1.89\ 10^{-3} \pm 5.70\ 10^{-4}$	$1.79\ 10^{-3} \pm 5.18\ 10^{-4}$	$1.83\ 10^{-3} \pm 5.08\ 10^{-4}$
JET50	$1.85\ 10^{-4} \pm 1.31\ 10^{-4}$	$5.79\ 10^{-4} \pm 1.83\ 10^{-4}$	$9.40\ 10^{-4} \pm 2.10\ 10^{-4}$	$1.15\ 10^{-3} \pm 2.22\ 10^{-4}$
JET70	$1.37\ 10^{-3} \pm 4.55\ 10^{-4}$	$1.63\ 10^{-3} \pm 3.86\ 10^{-4}$	$1.87\ 10^{-3} \pm 3.61\ 10^{-4}$	$2.41\ 10^{-3} \pm 3.81\ 10^{-4}$
JET100	$1.81\ 10^{-3} \pm 4.54\ 10^{-4}$	$2.00\ 10^{-3} \pm 3.60\ 10^{-4}$	$2.94\ 10^{-3} \pm 3.74\ 10^{-4}$	$3.42\ 10^{-3} \pm 3.67\ 10^{-4}$

Table 30: Fake ratios from the QCD data for various lepton categories versus the $\not\!\!E_T$ cut.

	No cuts	$f_{EM} > 0.5$ $E/P < 0.5$	$f_{EM} > 0.5$ $E/P < 1$	$f_{EM} > 0.8$ $E/P < 0.5$	$f_{EM} > 0.8$ $E/P < 1.$
CEM:	0.132±0.026±0.045	0.122±0.024±0.046	0.122±0.024±0.046	0.141±0.026±0.088	0.141±0.026±0.088
PHX:	0.239±0.019±0.075	0.244±0.019±0.077	0.244±0.019±0.077	0.290±0.028±0.133	0.290±0.028±0.133
CMUP:	0.224±0.063±0.118	0.055±0.026±0.035	0.114±0.035±0.061	0.055±0.026±0.035	0.114±0.035±0.061
CMU:	0.000±0.000±0.003	0.000±0.000±0.004	0.000±0.000±0.003	0.000±0.000±0.004	0.000±0.000±0.003
CMP:	0.114±0.048±0.055	0.047±0.024±0.016	0.078±0.034±0.033	0.047±0.024±0.016	0.078±0.034±0.033
CMX:	0.000±0.000±0.000	0.000±0.000±0.000	0.000±0.000±0.000	0.000±0.000±0.000	0.000±0.000±0.000
CMIO:	0.787±0.100±0.330	0.349±0.063±0.078	0.474±0.068±0.145	0.349±0.063±0.078	0.474±0.068±0.145
ee	0.232±0.027±0.038	0.226±0.026±0.078	0.226±0.026±0.078	0.247±0.031±0.133	0.247±0.031±0.133
$e\mu$	0.788±0.104±0.140	0.399±0.057±0.079	0.519±0.068±0.128	0.442±0.059±0.109	0.563±0.069±0.148
$\mu\mu$	0.476±0.075±0.111	0.193±0.047±0.058	0.287±0.052±0.107	0.193±0.047±0.058	0.287±0.052±0.107

Table 31: Fake estimates for different choices of denominator definitions.

Jets with E_T uncorrected > 20 GeV	
ee	0.247±0.031±0.133
$e\mu$	0.563±0.069±0.148
$\mu\mu$	0.287±0.052±0.107
Jets with E_T uncorrected $\times f_{EM} > 20$ GeV	
ee	0.318±0.041±0.058
$e\mu$	0.634±0.073±0.127
$\mu\mu$	0.287±0.052±0.107

Table 32: Fake estimates for different choices of fakeable electron jet energy definition.

events for which to calculate a fake ratio, so for this one category we loosen this cut to $\not\!\!E_T < 20$, realizing that this will introduce some contamination from real leptons (see below), but this effect is well contained within our systematic errors.

We have checked if the fake rates (with no track isolation for better statistics) vary as a function of P_T. In figures 9, 10 and 11 we see that within statistics there is no meaningful variation with P_T.

Our total fake contribution in about $200\,\mathrm{pb}^{-1}$ is 1.1 ± 0.5 events. By requiring OS on PHX the fake estimate goes down about 30%. Then requiring $|\eta| < 2.0$ rather than $|\eta| < 2.0$, reduces it another 20%.

CEM CEM	$0.063 \pm 0.046 \pm 0.013$
CEM PHX	$0.030 \pm 0.022 \pm 0.010$
CEM CMUP	$0.043 \pm 0.032 \pm 0.009$
CEM CMU	$0.001 \pm 0.0005 \pm 0.0001$
CEM CMP	$0.001 \pm 0.0005 \pm 0.0001$
CEM CMX	$0.023 \pm 0.0017 \pm 0.005$
CEM CMIO	$0.002 \pm 0.0018 \pm 0.0005$
PHX CEM	$0.21 \pm 0.13 \pm 0.06$
PHX PHX	$0.14 \pm 0.10 \pm 0.04$
PHX CMUP	$0.13 \pm 0.08 \pm 0.03$
PHX CMU	$0.002 \pm 0.0005 \pm 0.0001$
PHX CMP	$0.003 \pm 0.002 \pm 0.001$
PHX CMX	$0.071 \pm 0.040 \pm 0.017$
PHX CMIO	$0.007 \pm 0.004 \pm 0.002$
CMUP CEM	$0.015 \pm 0.025 \pm 0.007$
CMUP PHX	$0.006 \pm 0.010 \pm 0.003$
CMUP CMUP	$0.009 \pm 0.016 \pm 0.005$
CMUP CMX	$0.002 \pm 0.004 \pm 0.001$
CMUP CMIO	$0.0010 \pm 0.0012 \pm 0.0003$
CMU CEM	$0.002 \pm 0.004 \pm 0.001$
CMU PHX	$0.0004 \pm 0.0008 \pm 0.0002$
CMU CMUP	$0.0010 \pm 0.0015 \pm 0.0004$
CMU CMX	$0.000 \pm 0.0008 \pm 0.0002$
CMP CEM	$0.014 \pm 0.014 \pm 0.007$
CMP PHX	$0.008 \pm 0.008 \pm 0.004$
CMP CMUP	$0.006 \pm 0.006 \pm 0.003$
CMP CMX	$0.003 \pm 0.004 \pm 0.002$
CMX CEM	$0.009 \pm 0.006 \pm 0.004$
CMX PHX	$0.0004 \pm 0.0004 \pm 0.0002$
CMX CMUP	$0.003 \pm 0.002 \pm 0.002$
CMX CMP	$0.0004 \pm 0.0004 \pm 0.0002$
CMX CMX	$0.002 \pm 0.001 \pm 0.001$
CMIO CEM	$0.115 \pm 0.092 \pm 0.058$
CMIO PHX	$0.04 \pm 0.03 \pm 0.02$
CMIO CMUP	$0.091 \pm 0.073 \pm 0.045$
CMIO CMX	$0.033 \pm 0.027 \pm 0.017$
CEM	$0.16 \pm 0.12 \pm 0.05$
PHX	$0.58 \pm 0.26 \pm 0.16$
CMUP	$0.033 \pm 0.057 \pm 0.016$
CMU	$0.003 \pm 0.007 \pm 0.002$
CMP	$0.030 \pm 0.032 \pm 0.015$
CMX	$0.014 \pm 0.010 \pm 0.007$
CMIO	$0.28 \pm 0.23 \pm 0.14$
ee	$0.45 \pm 0.18 \pm 0.13$
$e\mu$	$0.49 \pm 0.17 \pm 0.18$
$\mu\mu$	$0.15 \pm 0.11 \pm 0.08$
TOTAL	$1.09 \pm 0.37 \pm 0.39$

Table 33: Fake estimates per dilepton category in about $200\,\mathrm{pb}^{-1}$. The first error is statistical, the second is systematic both from the QCD comparison and the various studies discussed in the text. The fake rates given for the individual lepton types correspond to the total dilepton contributions where that lepton type is the fakeable leg.

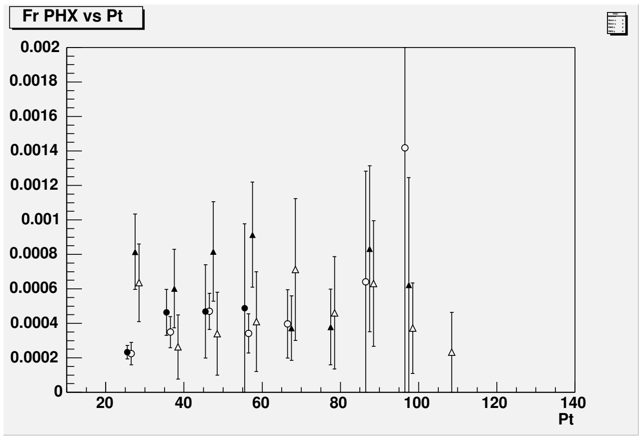

Figure 9: Fake ratio for CEM versus P_T, no track isolation requirement has been applied. Solid circles are jet-20, open circles jet-50, solid triangles jet-70, and open triangles jet-100.

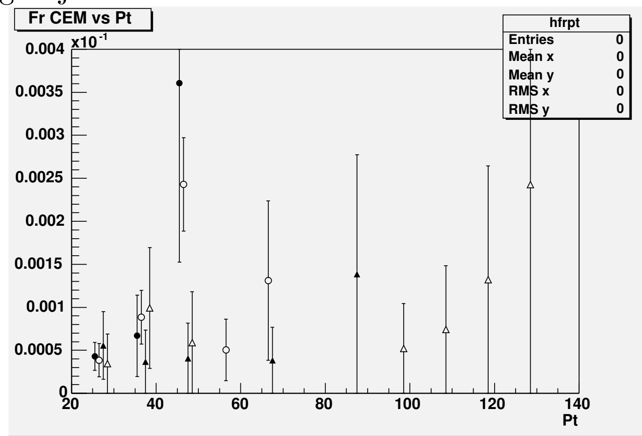

Figure 10: Fake ratio for PHX versus P_T. Same symbol definitions as for figure 9.

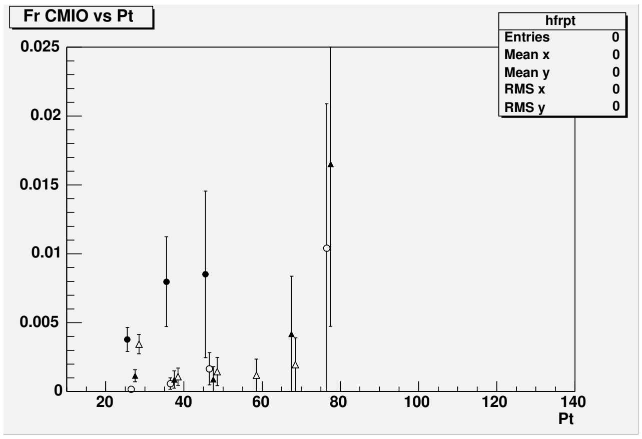

Figure 11: Fake ratio for CMIO versus P_T, no track isolation requirement has been applied.

7.7 Update on Fake Background after God-parent and Blessing Requests

The results from this section supersede those of the previous section, although a lot of the information on the method itself from the previous section is still relevant so we keep it here. The main differences in this latest result are as follows.

- Dependence of the fake ratios with the P_T of the numerator and denominator objects. Figures 12, 13, 14, 17, 15, 16, 18 and 19 show the P_T dependence of the fake ratios (top), the numerator objects (middle), and the denominator objects (bottom), found in the jet samples. Figure 20 shows the P_T spectrum of the fakeable objects found in the signal sample, in dilepton configurations where the first leg is the fakeable leg and the second leg is the baseline electron or muon. All the WW selection criteria have been applied to these dilepton configurations [2] (see also tables 38 and 39 for the total number of fakeable events in each dilepton category).

  Since the fake ratios have a dependence on P_T, if the P_T spectra of the denominator objects and the fakeable objects were different, then this dependence would affect our fake rates. Although this is not a huge effect, we decided to apply the fake ratios to the signal in three bins of P_T: $20 < P_T < 60$, $60 < P_T < 100$, $100 < P_T < 140$ instead of simply applying a constant ratio. We found almost no effect in the final fake estimate between both methods, mainly because most of the fakeable legs found in the signal are in the lowest P_T bin.

- Previously we were applying a $\not{E}_T$ cut to the numerator of the fake ratios in order to remove the W contamination in the jet samples. We were asked not to apply this cut because it could also remove some sources of fakes.

  - It was suggested to remove the W contamination by direct subtraction. For triggerable leptons: CEM, PHX, CMUP and CMX we count the number of $W + \geq 1\ jet$ events in the signal data sample that could have been triggered in the jet samples and thus contaminate them. For non triggerable leptons: CMU,CMP,CMIO and CMIO-*fidele* we have used PYTHIA MC wtop0m to estimate the ratios:

    $$\frac{N(W + \geq 1\ jet)^{\mathrm{CMU,CMP,CMIO,CMIO}-\textit{fidele}}}{N(W + \geq 1\ jet)^{\mathrm{CMUP}}} \tag{1}$$

    and we have used the CMUP P_T distribution of the $W + \geq 1\ jet$ events. In order to emulate the L3 JET 20,50,70 and 100 triggers in the MC we require at least one jet with $E_T >$ 38, 68, 90 and 122 GeV respectively (see reference [9]). These ratios are summarized in table 34.

[2]These fake rates are affected by W contamination in the jet samples.

Non triggering μ	Jet sample	$\frac{N(W(\rightarrow\mu_{\mu}\nu)+\geq 1 jets))}{(N(W(\rightarrow\mu_{\mathrm{CMUP}}\nu)+\geq 1 jets))}$
CMU	JET20	0.222 ± 0.011
CMU	JET50	0.234 ± 0.026
CMU	JET70	0.283 ± 0.050
CMU	JET100	0.282 ± 0.096
CMP	JET20	0.285 ± 0.013
CMP	JET50	0.278 ± 0.029
CMP	JET70	0.290 ± 0.051
CMP	JET100	0.333 ± 0.107
CMIO	JET20	0.694 ± 0.023
CMIO	JET50	0.634 ± 0.050
CMIO	JET70	0.641 ± 0.085
CMIO	JET100	0.692 ± 0.173
CMIO-fidele	JET20	0.340 ± 0.015
CMIO-fidele	JET50	0.287 ± 0.030
CMIO-fidele	JET70	0.276 ± 0.049
CMIO-fidele	JET100	0.256 ± 0.091

Table 34: Non triggering muon scale factors used for W subtraction method.

.

- The $W + \geq 1jet$ selection is based on a single baseline lepton with calorimeter isolation for CEM, CMUP or CMX, or for PHX, calorimeter isolation only. The same baseline identification criteria is used as in the current analysis. In addition we require $\not\!\!E_T > 20$ GeV, where the $\not\!\!E_T$ is corrected for identified muons, and at least one tight jet with corrected $E_T > 15$ GeV and $|\eta| < 2.5$. In addition, to ensure that these $W + \geq 1jets$ events will appear in the jet trigger sample we require the corresponding L3 trigger to have been fired: (L3_JET_20/50/70/100) respectively. In particular, when the baseline lepton is CEM or TCE we require the leading jet to have higher E_T than the electron, or in other words, we require the electron not to be the leading object, since leading jets are removed when building the electron fake rate. (See figure 21 for the lepton P_T spectrum of these events). Finally we subtract the W contamination from the jet data numerator and denominator for each P_T bin.

- In order to test that the lepton P_T spectrum of the $W + \geq 1jet$ events found in the signal data sample shown in figure 21 corresponds to events that are clearly W like, we compute the transverse mass $M_T = \sqrt{E_T^l \not\!\!E_T - (E_x^l \not\!\!E_T, x + E_y^l \not\!\!E_T, y)}$ for these events (see figure 22). To check that the M_T distributions in figure 22 are W like, especially the low M_T region, we show in figure 23 the three cases $W + 0\ jets$, $W + \geq 1\ jet$ and $W + n\ jet$. We have repeated the study using PYTHIA MC wtop0e ($W \to e\nu$) and wtop0m ($W \to \mu\nu$) (figures 24, 25 and 26), where we emulate the L3 JET 20,50,70 and 100 triggers by requiring at least one jet with $E_T > 38, 68, 90$ and 122 GeV respectively (see reference [9]). The MC P_T spectra suffer from lack of statistics for higher E_T jets.

  We conclude that the lepton P_T spectrum of the $W + \geq 1 - jet$ events found in the signal data sample used to subtract the real W contamination from the jet samples is mostly W like. Nevertheless we subtract a percentage of QCD background taken from the W inclusive analysis [29]: 3.5% (CEM), 5.76% (PHX), 9.43% (CMUP) and 9.21% (CMX) to avoid over-estimating the level of W contamination.

- We now use all the luminosity available to compute the fake rates, since we were using only ~ 72 pb^{-1} and almost ~ 200 pb^{-1} for the signal. We now use all the jet samples in our study which has given us much better statistics.

  - The fake rate estimate for CMX was affected by lack of statistics in the numerator. This problem has disappeared partially because we have removed the $\not\!\!E_T$ cut and because we now use all the luminosity available in the jet samples.
  - Independence of the fake rates with the run number has been rechecked as requested by the god-parents. We have computed the raw fake rates using all P_T bins for Jet20 and three different running periods (table 35).

After all these studies:

- The fake rates before and after W contamination subtraction are summarized in detail in tables 36 and 37.

  Please note that some of the zero values are due to over-subtraction of W contamination, (indicated by $(*)$ in table 37) and some are due to the lack of numerator statistics in certain P_T bins, as can also be seen in the P_T spectra of the numerator objects for the jet samples. This feature of our methodology affects only certain P_T bins and never all of them, for a given choice of lepton kind and jet sample. These instances are counted as zeroes when averaging over all samples and bins.

  For each P_T bin the resulting fake rate is the average of the jet20, jet50, jet70 and jet100 fake rates. The error is taken to be one half of the spread of the central values.

- We recomputed the fake background and the result is summarized in detail in tables 38 and 39. In these tables for a given dilepton category, the errors in the first column come from the propagation of the statistical error due to the number of fakeable events in the fake estimate. They have been added in quadrature over all dilepton categories. The errors in the second column come from the propagation of the error in the fake rate in the fake estimate: $(frmax - frmin)/2$. For dilepton categories where the fakeable leg is CEM or PHX, since we have used the charge asymmetry measurement in the prediction of the fake estimate, we have further propagated the error of our charge asymmetry measurement in the fake estimate: 0.63 ± 0.05 to both error contributions in the first and second column. We have added arithmetically those error contributions due to the fake rate error for dilepton categories with the same kind of fakeable leg. We have finally added quadratically those error contributions due to the number of fakeable events and due to the error in the fake rate, for different fakeable legs. The third error is our systematic error as before.

138838 (Feb 10,2002) - 158733 (Feb 13, 2003) Winter2003		
CEM	$\frac{28}{608730}$	$4.6 \cdot 10^{-5} \pm 0.8 \cdot 10^{-5}$
PHX	$\frac{80}{219035}$	$3.7 \cdot 10^{-4} \pm 0.4 \cdot 10^{-4}$
CMUP	$\frac{30}{21399}$	$1.4 \cdot 10^{-3} \pm 0.3 \cdot 10^{-3}$
CMU	$\frac{3}{5727}$	$5.2 \cdot 10^{-4} \pm 3.0 \cdot 10^{-4}$
CMP	$\frac{8}{7655}$	$1.1 \cdot 10^{-3} \pm 0.4 \cdot 10^{-3}$
CMX	$\frac{7}{9286}$	$7.5 \cdot 10^{-4} \pm 2.8 \cdot 10^{-4}$
CMIO	$\frac{57}{69391}$	$8.1 \cdot 10^{-4} \pm 1.1 \cdot 10^{-4}$
CMIOFIDELE	$\frac{37}{43517}$	$8.5 \cdot 10^{-4} \pm 1.4 \cdot 10^{-4}$
158733 (Feb 13,2003) - 163527 (Jun 2003) LP2003 (Summer data)		
CEM	$\frac{10}{173108}$	$5.8 \cdot 10^{-5} \pm 1.8 \cdot 10^{-5}$
PHX	$\frac{33}{95271}$	$3.5 \cdot 10^{-4} \pm 0.6 \cdot 10^{-4}$
CMUP	$\frac{7}{6827}$	$1.0 \cdot 10^{-3} \pm 0.4 \cdot 10^{-3}$
CMU	$\frac{2}{1840}$	$1.1 \cdot 10^{-3} \pm 0.8 \cdot 10^{-3}$
CMP	$\frac{6}{2354}$	$2.6 \cdot 10^{-3} \pm 1.0 \cdot 10^{-3}$
CMX	$\frac{5}{4711}$	$1.1 \cdot 10^{-3} \pm 0.5 \cdot 10^{-3}$
STUBLESS	$\frac{23}{24191}$	$9.5 \cdot 10^{-4} \pm 1.9 \cdot 10^{-4}$
STUBLESSFIDELE	$\frac{10}{15215}$	$6.6 \cdot 10^{-4} \pm 2.1 \cdot 10^{-4}$
163527 (Jun 2003) -168889 (Sep 09,2003) September data		
CEM	$\frac{9}{207051}$	$4.4 \cdot 10^{-5} \pm 1.4 \cdot 10^{-5}$
PHX	$\frac{25}{95245}$	$2.6 \cdot 10^{-4} \pm 0.5 \cdot 10^{-4}$
CMUP	$\frac{11}{8297}$	$1.3 \cdot 10^{-3} \pm 0.4 \cdot 10^{-3}$
CMU	$\frac{1}{2191}$	$4.6 \cdot 10^{-4} \pm 4.6 \cdot 10^{-4}$
CMP	$\frac{3}{2958}$	$1.0 \cdot 10^{-3} \pm 0.6 \cdot 10^{-3}$
CMX	$\frac{5}{5501}$	$9.1 \cdot 10^{-4} \pm 4.1 \cdot 10^{-4}$
STUBLESS	$\frac{21}{28915}$	$7.3 \cdot 10^{-4} \pm 1.6 \cdot 10^{-4}$
STUBLESSFIDELE	$\frac{7}{18455}$	$3.8 \cdot 10^{-4} \pm 1.4 \cdot 10^{-4}$

Table 35: Raw fake rates for Jet20 and 3 different periods of CDF data taking.

.

P_T	$20 < P_T < 60$	$60 < P_T < 100$	$100 < P_T < 140$
JET20 CEM	0.00005 ± 0.00001	0. ± 0.	0. ± 0.
JET50 CEM	0.00010 ± 0.00001	0.00010 ± 0.00002	0.00023 ± 0.00012
JET70 CEM	0.00007 ± 0.00001	0.00008 ± 0.00001	0.00014 ± 0.00006
JET100 CEM	0.00015 ± 0.00001	0.00013 ± 0.00001	0.00014 ± 0.00002
CEM	0.00009 ± 0.00005	0.00008 ± 0.00006	0.00013 ± 0.00012
JET20 PHX	0.00034 ± 0.00003	0. ± 0.	0.00658 ± 0.00660
JET50 PHX	0.00048 ± 0.00002	0.00085 ± 0.00011	0.00134 ± 0.00067
JET70 PHX	0.00061 ± 0.00004	0.00094 ± 0.00009	0.00124 ± 0.00041
JET100 PHX	0.00078 ± 0.00005	0.00121 ± 0.00008	0.00117 ± 0.00015
PHX	0.00055 ± 0.00022	0.00075 ± 0.00060	0.00258 ± 0.00270
JET20 CMUP	0.00101 ± 0.00017	0.01422 ± 0.00477	0.00452 ± 0.00454
JET50 CMUP	0.00061 ± 0.00008	0.00920 ± 0.00181	0.02784 ± 0.00815
JET70 CMUP	0.00073 ± 0.00011	0.00488 ± 0.00098	0.02353 ± 0.00636
JET100 CMUP	0.00086 ± 0.00010	0.00385 ± 0.00054	0.01358 ± 0.00216
CMUP	0.00080 ± 0.00020	0.00804 ± 0.00518	0.01737 ± 0.01166
JET20 CMU	0.00063 ± 0.00026	0. ± 0.	0. ± 0.
JET50 CMU	0.00057 ± 0.00015	0.00524 ± 0.00262	0. ± 0.
JET70 CMU	0.00057 ± 0.00019	0.00553 ± 0.00196	0.01418 ± 0.01010
JET100 CMU	0.00075 ± 0.00018	0.00274 ± 0.00087	0.00654 ± 0.00294
CMU	0.00063 ± 0.00009	0.00338 ± 0.00277	0.00518 ± 0.00709
JET20 CMP	0.00134 ± 0.00032	0. ± 0.	0. ± 0.
JET50 CMP	0.00066 ± 0.00012	0.00431 ± 0.00193	0.03226 ± 0.01639
JET70 CMP	0.00049 ± 0.00012	0.00292 ± 0.00120	0.00930 ± 0.00661
JET100 CMP	0.00052 ± 0.00010	0.00204 ± 0.00055	0.01821 ± 0.00411
CMP	0.00075 ± 0.00042	0.00232 ± 0.00215	0.01494 ± 0.01613
JET20 CMX	0.00079 ± 0.00020	0.00604 ± 0.00429	0. ± 0.
JET50 CMX	0.00047 ± 0.00009	0.00625 ± 0.00189	0.00926 ± 0.00658
JET70 CMX	0.00055 ± 0.00012	0.00545 ± 0.00133	0.01520 ± 0.00685
JET100 CMX	0.00088 ± 0.00012	0.00261 ± 0.00054	0.00887 ± 0.00230
CMX	0.00067 ± 0.00020	0.00509 ± 0.00182	0.00833 ± 0.00760
JET20 CMIO	0.00066 ± 0.00007	0.00149 ± 0.00086	0.00152 ± 0.00152
JET50 CMIO	0.00094 ± 0.00005	0.00434 ± 0.00065	0.00521 ± 0.00198
JET70 CMIO	0.00201 ± 0.00010	0.00330 ± 0.00043	0.01094 ± 0.00240
JET100 CMIO	0.00470 ± 0.00012	0.00358 ± 0.00027	0.00529 ± 0.00075
CMIO	0.00208 ± 0.00202	0.00318 ± 0.00142	0.00574 ± 0.00471
JET20 CMIOFIDELE	0.00049 ± 0.00008	0.00143 ± 0.00101	0.00214 ± 0.00214
JET50 CMIOFIDELE	0.00104 ± 0.00007	0.00464 ± 0.00086	0.00674 ± 0.00276
JET70 CMIOFIDELE	0.00268 ± 0.00014	0.00397 ± 0.00059	0.01066 ± 0.00297
JET100 CMIOFIDELE	0.00616 ± 0.00018	0.00440 ± 0.00038	0.00565 ± 0.00096
CMIOFIDELE	0.00259 ± 0.00283	0.00361 ± 0.00160	0.00630 ± 0.00426

Table 36: Fake ratios before W contamination subtraction. Null ratios are due to empty numerators.

P_T	$20 < P_T < 60$	$60 < P_T < 100$	$100 < P_T < 140$
JET20 CEM	0.00004 ± 0.00001	0. ± 0.	0. ± 0.
JET50 CEM	0.00007 ± 0.00001	0.00006 ± 0.00002	0.00006 ± 0.00006
JET70 CEM	0.00003 ± 0.00001	0.00004 ± 0.00001	0.00010 ± 0.00005
JET100 CEM	0.00005 ± 0.00001	0.00004 ± 0.00001	0.00007 ± 0.00001
CEM	0.00005 ± 0.00002	0.00003 ± 0.00003	0.00006 ± 0.00005
JET20 PHX	0.00033 ± 0.00003	0. ± 0.	0.00658 ± 0.00660
JET50 PHX	0.00044 ± 0.00002	0.00068 ± 0.00010	0.00102 ± 0.00058
JET70 PHX	0.00043 ± 0.00004	0.00084 ± 0.00008	0.00111 ± 0.00039
JET100 PHX	0.00036 ± 0.00004	0.00085 ± 0.00007	0.00100 ± 0.00014
PHX	0.00039 ± 0.00005	0.00059 ± 0.00042	0.00243 ± 0.00279
JET20 CMUP	0.00081 ± 0.00015	0.01136 ± 0.00426	0.00452 ± 0.00454
JET50 CMUP	0.00021 ± 0.00005	0.00375 ± 0.00115	0.01944 ± 0.00678
JET70 CMUP	0.00031 ± 0.00007	0.00223 ± 0.00066	0.00983 ± 0.00408
JET100 CMUP	0.00036 ± 0.00007	0.00118 ± 0.00030	0.00743 ± 0.00159
CMUP	0.00042 ± 0.00030	0.00463 ± 0.00509	0.01031 ± 0.00746
JET20 CMU	0.00046 ± 0.00022	0. ± 0.	0. ± 0.
JET50 CMU	0.00024 ± 0.00010	0.00051 ± 0.00082	0. ± 0.
JET70 CMU	0.00015 ± 0.00010	0.00288 ± 0.00141	0. ± 0. (∗)
JET100 CMU	0.00023 ± 0.00010	0.00001 ± 0.00005	0. ± 0. (∗)
CMU	0.00027 ± 0.00016	0.00085 ± 0.00144	0. ± 0.
JET20 CMP	0.00117 ± 0.00030	0. ± 0.	0. ± 0.
JET50 CMP	0.00043 ± 0.00010	0.00063 ± 0.00073	0.02415 ± 0.01412
JET70 CMP	0.00028 ± 0.00009	0.00101 ± 0.00070	0. ± 0. (∗)
JET100 CMP	0.00025 ± 0.00007	0.00032 ± 0.00022	0.01272 ± 0.00342
CMP	0.00053 ± 0.00046	0.00049 ± 0.00050	0.00922 ± 0.01208
JET20 CMX	0.00065 ± 0.00019	0.00056 ± 0.00130	0. ± 0.
JET50 CMX	0.00020 ± 0.00006	0.00264 ± 0.00123	0. ± 0. (∗)
JET70 CMX	0.00028 ± 0.00008	0.00225 ± 0.00085	0.00140 ± 0.00206
JET100 CMX	0.00034 ± 0.00008	0.00024 ± 0.00017	0.00350 ± 0.00144
CMX	0.00037 ± 0.00022	0.00142 ± 0.00120	0.00123 ± 0.00175
JET20 CMIO	0.00062 ± 0.00007	0.00086 ± 0.00066	0.00152 ± 0.00152
JET50 CMIO	0.00088 ± 0.00005	0.00340 ± 0.00057	0.00350 ± 0.00162
JET70 CMIO	0.00194 ± 0.00009	0.00281 ± 0.00040	0.00822 ± 0.00208
JET100 CMIO	0.00461 ± 0.00012	0.00308 ± 0.00025	0.00396 ± 0.00065
CMIO	0.00201 ± 0.00199	0.00254 ± 0.00127	0.00430 ± 0.00335
JET20 CMIOFIDELE	0.00046 ± 0.00008	0.00099 ± 0.00084	0.00214 ± 0.00214
JET50 CMIOFIDELE	0.00099 ± 0.00007	0.00393 ± 0.00079	0.00557 ± 0.00251
JET70 CMIOFIDELE	0.00263 ± 0.00014	0.00364 ± 0.00057	0.00882 ± 0.00270
JET100 CMIOFIDELE	0.00610 ± 0.00018	0.00410 ± 0.00037	0.00490 ± 0.00089
CMIOFIDELE	0.00255 ± 0.00282	0.00316 ± 0.00155	0.00536 ± 0.00334

Table 37: Fake ratios after W contamination subtraction. Null ratios are due to zero statistics in the numerator in a particular P_T bin. Null ratios with a star symbol are due to over-subtraction and they are reset to zero before averaging.

CEM CEM	2281	0.070±0.006±0.026±0.020
CEM PHX	995	0.030±0.003±0.011±0.008
CEM CMUP	1571	0.048±0.004±0.018±0.013
CEM CMU	18	0.001±0.000±0.000±0.000
CEM CMP	21	0.001±0.000±0.000±0.000
CEM CMX	825	0.025±0.002±0.010±0.007
CEM CMIO	88	0.003±0.000±0.001±0.001
CEM		0.177±0.008±0.067±0.049
PHX CEM	987	0.267±0.022±0.077±0.075
PHX PHX	597	0.150±0.013±0.043±0.042
PHX CMUP	617	0.155±0.013±0.045±0.043
PHX CMU	7	0.002±0.001±0.001±0.001
PHX CMP	11	0.003±0.001±0.001±0.001
PHX CMX	327	0.084±0.008±0.024±0.024
PHX CMIO	30	0.008±0.001±0.002±0.002
PHX		0.668±0.030±0.192±0.187
CMUP CEM	25	0.015±0.003±0.007±0.007
CMUP PHX	8	0.003±0.001±0.002±0.002
CMUP CMUP	16	0.007±0.002±0.003±0.003
CMUP CMU	0	0.000±0.000±0.000±0.000
CMUP CMP	0	0.000±0.000±0.000±0.000
CMUP CMX	4	0.002±0.001±0.001±0.001
CMUP CMIO	1	0.000±0.000±0.000±0.000
CMUP		0.027±0.004±0.013±0.013
CMU CEM	10	0.003±0.001±0.001±0.001
CMU PHX	2	0.001±0.000±0.000±0.000
CMU CMUP	4	0.001±0.001±0.000±0.001
CMU CMU	0	0.000±0.000±0.000±0.000
CMU CMP	0	0.000±0.000±0.000±0.000
CMU CMX	2	0.001±0.001±0.000±0.001
CMU CMIO	0	0.000±0.000±0.000±0.000
CMU		0.005±0.001±0.002±0.003

Table 38: Number of fakeable events found in the signal sample for each dilepton category and the corresponding fake estimates (continued in table 39).

CMP CEM	12	0.006±0.002±0.004±0.003
CMP PHX	7	0.004±0.001±0.002±0.002
CMP CMUP	5	0.003±0.001±0.002±0.001
CMP CMU	0	0.000±0.000±0.000±0.000
CMP CMP	0	0.000±0.000±0.000±0.000
CMP CMX	3	0.002±0.001±0.001±0.001
CMP CMIO	0	0.000±0.000±0.000±0.000
CMP		0.014±0.003±0.009±0.007
CMX CEM	23	0.012±0.002±0.005±0.006
CMX PHX	1	0.001±0.000±0.001±0.001
CMX CMUP	8	0.003±0.001±0.001±0.001
CMX CMU	0	0.000±0.000±0.000±0.000
CMX CMP	1	0.000±0.000±0.000±0.000
CMX CMX	4	0.001±0.001±0.001±0.001
CMX CMIO	0	0.000±0.000±0.000±0.000
CMX		0.018±0.003±0.008±0.009
CMIO CEM	83	0.214±0.023±0.200±0.107
CMIO PHX	25	0.064±0.013±0.060±0.032
CMIO CMUP	52	0.105±0.015±0.098±0.053
CMIO CMU	0	0.000±0.000±0.000±0.000
CMIO CMP	1	0.002±0.002±0.002±0.001
CMIO CMX	19	0.039±0.009±0.036±0.019
CMIO CMIO	1	0.002±0.002±0.002±0.001
CMIO		0.426±0.032±0.399±0.213
ee		0.516±0.027±0.126±0.145
$e\mu$		0.651±0.032±0.272±0.253
$\mu\mu$		0.168±0.018±0.139±0.084
Total		1.335±0.045±0.448±0.482

Table 39: Continued from table 38: Number of fakeable events found in the signal sample for each dilepton category and the corresponding fake estimates.

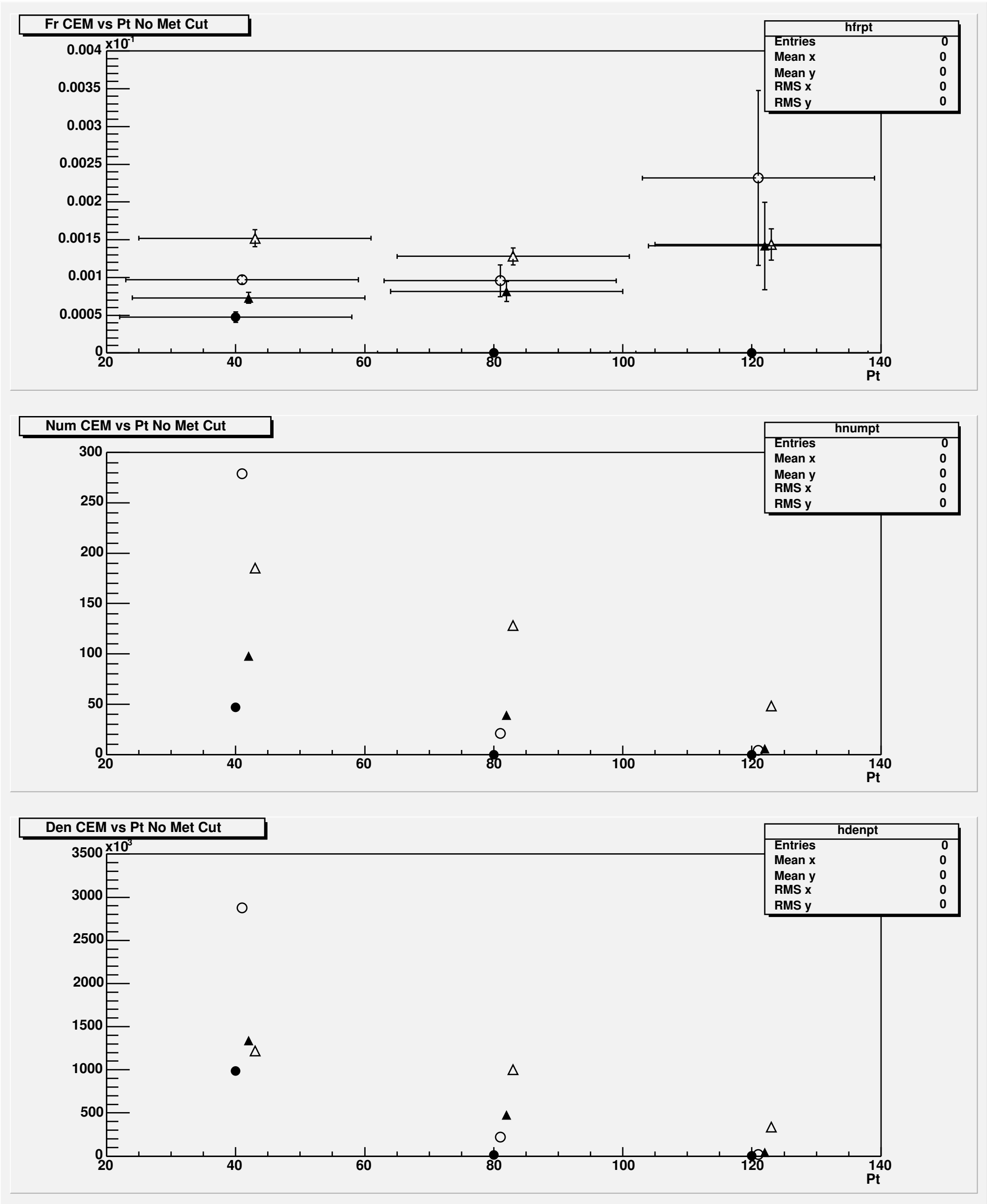

Figure 12: Fake ratios for CEM versus P_T, no track isolation requirement has been applied. Solid circles are jet-20, open circles jet-50, solid triangles jet-70, and open triangles jet-100.

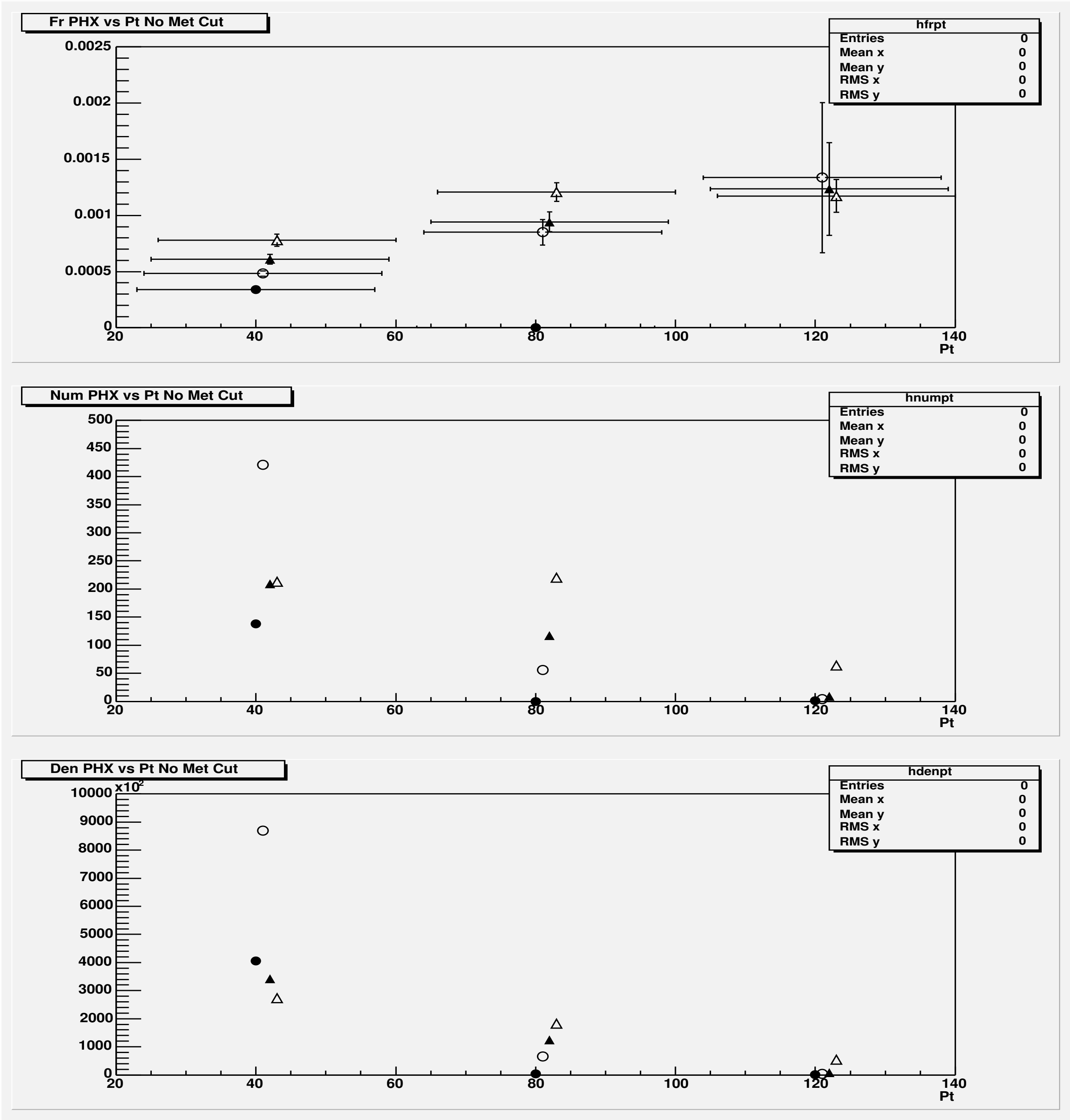

Figure 13: Fake ratio for PHX versus P_T. Same symbol definitions as for figure 12.

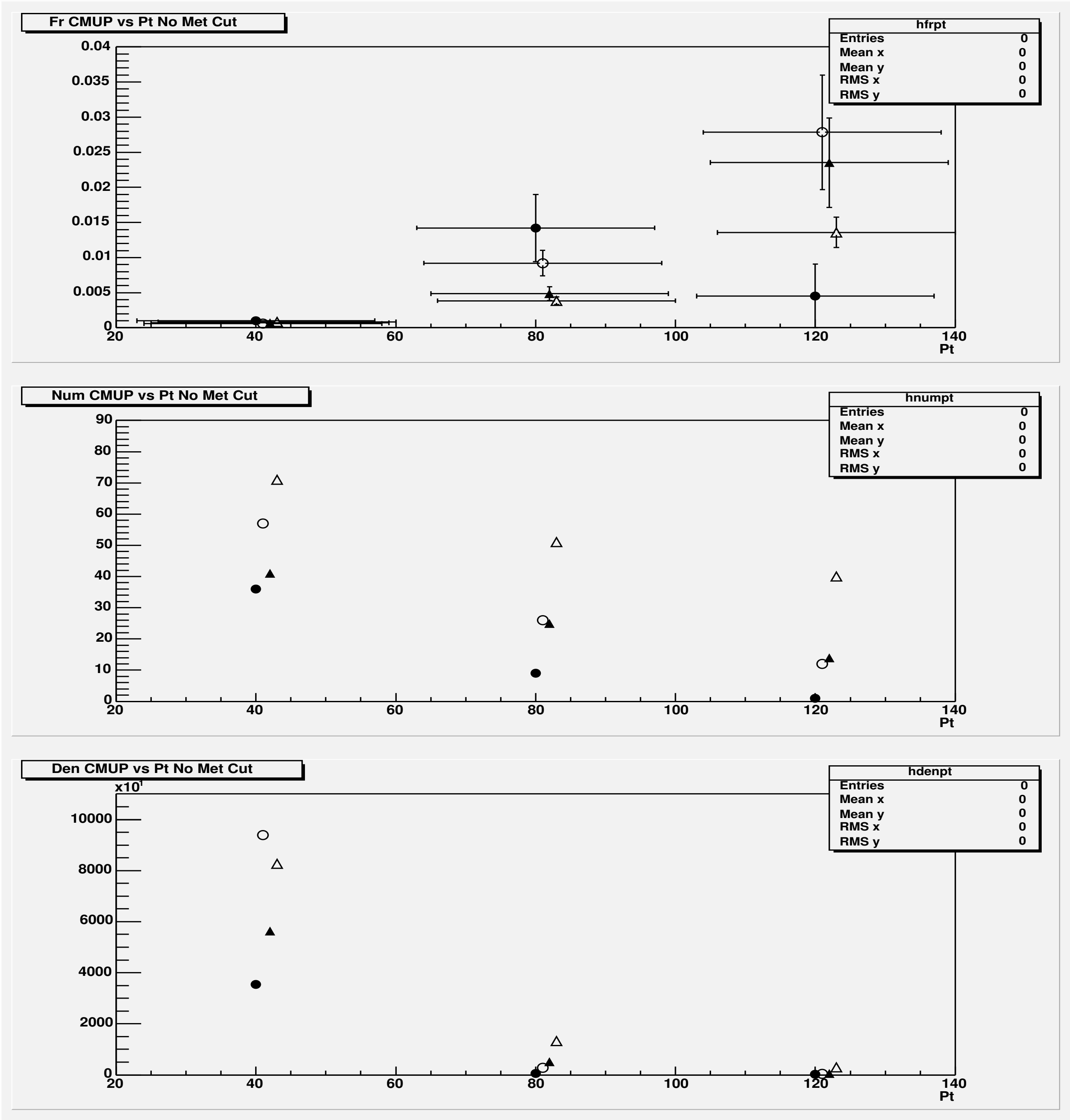

Figure 14: Fake ratio for CMUP versus P_T. Same symbol definitions as for figure 12.

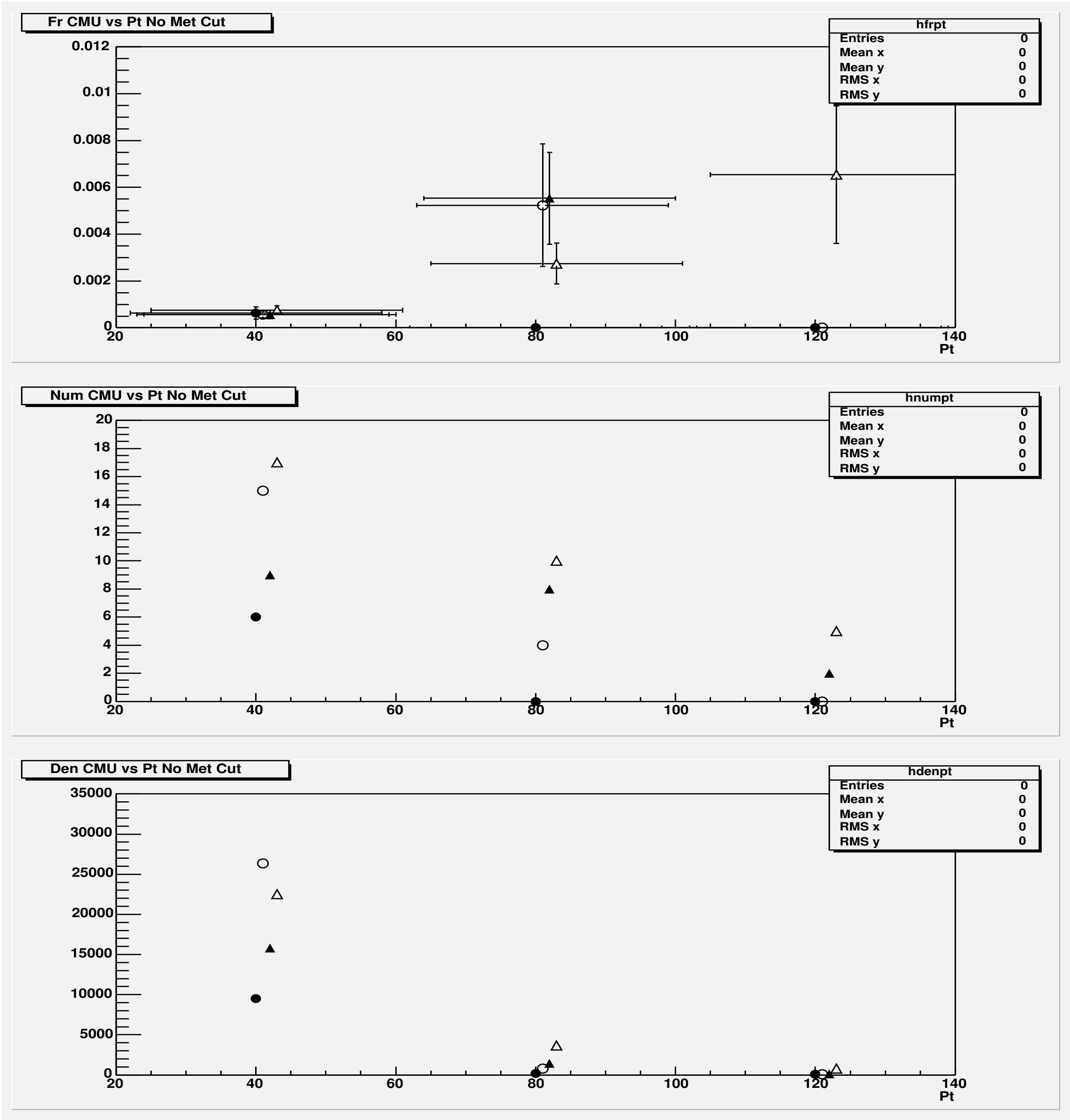

Figure 15: Fake ratio for CMU versus P_T. Same symbol definitions as for figure 12.

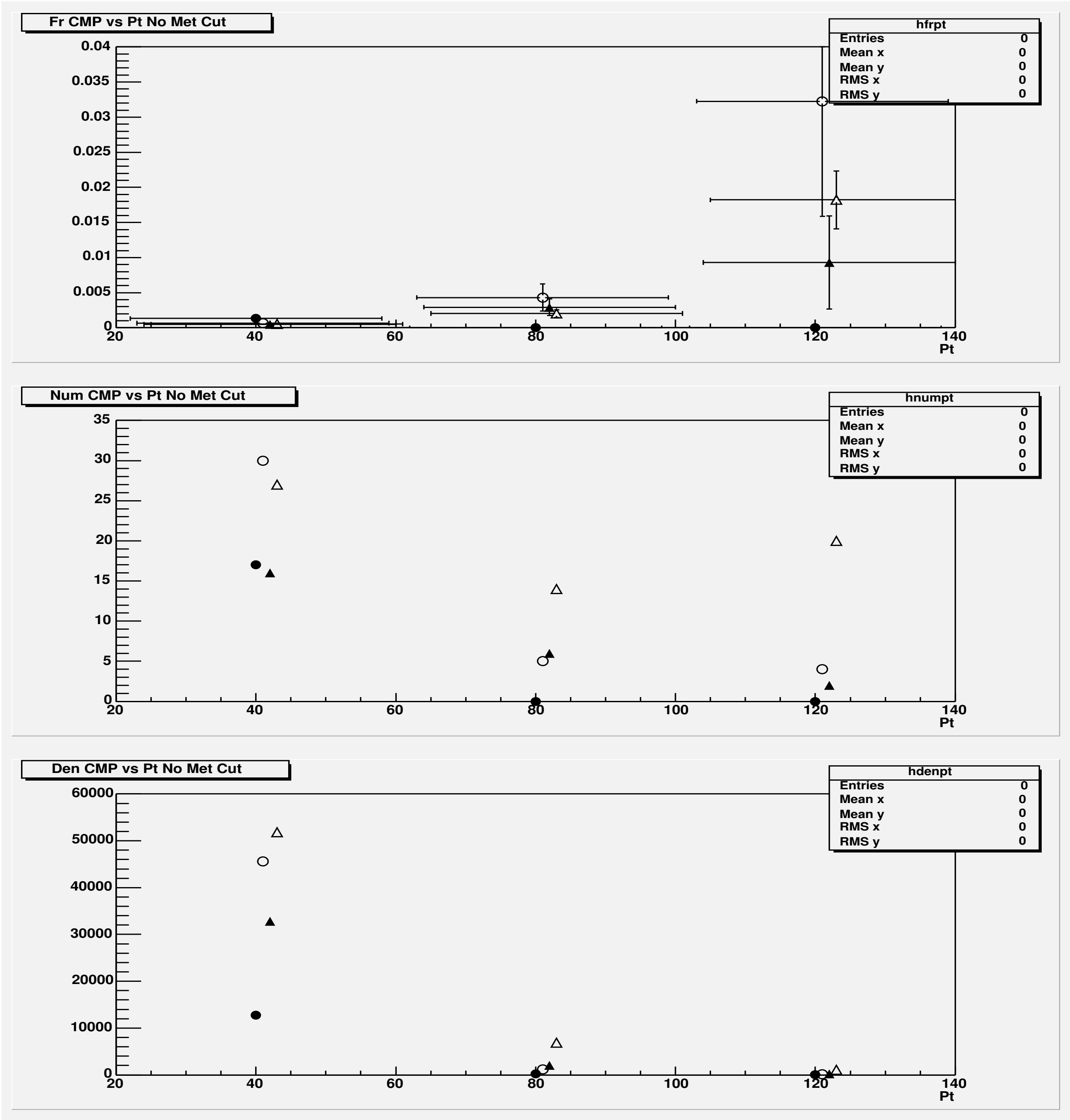

Figure 16: Fake ratio for CMP versus P_T. Same symbol definitions as for figure 12.

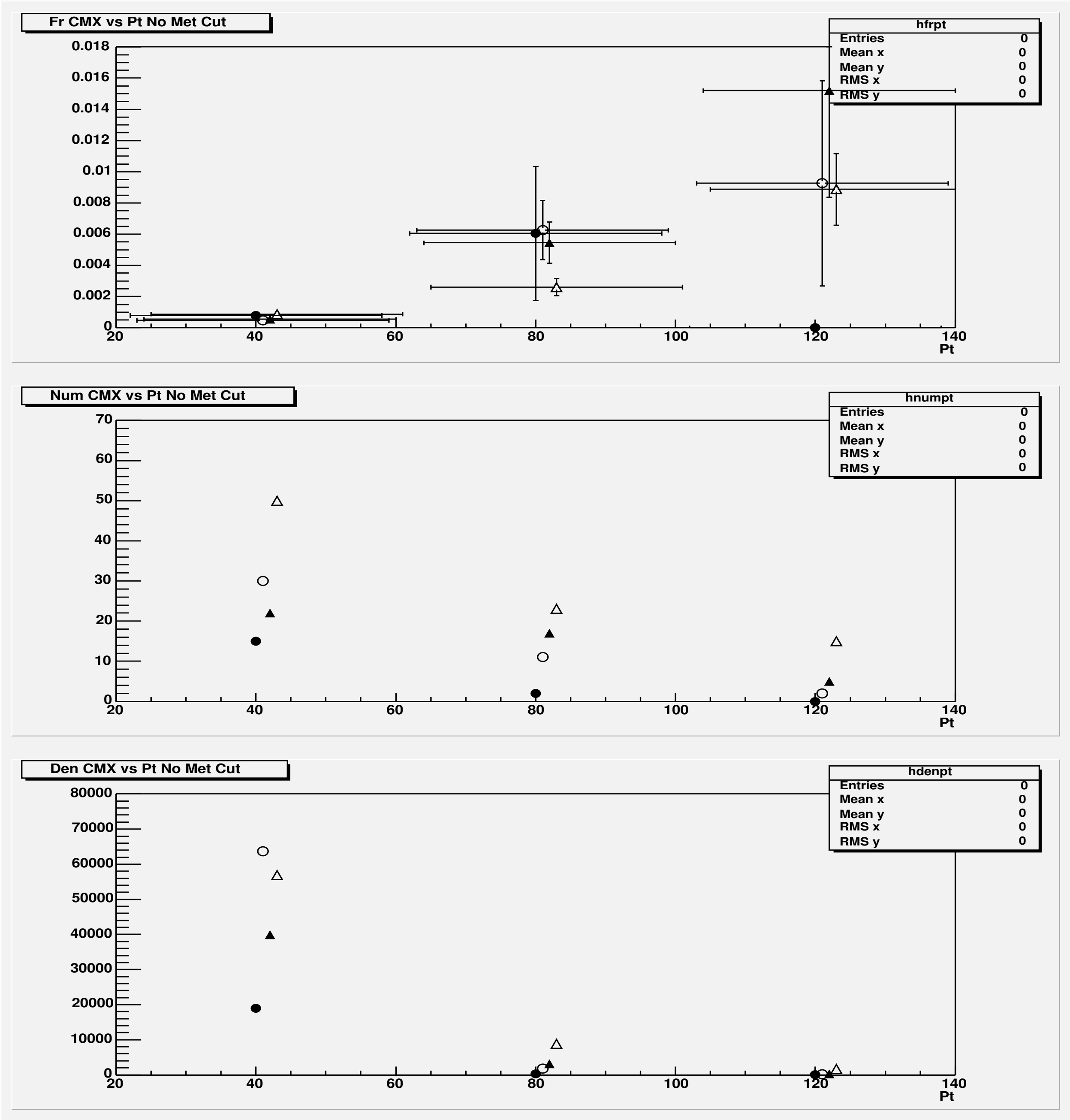

Figure 17: Fake ratio for CMX versus P_T. Same symbol definitions as for figure 12.

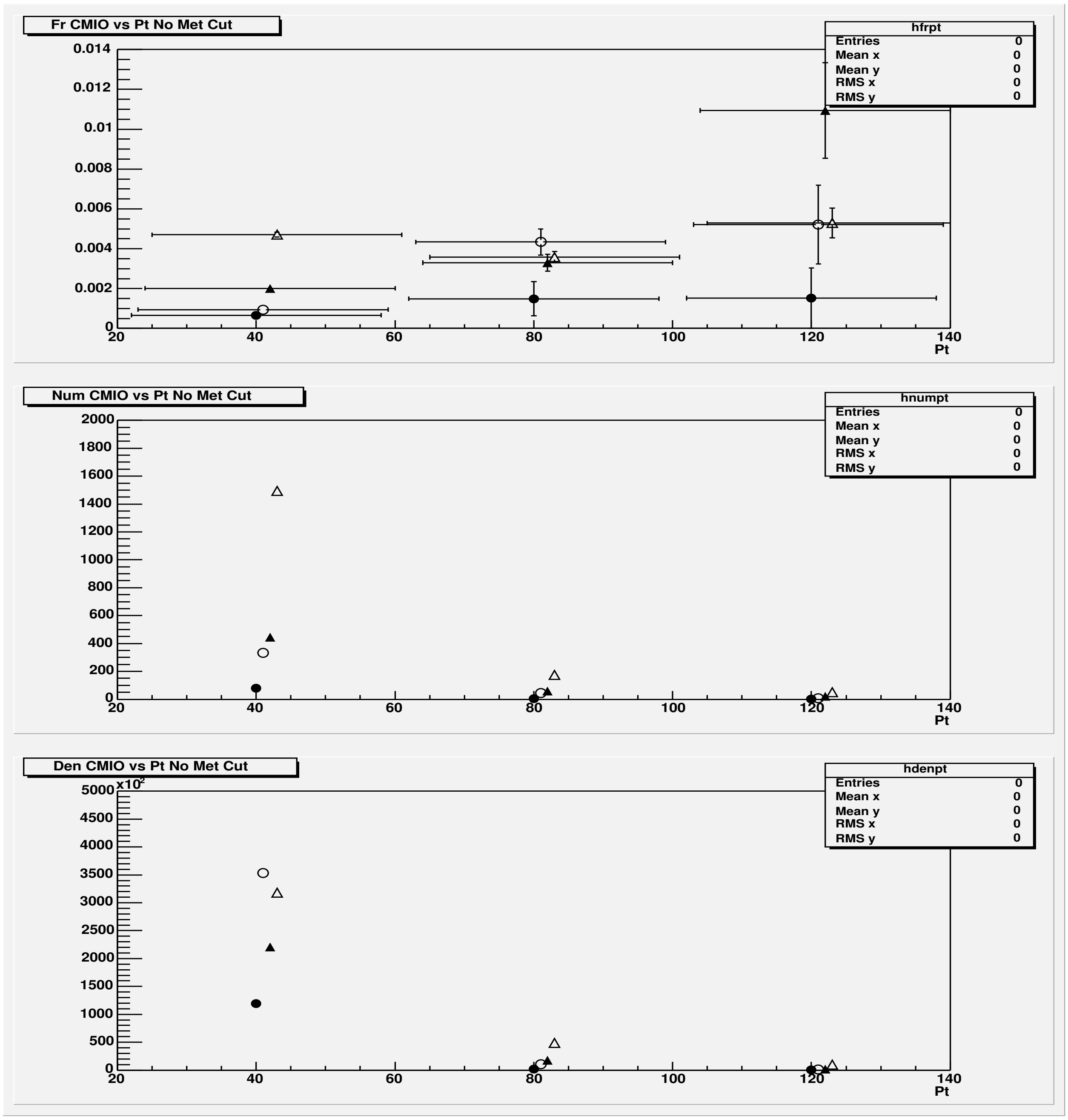

Figure 18: Fake ratio for CMIO versus P_T. Same symbol definitions as for figure 12.

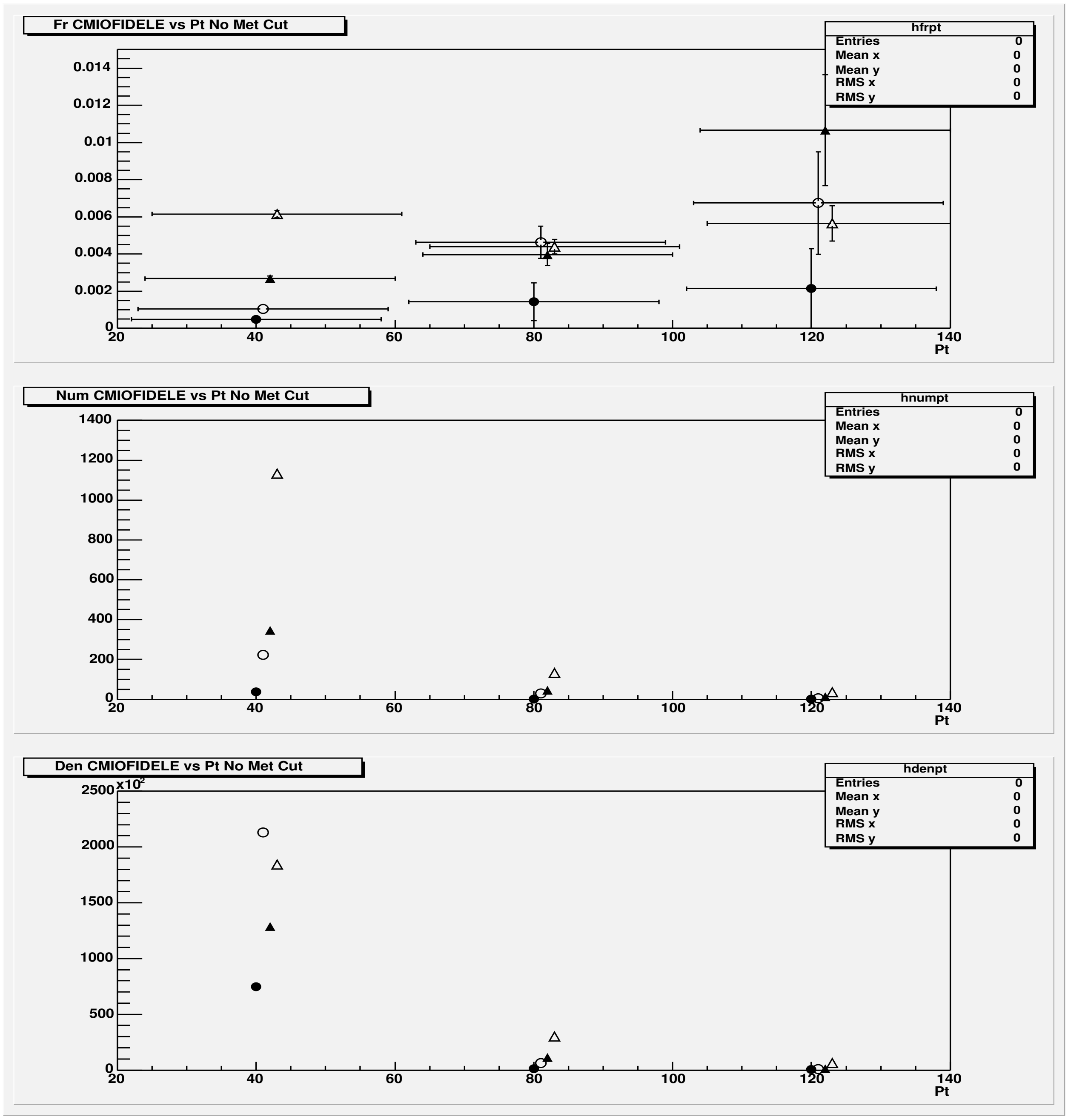

Figure 19: Fake ratio for CMIO-*fidele* versus P_T. Same symbol definitions as for figure 12.

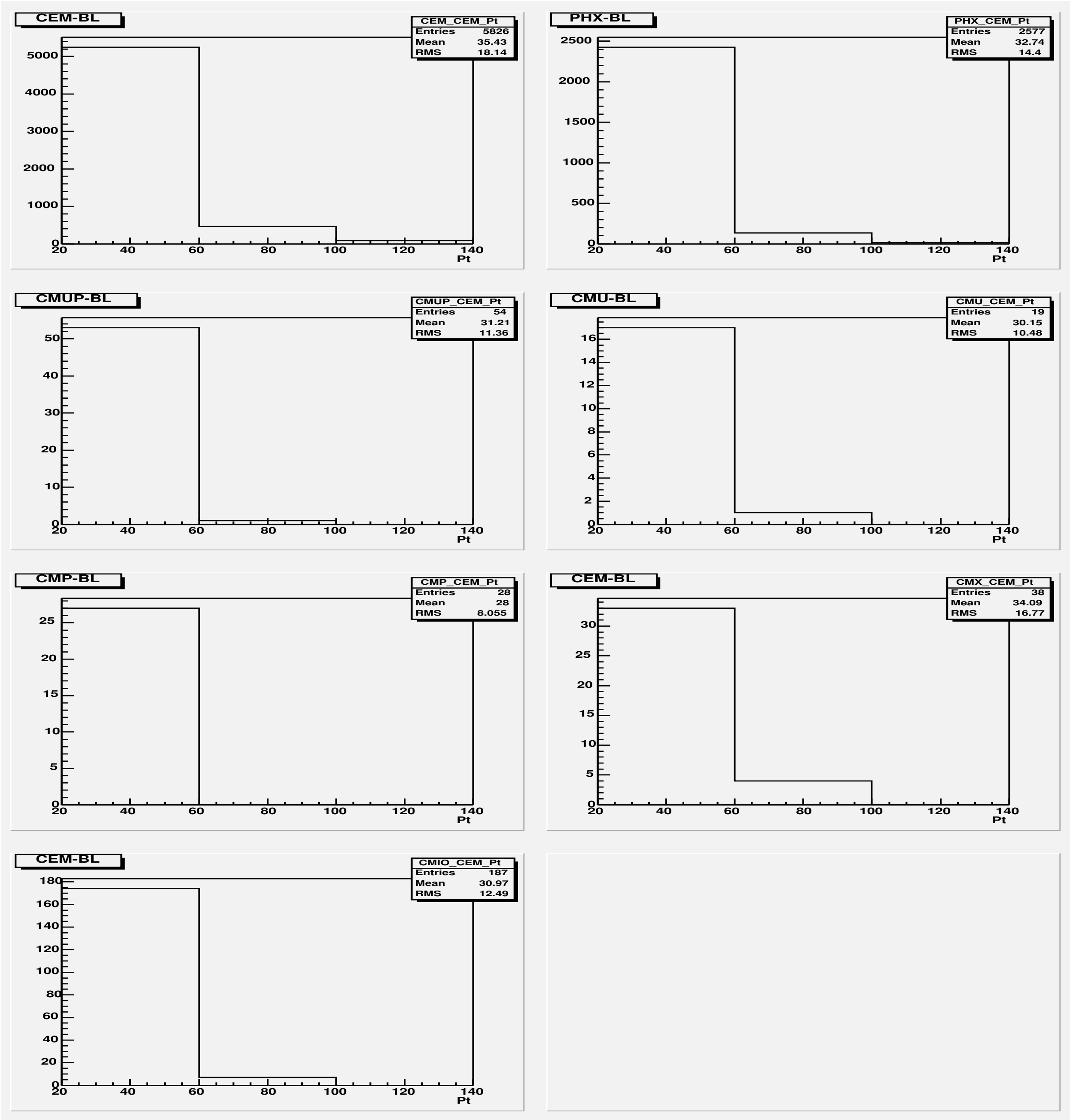

Figure 20: P_T spectrum of the fakeable electrons and muons found in the signal sample.

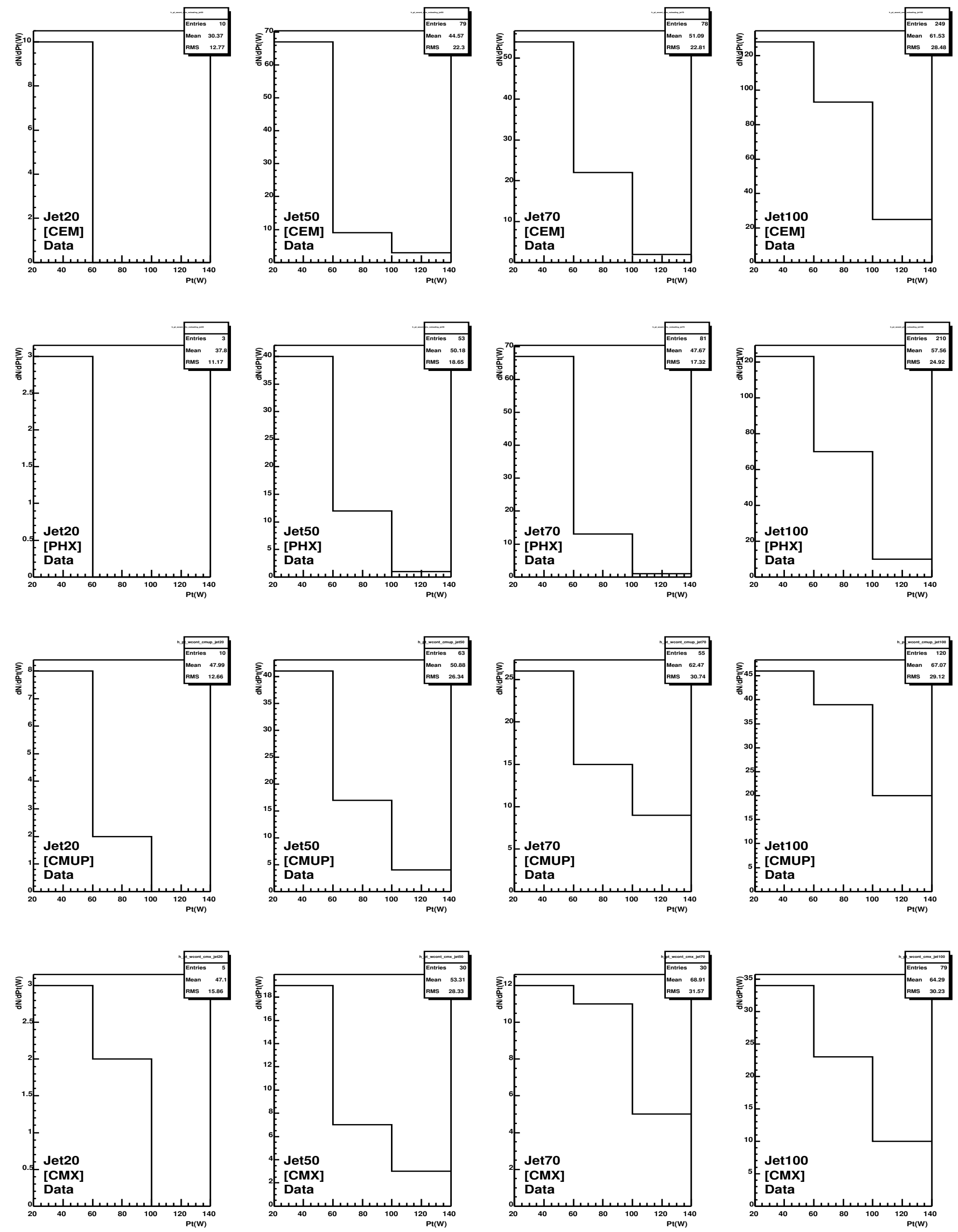

Figure 21: Lepton P_T spectrum of the $W + \geq 1$ jet events found in the signal data sample, triggerable in the jet samples.

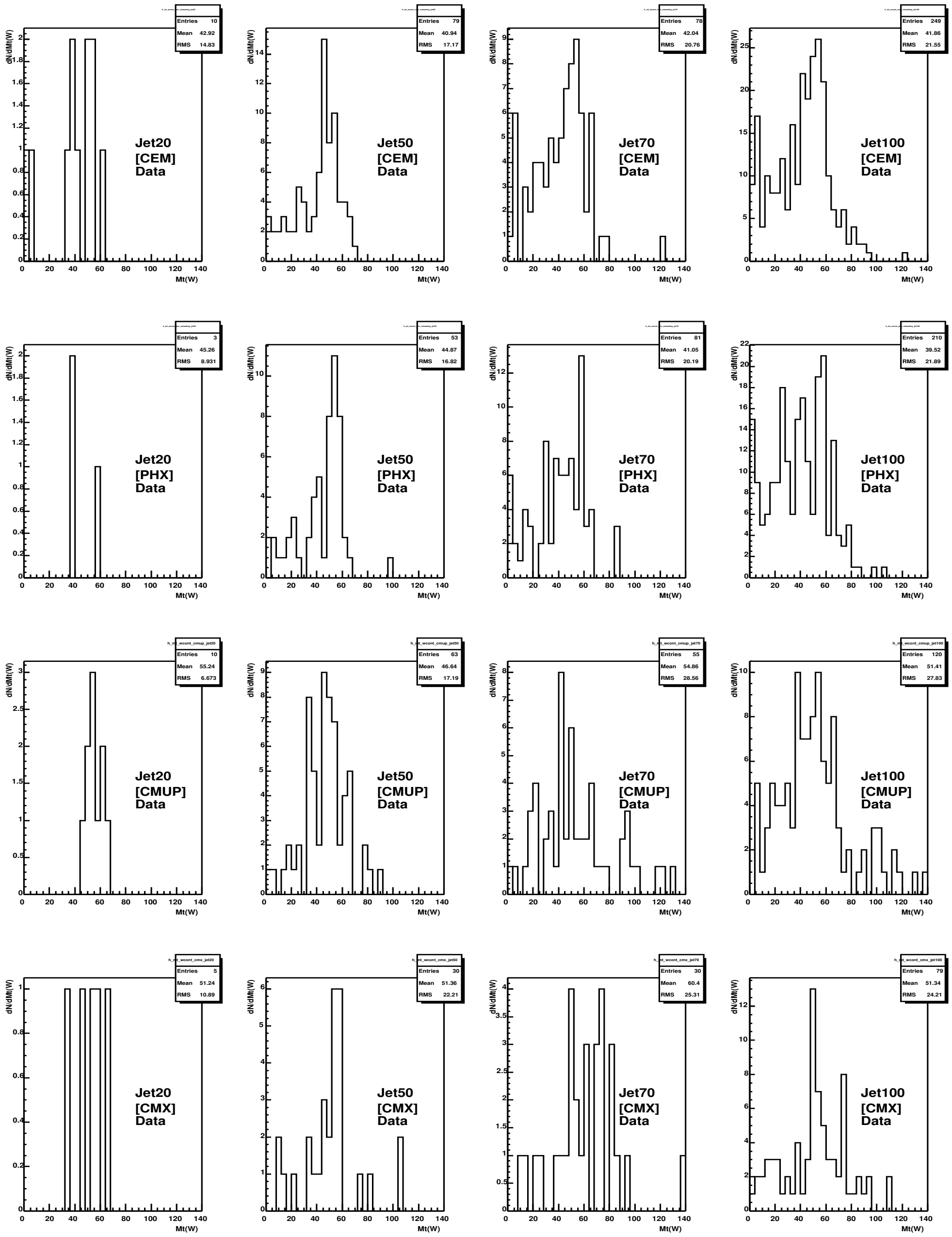

Figure 22: M_T spectrum of the $W+\geq 1$ jet events found in the signal data sample, triggerable in the jet samples.

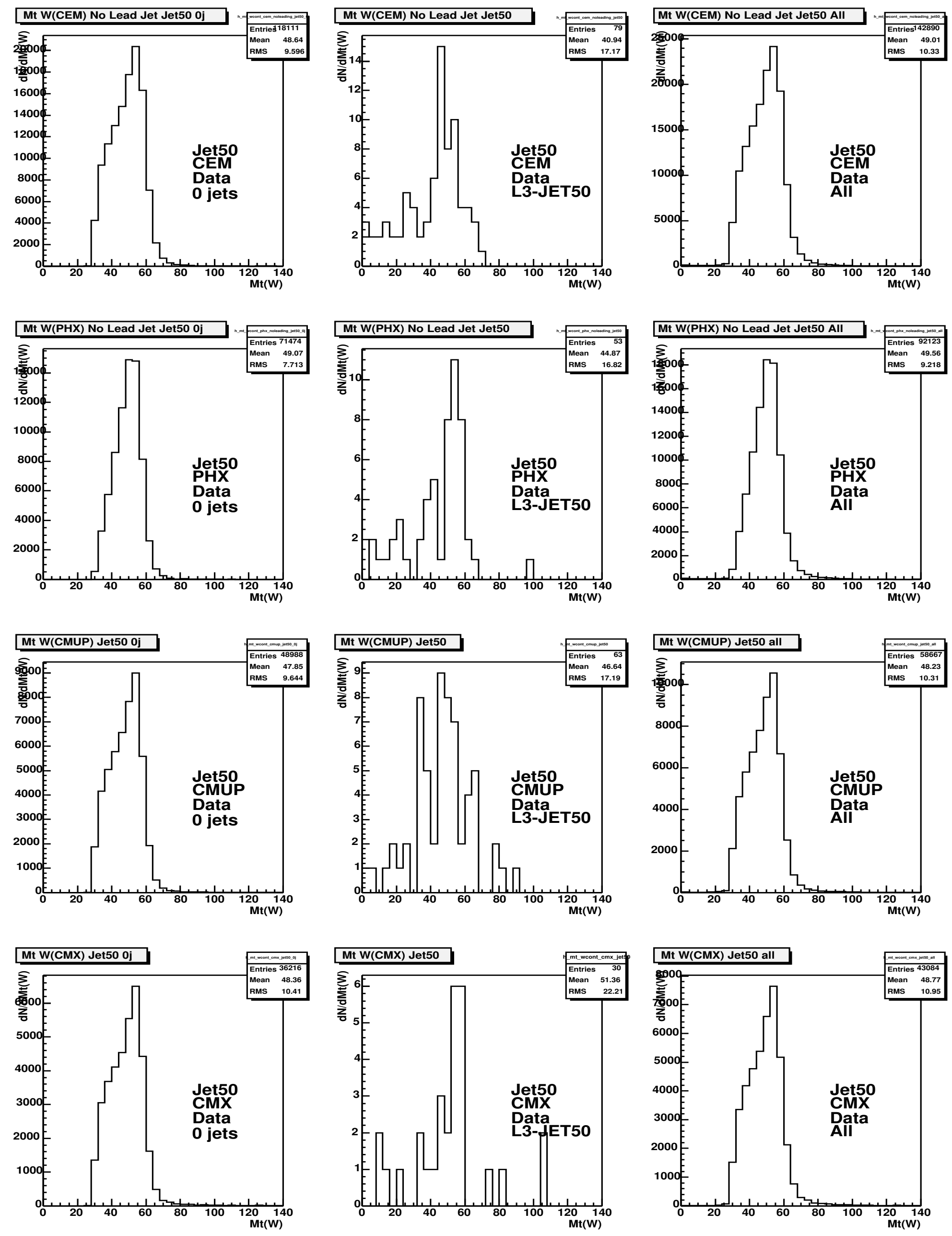

Figure 23: M_T spectrum of the $W + 0\ jets$, $W + \geq 1\ jet$ and $W + n\ jet$ events found in the signal data sample, triggerable in the JET50 samples.

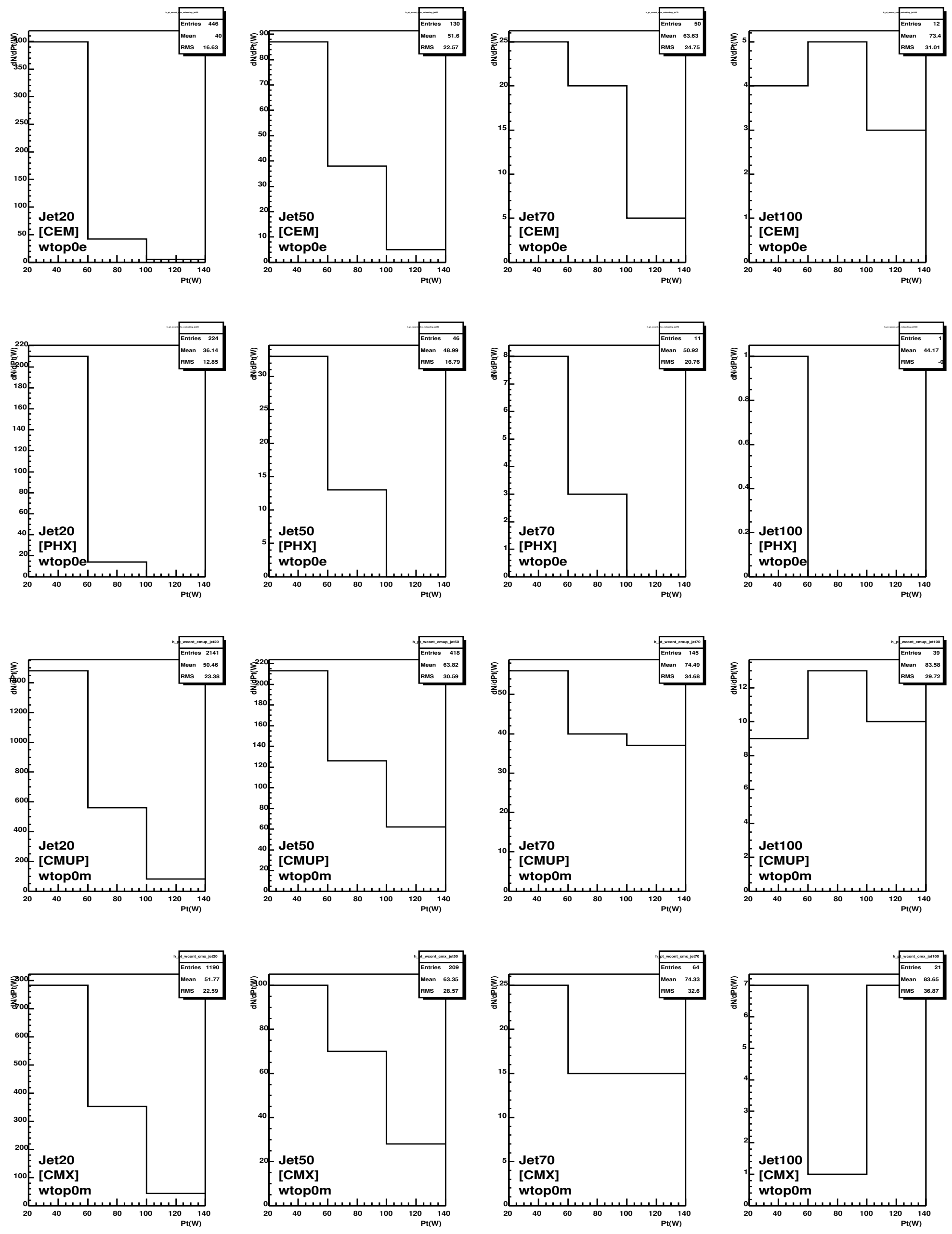

Figure 24: Lepton P_T spectrum of the $W + \geq 1\ jet$ events found in the $W \rightarrow \ell\nu$ PYTHIA MC samples wtop0e and wtop0m.

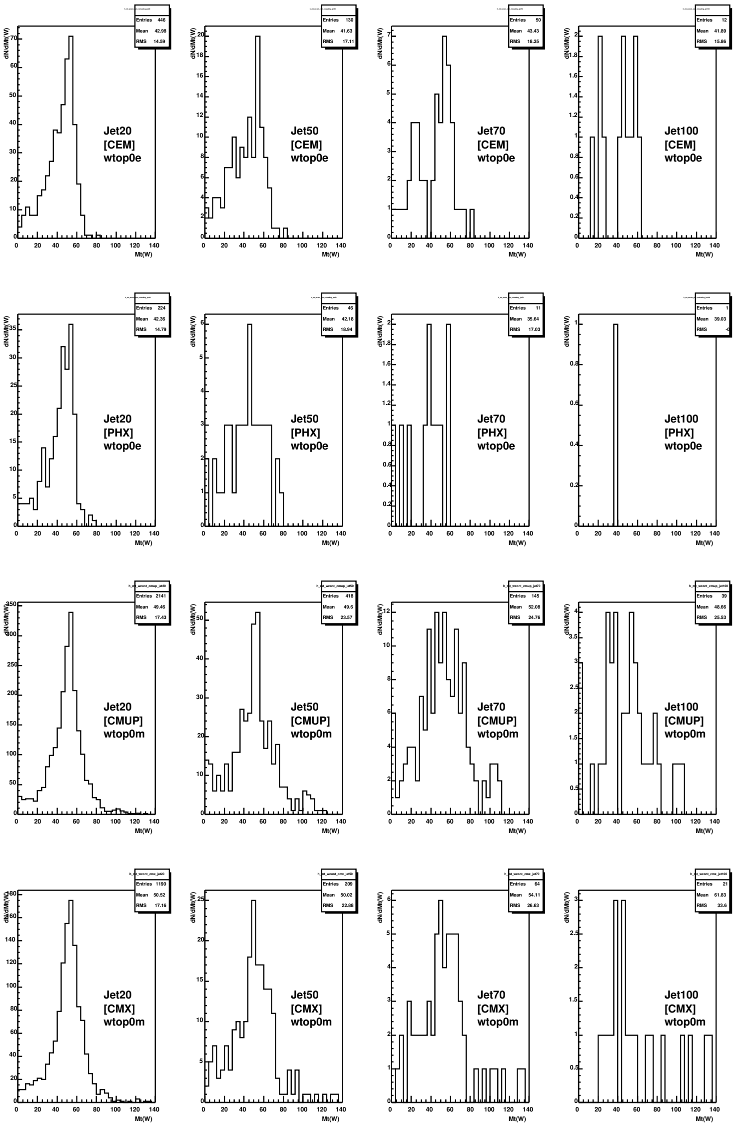

Figure 25: The M_T spectrum of the $W + \geq 1$ jet events found in the $W \to \ell\nu$ PYTHIA MC samples wtop0e and wtop0m.

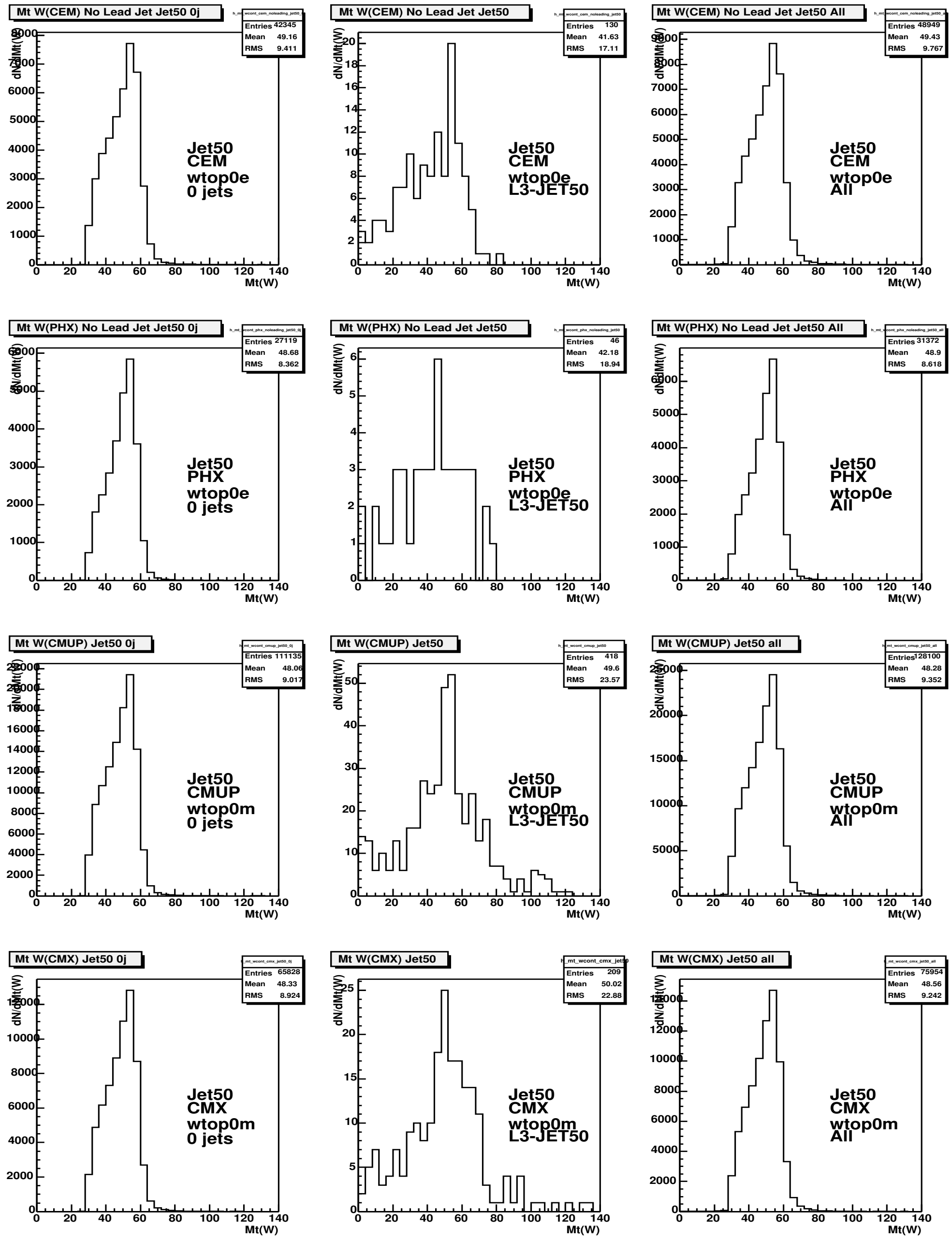

Figure 26: M_T spectrum of the $W + 0\ jets$, $W + \geq 1\ jet$ and $W + n\ jet$ events found in the $W \to \ell\nu$ PYTHIA MC samples wtop0e and wtop0m.

7.8 Contribution from Heavy Flavor

The requirement that both leptons be isolated is expected to significantly reduce any $b\bar{b}$, $c\bar{c}$ or $Wb\bar{b}$ background. In addition some of the heavy flavor contribution will be included in the fake estimate (however, not all, as the ratio of heavy flavor in the jet samples, used to calculate the fake ratio, and the lepton + jets samples, used to apply the fake ratio, is not necessarily the same) . The two main contributions are QCD with heavy flavor and $Wb\bar{b}$.

7.8.1 QCD + HF

We estimate the $b\bar{b}$ contribution by running on a HERWIG $b\bar{b}$ sample (btop1a, cdfptop, herwig_bbar_v01) with an effective luminosity of $733\,\mathrm{pb}^{-1}$.

We find after lepton ID and isolation requirements only (that is, no WW specific event selection cuts), 1 ee, 2 $e\mu$ and 0 $\mu\mu$ $b\bar{b}$ events remaining. (If we lift any isolation requirement on one lepton leg we see 34 events remaining, indicating the effectiveness of isolation in removing heavy flavor.)

To get a rough upper limit from these numbers on the $b\bar{b}$ contribution we assume the $\not\!\!E_T > 25\,\mathrm{GeV}$ cut efficiency to be roughly the same as that in $Z \to \tau\tau$, that is 5% (see table 17). By not applying *any* other cut efficiencies, this gives us a $b\bar{b}$ contribution of 0.04 events. We therefore neglect this as a source of background in our analysis.

7.8.2 $Wb\bar{b}$

We have analyzed in detail $Wb\bar{b}$ production as a potential background source, as well as the possible overlap of a Monte Carlo estimation of this background with our data-based fake background estimate. Table 40 gives details of the dataset used and the numbers of events passing the WW selection cuts. Normalizing to the data luminosity, fewer than 0.01 events are expected to remain after all cuts. As a cross check, we have applied the fake rates computed with jet triggered data to the number of fakeable events found in the $Wb\bar{b}$ sample, the results of which are shown in table 41. The results are in agreement with the direct cuts-based estimate within large statistical errors and also indicate this background source to be negligible. Any possible overlap with our data based fake estimate must also therefore be negligible.

7.9 Contribution from $W + \gamma$

The background from radiative W production can be significant, contributing in particular to dilepton categories in which one leg is a PHX electron, due to the lack of conversion rejection and track isolation requirements for such leptons.

We have estimated this background by running over approximately 425k $W + \gamma$ Monte Carlo events, generated using the Monte Carlo program WGAMMA and described in [21] and references therein. The $k-$factor corrected cross section is $\sigma(W\gamma) \times BR(W \to l\nu) = 44.7$ pb (for $E_T^\gamma > 5$ GeV, $|\eta^\gamma| < 10$, and $\Delta R(l, \gamma) > 0.2$). Since the Monte Carlo datasets include both electron and muon decays, the effective integrated luminosity of the sample is 4.74 fb^{-1}. Running the Monte Carlo sample through the full analysis chain, a total of 35 events survive all cuts, corresponding to an estimated background of 1.1 ± 0.2 events in 184 pb^{-1} after the application of all relevant luminosity and lepton scale factors. The breakdown by dilepton category is given in table 42.

In order to estimate any possible overlap between this estimate and the data based fake background estimate, we have run over the $W + \gamma$ Monte Carlo and applied fake ratios derived from QCD data. We find the total expected number of events calculated this way to be negligible, and therefore assume no overlap between these two background estimates.

8 ZZ background

The ZZ background has been revisited after the introduction of the missing-E_T significance cut to recover WW acceptance in the Z-mass window. In particular, we now let in significantly more background due to $ZZ \to l^+l^-\nu\bar{\nu}$ events, where the dilepton mass is consistent with the Z-mass and there is large real missing-E_T.

We evaluate this background by running on a sample of 290541 PYTHIA generated ZZ events. PYTHIA includes γ^* in addition to Z in a consistent way. At the generator level we require each Z/γ^* to have a mass greater than 30 GeV. We expect very little acceptance at lower masses. We take the PYTHIA LO cross-section and apply an MCFM calculated $k-$factor with identical kinematic cuts, to give an estimated $\sigma^{ZZ}_{NLO} = 1.30$ pb. A post-generator HEPG filter required at least two generator level electrons or muons with $P_T >$ 1 GeV, with a resulting efficiency of 21.3%. The effective luminosity of the sample is therefore ~ 1 fb^{-1}.

The numbers of events surviving each cut are shown in table 43. It can be seen that the Z-veto is not as effective at removing these events as it is at removing Drell-Yan events, due to the fraction of ZZ events with real missing-E_T. The final number of background events expected from ZZ production is 0.70 ± 0.06. This is close to the number reported in [9] for similar but not identical cuts, and is of the same order as the background from WZ production. We apply a systematic error of 10% to this estimate, the same as for our WW signal.

Cut	$W(\to e\nu)b\bar{b}$ (atop0,cdfptop), $N_{analyzed}=233613$, $\sigma_{Wb\bar{b}}=2.914\ pb$					
	ee		$\mu\mu$		$e\mu$	
		%		%		%
Lepton ID	38.00	0.00 ± 0.00	1.00	0.00 ± 0.00	48.00	0.00 ± 0.00
Isolation	3.00	7.89 ± 4.37	0.00	0.00 ± 0.00	3.00	6.25 ± 3.49
Conv+Cosmic	3.00	100.00 ± 0.00	0.00	0.00 ± 0.00	3.00	100.00 ± 0.00
Z-veto	3.00	100.00 ± 0.00	0.00	0.00 ± 0.00	3.00	100.00 ± 0.00
$\not{E}_T$ >25 GeV :	3.00	100.00 ± 0.00	0.00	0.00 ± 0.00	3.00	100.00 ± 0.00
$\Delta\Phi > 20°$ if $\not{E}_T$ <50	2.00	66.67 ± 27.22	0.00	0.00 ± 0.00	3.00	100.00 ± 0.00
0 jets	1.00	50.00 ± 35.36	0.00	0.00 ± 0.00	0.00	0.00 ± 0.00
Opposite Sign	0.94	94.17 ± 23.43	0.00	0.00 ± 0.00	0.00	0.00 ± 0.00
	$N_{predicted}=0.0017\pm0.0017$					
	$W(\to\mu\nu)b\bar{b}$ (atop6,cdfptop),$N_{analyzed}=220768$, $\sigma_{Wb\bar{b}}=2.914\ pb$					
Lepton ID	0.00	0.00 ± 0.00	43.00	0.00 ± 0.00	29.00	0.00 ± 0.00
Isolation	0.00	0.00 ± 0.00	0.00	0.00 ± 0.00	1.00	3.45 ± 3.39
Conv+Cosmic	0.00	0.00 ± 0.00	0.00	0.00 ± 0.00	1.00	100.00 ± 0.00
Z-veto	0.00	0.00 ± 0.00	0.00	0.00 ± 0.00	1.00	100.00 ± 0.00
$\not{E}_T$ >25 GeV :	0.00	0.00 ± 0.00	0.00	0.00 ± 0.00	1.00	100.00 ± 0.00
$\Delta\Phi > 20°$ if $\not{E}_T$ <50	0.00	0.00 ± 0.00	0.00	0.00 ± 0.00	1.00	100.00 ± 0.00
0 jets	0.00	0.00 ± 0.00	0.00	0.00 ± 0.00	0.00	0.00 ± 0.00
Opposite Sign	0.00	0.00 ± 0.00	0.00	0.00 ± 0.00	0.00	0.00 ± 0.00
	$N_{predicted}=0$					

Table 40: ALPGEN+HERWIG $Wb\bar{b}$ events passing dilepton cuts for each dilepton category, and the associated efficiencies of each cut (after all previous cuts have been applied). Errors are statistical only. The numbers of events expected in the data luminosity are also indicated.

$W(\to e\nu)b\bar{b}$ (atop0,cdfptop), $N_{analyzed} = 233613$, $\sigma_{Wb\bar{b}} = 2.914\ pb$	
ee	1.274±0.071±0.387±0.357
$e\mu$	0.111±0.016±0.083±0.055
$\mu\mu$	0.000±0.000±0.000±0.000
Total 80169 pb^{-1}	1.385±0.072±0.396±0.412
Total 200 pb^{-1}	$\sim$ 0.0035
$W(\to \mu\nu)b\bar{b}$ (atop6,cdfptop),$N_{analyzed} = 220768$, $\sigma_{Wb\bar{b}} = 2.914\ pb$	
ee	0.000±0.000±0.000±0.000
$e\mu$	1.484±0.053±0.412±0.416
$\mu\mu$	0.150±0.017±0.104±0.075
Total 75761 pb^{-1}	1.634±0.056±0.425±0.49
Total 200 pb^{-1}	$\sim$ 0.0043

Table 41: W$b\bar{b}$ background estimated using fake rates applied to Monte Carlo.

$W(\gamma) \to e\nu\gamma$	
TCE-TCE	0.08 ± 0.06
TCE-PHX	0.31 ± 0.10
PHX-PHX	0.09 ± 0.05
Total	0.48 ± 0.13
$W(\gamma) \to \mu\nu\gamma$	
μ-TCE	0.07 ± 0.05
μ-PHX	0.50 ± 0.12
Total	0.57 ± 0.13
Combined	
Total	1.05 ± 0.19

Table 42: The breakdown by dilepton category of the background in 184 pb^{-1} due to radiative W production. See text for details.

Cut	ZZ					
	ee		$\mu\mu$		$e\mu$	
		%		%		%
Lepton ID	23364.00	0.00 ± 0.00	21926.00	0.00 ± 0.00	1714.00	0.00 ± 0.00
Isolation	19666.00	84.17 ± 0.24	18563.00	84.66 ± 0.24	1090.00	63.59 ± 1.16
Conv+Cosmic	19279.00	98.03 ± 0.10	18563.00	100.00 ± 0.00	1074.00	98.53 ± 0.36
Z-veto with $\not{E}_T^{sig}$	4926.00	25.55 ± 0.31	4812.00	25.92 ± 0.32	1074.00	100.00 ± 0.00
$\not{E}_T$ >25 GeV :	3514.00	71.34 ± 0.64	3645.00	75.75 ± 0.62	650.00	60.52 ± 1.49
$\Delta\Phi > 20°$ if $\not{E}_T$ <50	3229.00	91.89 ± 0.46	3384.00	92.84 ± 0.43	512.00	78.77 ± 1.60
0 jets	2343.00	72.56 ± 0.79	2445.00	72.25 ± 0.77	145.00	28.32 ± 1.99
Opposite Sign	2168.53	92.55 ± 0.54	2376.00	97.18 ± 0.33	74.29	51.23 ± 4.15

Table 43: PYTHIA ZZ events passing dilepton cuts for each dilepton category, and the associated efficiencies of each cut (after all previous cuts have been applied). Errors are statistical only.

9 Grand summary

The summary of all the backgrounds, signal acceptances, and data analysis for $184\,\mathrm{pb}^{-1}$, all of which has been detailed above, is given in table 44. The signal to background ratio in this analysis is about 2:1. These results will be used to calculate the WW production cross-section in Section 11.1.

	CDF Run II Preliminary			
Source	ee	$\mu\mu$	$e\mu$	$\ell\ell$
Drell-Yan e^+e^-	0.75 ± 0.34	0.00 ± 0.00	0.052 ± 0.043	0.80 ± 0.34
Drell-Yan $\mu^+\mu^-$	0.00 ± 0.00	0.61 ± 0.27	0.28 ± 0.13	0.89 ± 0.30
Drell-Yan $\tau^+\tau^-$	0.047 ± 0.021	0.046 ± 0.020	0.099 ± 0.041	0.19 ± 0.05
WZ	0.29 ± 0.03	0.33 ± 0.03	0.15 ± 0.02	0.76 ± 0.06
ZZ	0.35 ± 0.04	0.34 ± 0.04	0.011 ± 0.002	0.70 ± 0.07
$W+\gamma$	0.48 ± 0.13	0.00 ± 0.00	0.57 ± 0.13	1.06 ± 0.19
$t\bar{t}$	0.021 ± 0.011	0.012 ± 0.007	0.046 ± 0.018	0.078 ± 0.023
Fake	0.52 ± 0.19	0.17 ± 0.16	0.65 ± 0.37	1.34 ± 0.66
Total Background	2.46 ± 0.42	1.51 ± 0.33	1.86 ± 0.43	5.82 ± 0.86
$WW \to$ dileptons	2.61 ± 0.31	2.48 ± 0.29	5.11 ± 0.60	10.20 ± 1.19
Total Expectation	5.07 ± 0.56	3.99 ± 0.46	6.97 ± 0.76	16.0 ± 1.6
Run 2 Data	6	6	5	17

Table 44: The estimated backgrounds and WW signal in $184\,\mathrm{pb}^{-1}$, and the number of events observed in the data, for each of the dilepton categories. The WW expectation uses the theoretical cross-section and BR discussed in Section 1.

10 WW Acceptance Systematic Errors

Potential sources of systematic uncertainty on the $WW \to l^+l^-\nu\bar{\nu}$ acceptance are summarized in table 45 and described below.

10.1 Jet Veto Uncertainty ("ISR")

The largest potential uncertainty in the acceptance calculation for WW events derives from the zero-jet requirement. The zero jet fraction is not expected to be well reproduced by leading-order Monte Carlo programs such as PYTHIA that we use to determine the central value for our acceptance.

Source	Systematic Error
Jet Veto ("ISR")	6%
Generator/Parton-Shower Model	4%
[PDF/QCD-Scale Cross Section	5%]
PDF Acceptance	1%
Jet Energy Scale	3%
Lepton ID	2%
Track Isolation	4%
Trigger Efficiency	1%
METSIG	2%
Combined	10%

Table 45: Sources of systematic uncertainty on the $WW \rightarrow l^+l^-\nu\bar{\nu}$ acceptance. The PDF/QCD-Scale systematic is included here from the studies described later in this section, but does not contribute to the systematic on the acceptance, but is included in the systematic on the expected WW yield.

To address this uncertainty we have used Drell-Yan data and the next-to-leading order WW production Monte Carlo program MC@NLO [10]. Figure 27(a) shows the zero-jet fraction (using an identical jet definition to the full WW analysis) for Drell-Yan e^+e^- data and PYTHIA Monte Carlo events (central-central only, to avoid background issues) over a wide range of mass. The points are plotted at the average mass for each bin. There is a weak dependence of the zero-jet fraction on mass, and the data is consistently below the leading order Monte Carlo prediction, as expected. The (data/MC) scale factor is shown in figure 27(c). Integrating over the full mass range gives an average value of 0.955 ± 0.009. Figure 27(b) shows the zero-jet fraction for PYTHIA and MC@NLO WW samples, also as a function of the dilepton mass. The average ratio (MC@NLO/PYTHIA) is 0.955 ± 0.010. The very similar value to that derived from the Drell-Yan comparison gives us some confidence that MC@NLO describes well the migration of events from the zero-jet to $\geq$ 1-bins due to hard QCD radiation. However the overall zero-jet fraction is 6% different in Drell-Yan events and WW events due to the different $\hat{s}$ distribution for the two processes, and the fact that QCD corrections are not exactly process independent. We use this difference as an estimate of the systematic uncertainty on the WW acceptance due to QCD corrections to the zero-jet fraction. A scale factor of 0.955 is applied to all WW yield estimates after applying the jet veto requirement, based on this study.

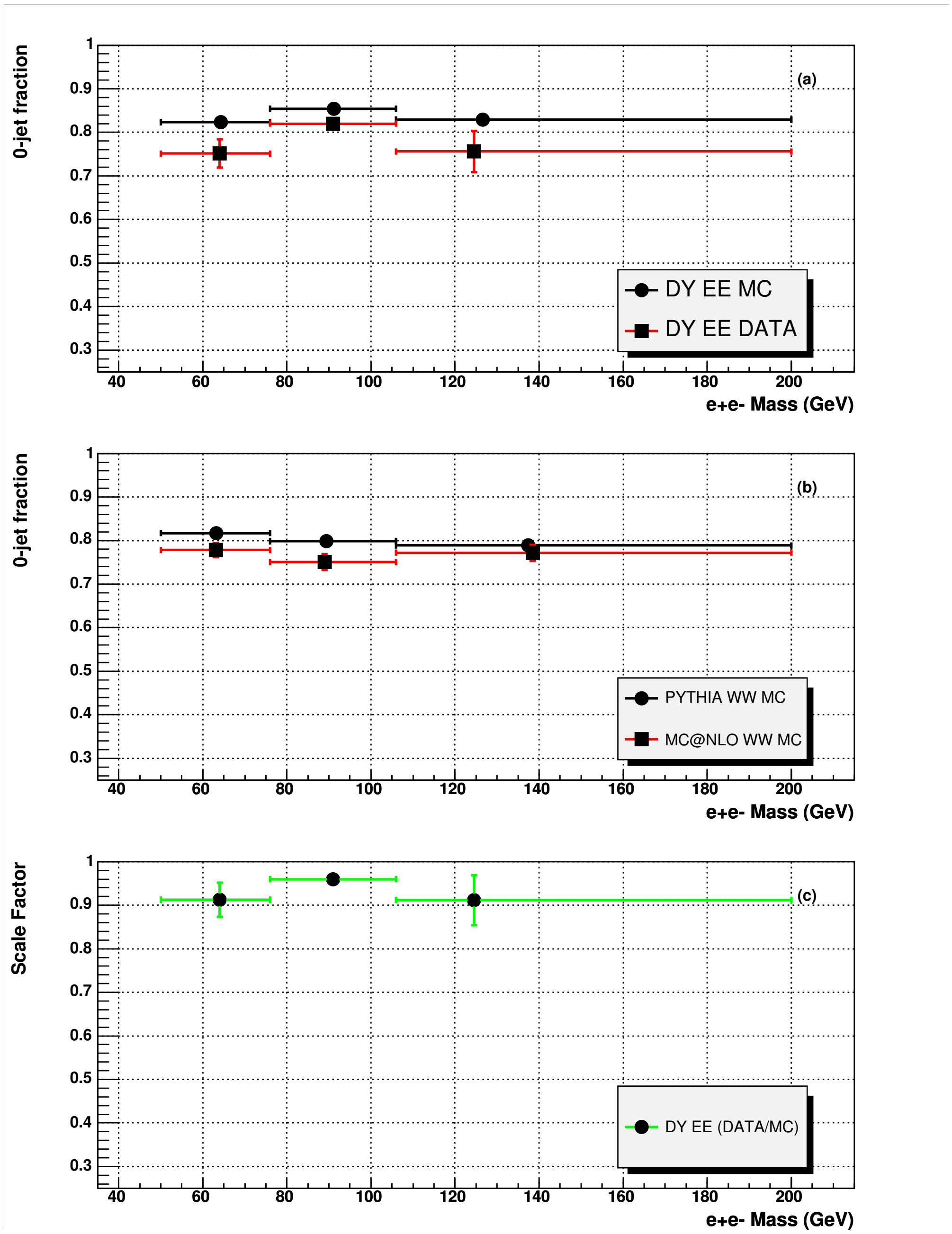

Figure 27: A comparison of zero-jet fractions for (a) Drell-Yan e^+e^- data and Monte Carlo and (b) MC@NLO and PYTHIA WW Monte Carlo. The (data/MC) scale factor computed from (a) is shown in (c).

10.2 Generator

HERWIG and PYTHIA have different parton showering models which can affect multiplicities and therefore Monte Carlo estimated isolation and other cut efficiencies. Our default acceptances and efficiencies are calculated using a PYTHIA WW sample (wtop0f). For HERWIG we use a sample of ALPGEN+HERWIG generated $WW + 0p$ events (atop4x). We find a difference in acceptance of 6.3% between these two samples. However, the PYTHIA sample requires both W's to decay leptonically, whereas this is only a requirement of one of the W's in the ALPGEN sample. A more detailed study, taking into account differences in branching ratios between the two generators, is described in section 12.4. We find a 2.2% systematic error associated to the generator.

10.3 PDF uncertainty studies and the Q^2 dependence of the NLO WW cross-section

The NLO WW total cross-section is calculated at $\sqrt{s} = 2$ TeV by the Monte Carlo program MCFM [3, 22] using the CTEQ6 LHAPDF [23]. The Hessian method [24] was used to estimate the uncertainty on the cross-section due to input PDF uncertainties. 40 member PDFs in the CTEQ6 family are used in the calculation. The cross-section has a predicted value

$$\sigma_0 = 12.4\,\text{pb}$$

and a range of uncertainty

$$(\sigma_0 - \delta\sigma_-, \sigma_0 + \delta\sigma_+) = \sigma_0\,(1 - 3.9\%, 1 + 4.6\%)$$

where $\delta\sigma_\pm$ is given by

$$(\delta\sigma_\pm)^2 = \sum_{i=1}^{20} [\sigma_i^\pm - \sigma_0]^2$$

The cross-section is also calculated at three different Q^2 values. Table 46 gives the Q^2 dependence of the NLO WW cross-section.

Q^2	σ (pb)	$\delta\sigma/\sigma_0$
$(M_W)^2$	12.4	-
$(\frac{M_W}{2})^2$	13.0	4.6%
$(2M_W)^2$	11.9	-4.4%

Table 46: Q^2 dependence of the total cross-section of $\mathrm{p\bar{p}} \to W^+W^-$

We find a combined maximal variation of about 6% in the predicted WW cross-section due to the choice of PDF and QCD scale. Note that this is NOT a systematic in the WW

acceptance, but rather on the WW yield, so we only propagate it to the expected number of WW events in table 44.

We furthermore estimate the uncertainty on the acceptance for $WW \to lvlv$ due to input PDF uncertainties. MCFM is run in leading-order mode with NLO CTEQ6 PDFs. Table 47 gives the acceptance and uncertainty with cuts of $|\eta^l| < 1$ and $P_T^l > 20$ GeV for both leptons and $\not\!\!E_T > 25$ GeV calculated from the neutrinos. 21.84 events pass all three cuts, corresponding to an overall acceptance of $19^{+1.1}_{-1.0}\%$. Table 48 gives the results for a larger rapidity acceptance interval, $|\eta^l| < 2$. Tables 47 and 48 show that for a wider range of lepton pseudorapidity acceptance the uncertainty is reduced, as expected. Conservatively we assign an acceptance systematic error of 1% due to PDF uncertainty.

Cuts	ee events	Acceptance	Uncertainty Range (%)
–	113.48	–	–
$\|\eta\| < 1$	40.48	0.36	(-1.0 , 1.2)
$P_T > 20$	31.05	0.77	(-0.4 , 0.4)
$\not\!\!E_T > 25$	21.84	0.70	(-0.3 , 0.3)
overall	21.84	0.19	(-1.0 , 1.1)

Table 47: Acceptance uncertainty due to PDF variation in the $WW \to ll$ channel, for $|\eta^l| < 1$.

Cuts	ee events	Acceptance	Uncertainty Range (%)
–	113.48	–	–
$\|\eta\| < 2$	93.45	0.82	(-0.4 , 0.4)
$P_T > 20$	69.74	0.75	(-0.4 , 0.4)
$\not\!\!E_T > 25$	49.11	0.70	(-0.1 , 0.1)
overall	49.11	0.43	(-0.3 , 0.4)

Table 48: Acceptance uncertainty due to PDF variation in the $WW \to ll$ channel, for $|\eta^l| < 2$.

10.4 Jet Energy Scale

The jet energy corrections are varied by $\pm 1\sigma$ and an overall $\approx 3\%$ variation in the WW acceptance is observed.

10.5 Lepton ID

Calculated (data/MC) scale factors for central leptons that are applied in this analysis typically have $\approx$ 1% errors. However approximately 25% of our events are expected to contain Phoenix electron, for which we conservatively assume the uncertainty to be several percent. This results in an overall uncertainty of $\approx 2\%$ in the WW acceptance.

10.6 Track Isolation

We have investigated the possibility that track isolation efficiencies are not well modelled in Monte Carlo. Comparison of Z yields with and without track isolation shows no systematic difference between data and Monte Carlo, with a maximum variation of 4% depending on the lepton category. We take this to be an estimate of the systematic uncertainty on the signal acceptance due to the track isolation requirement.

10.7 Missing E_T Significance

The $\not\!\!E_T^{sig}$ distribution for Drell-Yan data is well modelled by Monte Carlo. However the $\not\!\!E_T^{sig}$ distribution for W data shows possible discrepancies at the level of 10% in the fraction of events passing a cut at 3.0 (see reference [9] for this study, which uses an identical $\not\!\!E_T^{sig}$ cut). Since this cut affects 15% of our acceptance, we add 2% to our total WW acceptance uncertainty from this source.

10.8 Trigger Efficiency

Central trigger uncertainties are $\leq 1\%$. By far the largest uncertainty in this analysis is the MET-PEM trigger efficiency, which is calculated in section 5.1. However only 10% of WW dilepton events rely on the plug electron for triggering, reducing the overall uncertainty on the acceptance to $\approx 1\%$.

10.9 Combined Acceptance Systematic

Adding in quadrature the sources of uncertainty listed in table 45 results in a 10% uncertainty on the WW acceptance in the dilepton channel. This is assumed to be completely correlated between the ee, $\mu\mu$ and $e\mu$ channels.

11 Conclusions

11.1 Cross-Section Determination

The measured WW cross-section is given by the formula :

$$\sigma^{WW}_{meas} = \frac{(N_{obs} - N_{bk})}{\epsilon_{tot} \times \mathcal{L}} = \frac{(N_{obs} - N_{bk})}{\epsilon_{lep} \times [3 \times \mathrm{BR}(W \to l\nu)]^2 \times \mathcal{L}} \ , \tag{2}$$

where N_{obs} and N_{bk} are the number of events observed and the expected number of background events, respectively. The total efficiency ϵ_{tot} would be the fraction of WW events in all decay channels selected by this analysis. In practice we have calculated ϵ_{lep} using a Monte Carlo sample containing only the leptonic W decays, and we multiply by the appropriate factor involving the W leptonic branching ratio to determine the overall efficiency. As discussed in section 1, we use the Standard Model value $\mathrm{BR}(W \to l\nu) = 0.108$.

The product of efficiency, integrated luminosity and branching ratio appearing in the denominator can be re-expressed using the following expression for the expected number of WW events :

$$N^{WW}_{exp} = \sigma^{WW}_{theory} \times \epsilon_{tot} \times \mathcal{L} = \sigma^{WW}_{theory} \times \epsilon_{lep} \times [3 \times \mathrm{BR}(W \to l\nu)]^2 \times \mathcal{L} \ . \tag{3}$$

Combining equations 2 and 3 gives :

$$\sigma^{WW}_{meas} = \frac{(N_{obs} - N_{bk})}{N_{exp}} \times \sigma^{WW}_{theory} \ . \tag{4}$$

The advantage of using equation 4 is that the different efficiencies, luminosities and scale factors that pertain to each dilepton category are naturally taken into account in the evaluation of N^{WW}_{exp}. Note that we are not sensitive to the assumed value of σ^{WW}_{theory}, which in effect cancels in the numerator and denominator of equation 4. However we are sensitive to the assumption we make regarding the value of the leptonic branching ratio, as is clear from equation 2.

Since the sample size is small, we use the method developed in [31] to calculate a 68.27% ("1-sigma") confidence interval for the signal. This technique, which takes the number of observed events and the central value for the expected background as inputs, is equally valid for placing upper limits on signals and providing two-sided confidence intervals. If the lower limit on the two-sided confidence interval for the required confidence level is greater than zero, a cross-section can be stated. The central value for the cross-section is then given by equation 4. We find :

$$\sigma^{WW}_{meas} = 13.6^{+5.8}_{-5.1} \ \text{(stat)} \ \text{pb} \ . \tag{5}$$

11.1.1 Systematic Errors

We propagate errors on the acceptance, background and luminosity using equation 2. A fractional error on the acceptance of 10% is taken from section 10 and the uncertainties on the various background estimates discussed above are also taken into account. The systematic uncertainty on the integrated luminosity is taken to be 6%. We then find :

$$\sigma_{meas}^{WW} \quad = \quad 13.6^{+5.8}_{-5.1} \text{ (stat)} \ \pm \ 1.7 \text{ (syst)} \ \pm \ 0.8 \text{ (lum) pb} \ . \tag{6}$$

This is our final estimate of the WW cross-section in this analysis. However as a cross-check, we can take the Drell-Yan background estimated using the data rather than the Monte Carlo to give :

$$\sigma_{meas}^{WW}(\text{cross check}) \quad = \quad 14.2^{+5.8}_{-5.1} \text{ (stat)} \ \pm \ 2.7 \text{ (syst)} \ \pm \ 0.9 \text{ (lum) pb} \ . \tag{7}$$

The difference in central values is well within the statistical error and the final combined statistical plus systematic errors for the two cross-sections are different by less than 10%.

11.2 Kinematic Comparisons of Data with Monte Carlo

Figures 28 through 37 display some kinematic features of our candidate events compared with Monte Carlo predictions.

11.3 Event displays for the data candidates

In figures 38 through 42 we show the events displays of a few of our candidate events. We have not yet added any further event displays from those shown in CDF-6611.

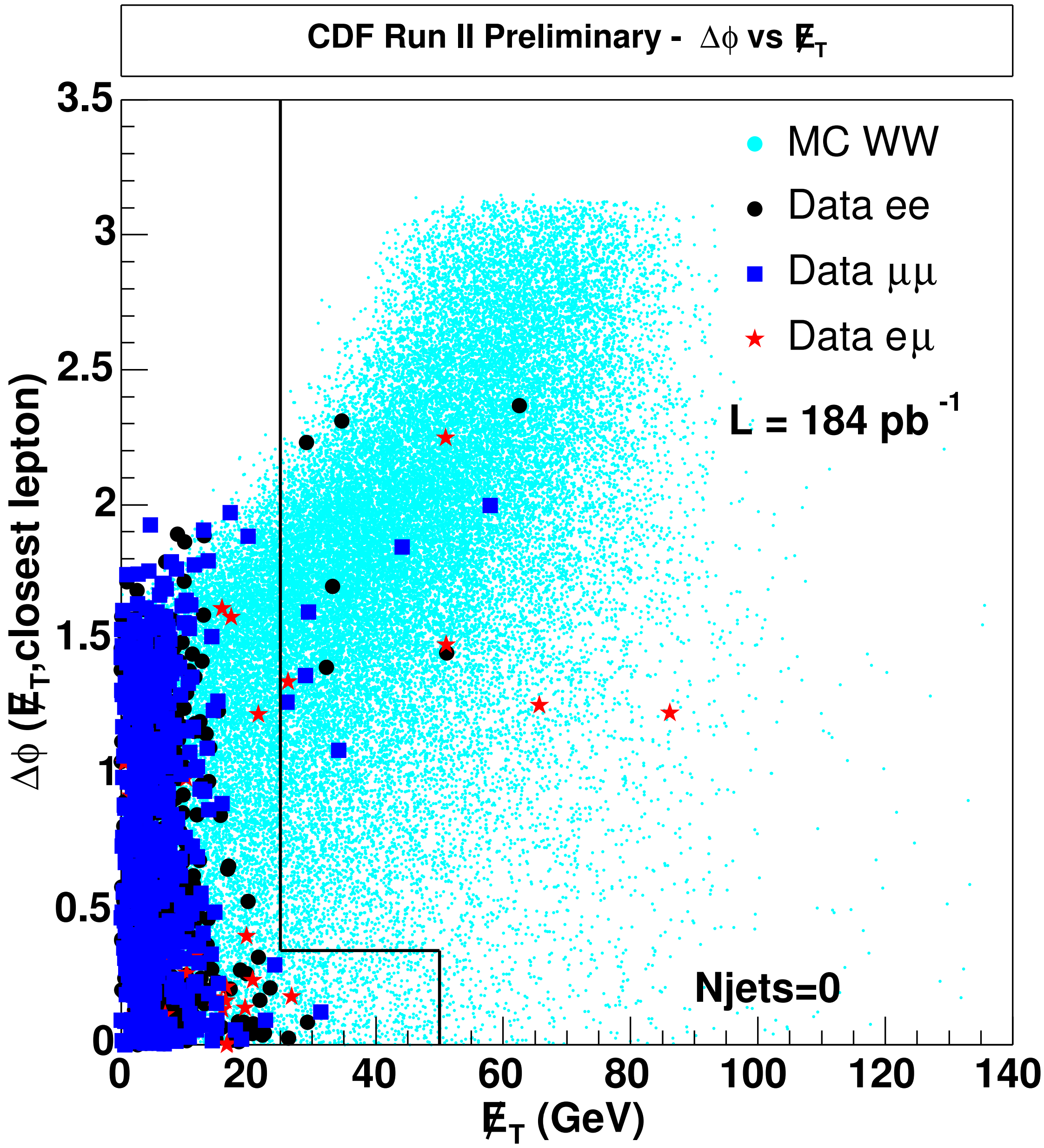

Figure 28: The azimuthal separation between the $\not\!\!E_T$ and the closest lepton or jet versus the $\not\!\!E_T$. The data is overlayed on the $WW \rightarrow l^+l^-\nu\bar{\nu}$ Monte Carlo expectation after all cuts except $\not\!\!E_T > 25$, $\Delta\phi(\not\!\!E_T$, nearest l or j) $> 20°$ if $\not\!\!E_T < 50$ GeV and opposite sign requirement.

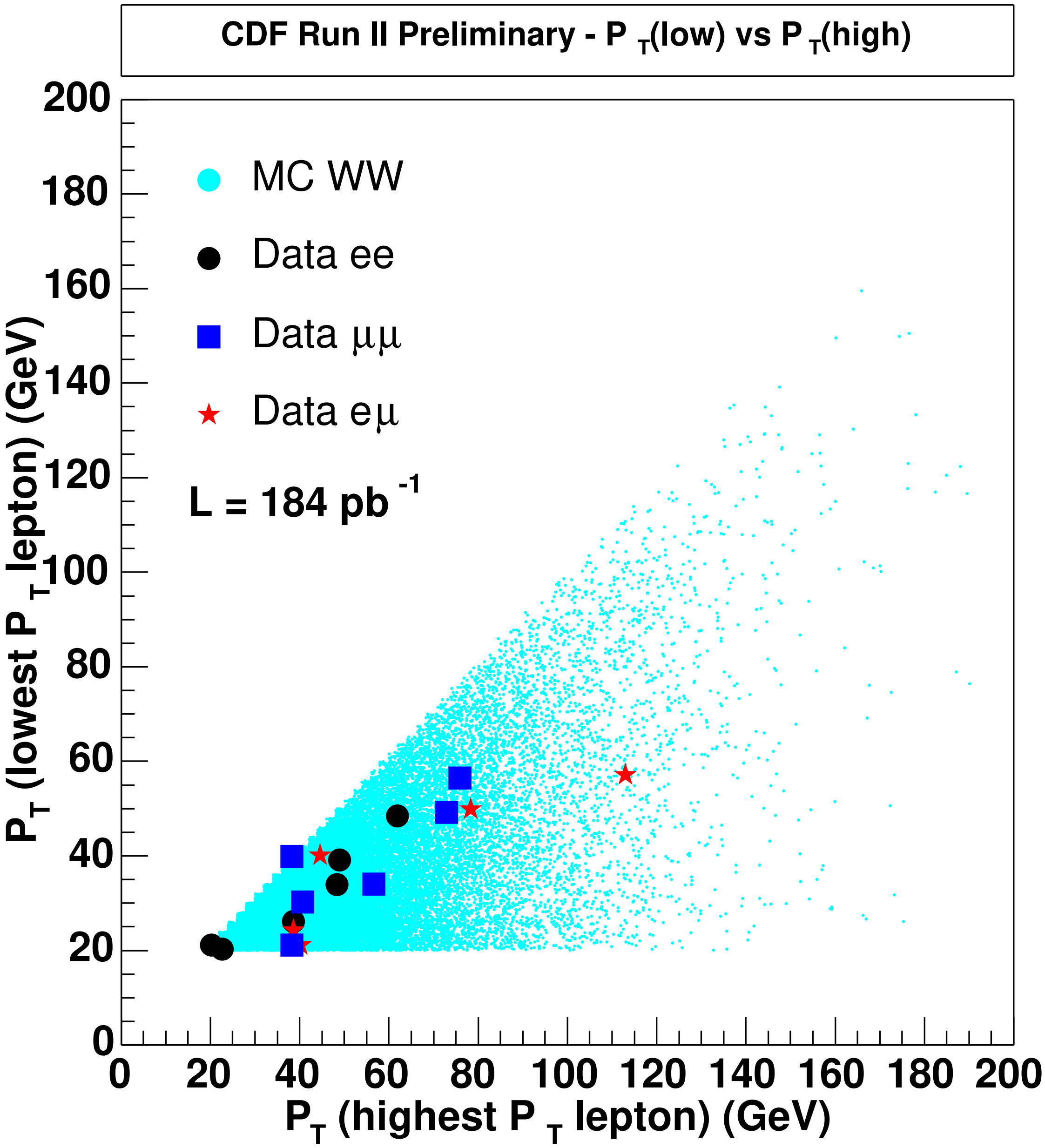

Figure 29: Correlation between P_T of the leading lepton and the second lepton. The data is overlayed on the $WW \to l^+l^-\nu\bar{\nu}$ Monte Carlo expectation after all cuts.

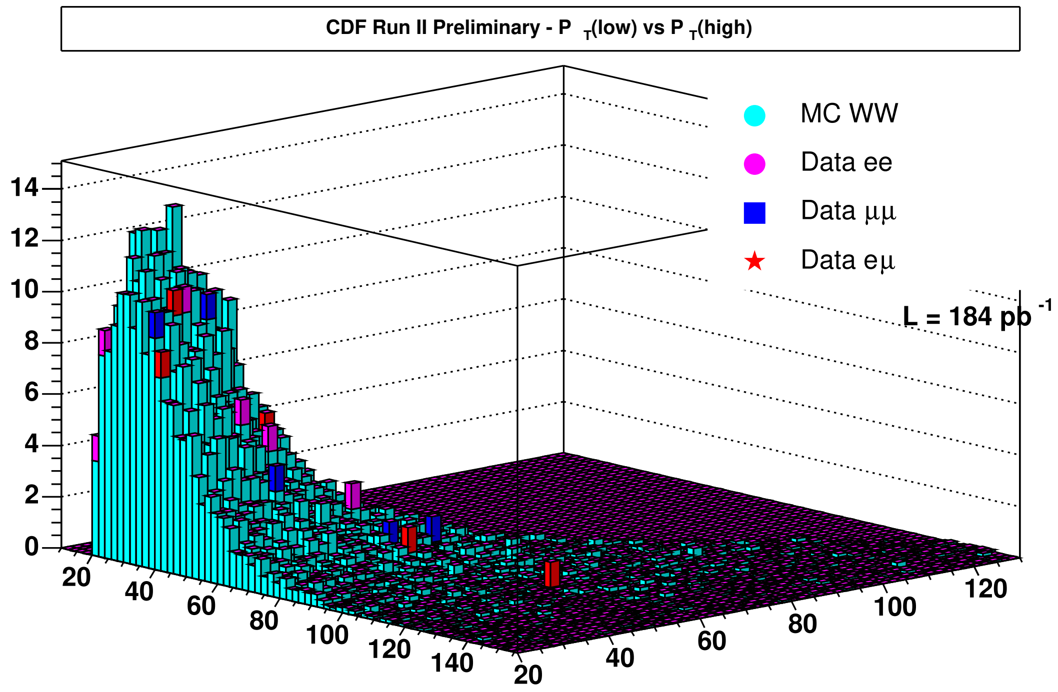

Figure 30: Lego version of figure 29. The WW Monte Carlo is scaled by 0.5 to make the candidates visible

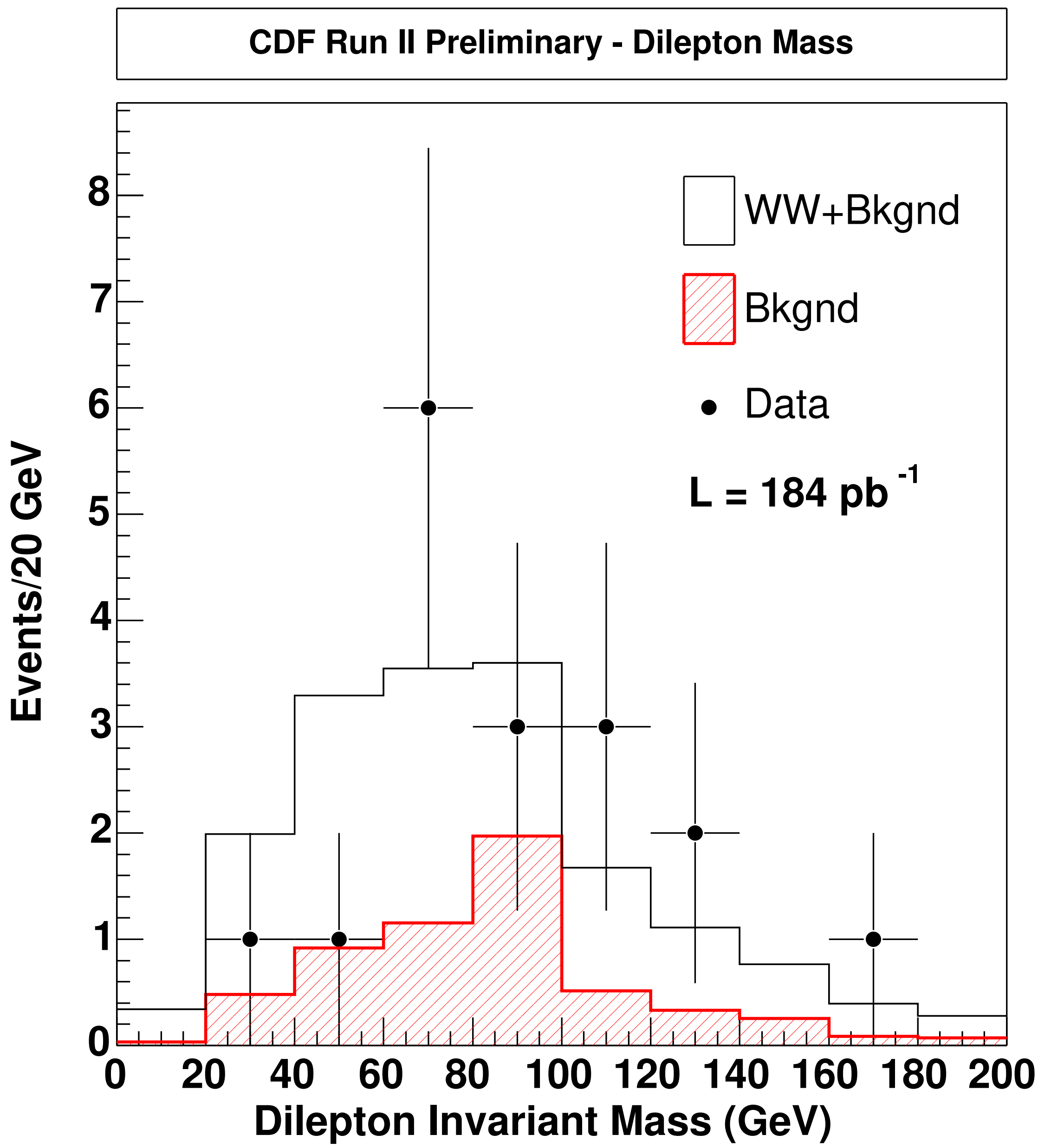

Figure 31: The dilepton invariant mass. The data is overlayed on the WW plus all backgrounds Monte Carlo expectation after all cuts(black line histogram). The solid histogram is backgrounds only.

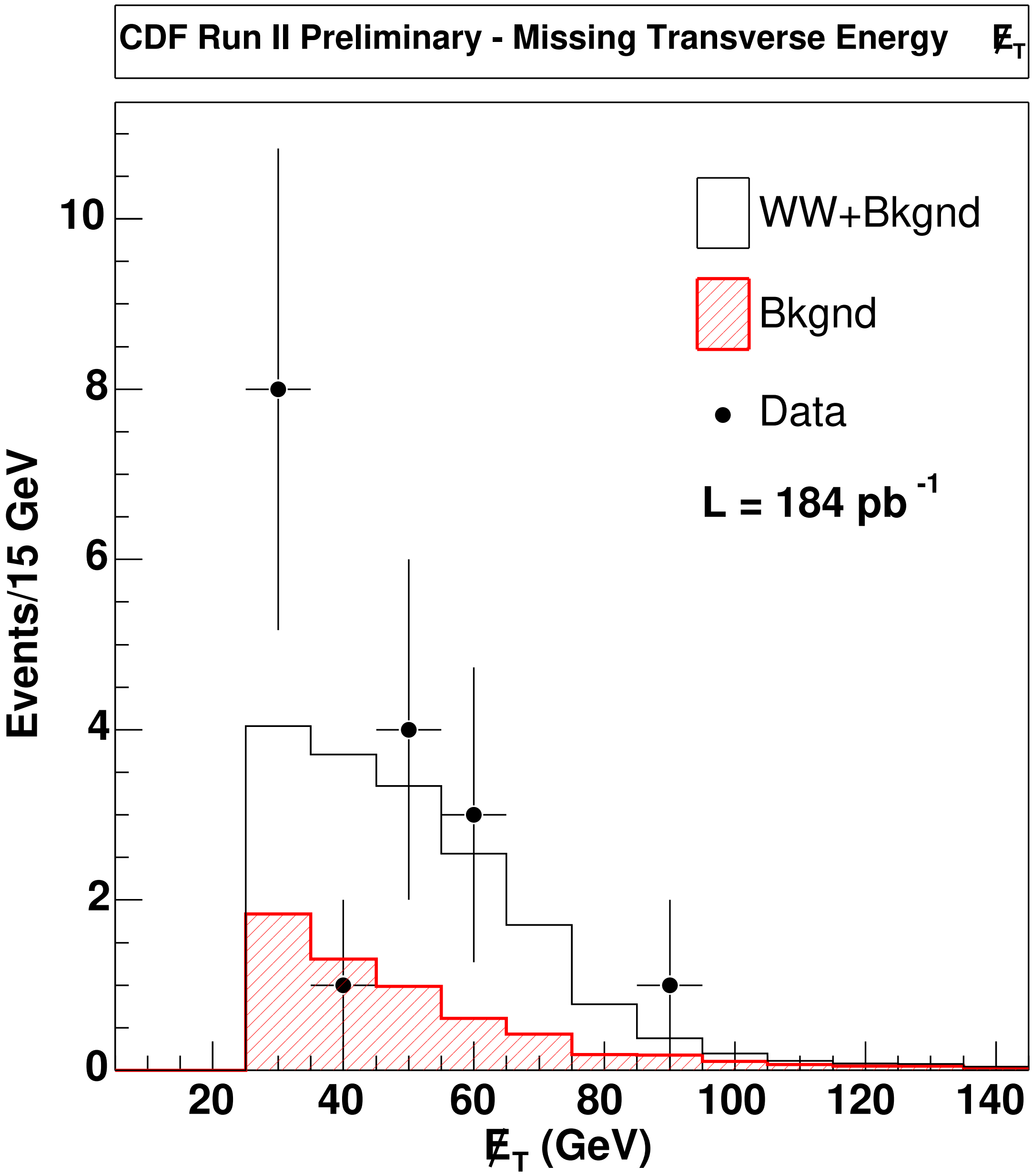

Figure 32: The missing transverse energy. The data is overlayed on the WW plus all backgrounds Monte Carlo expectation after all cuts(black line histogram). The solid histogram is backgrounds only.

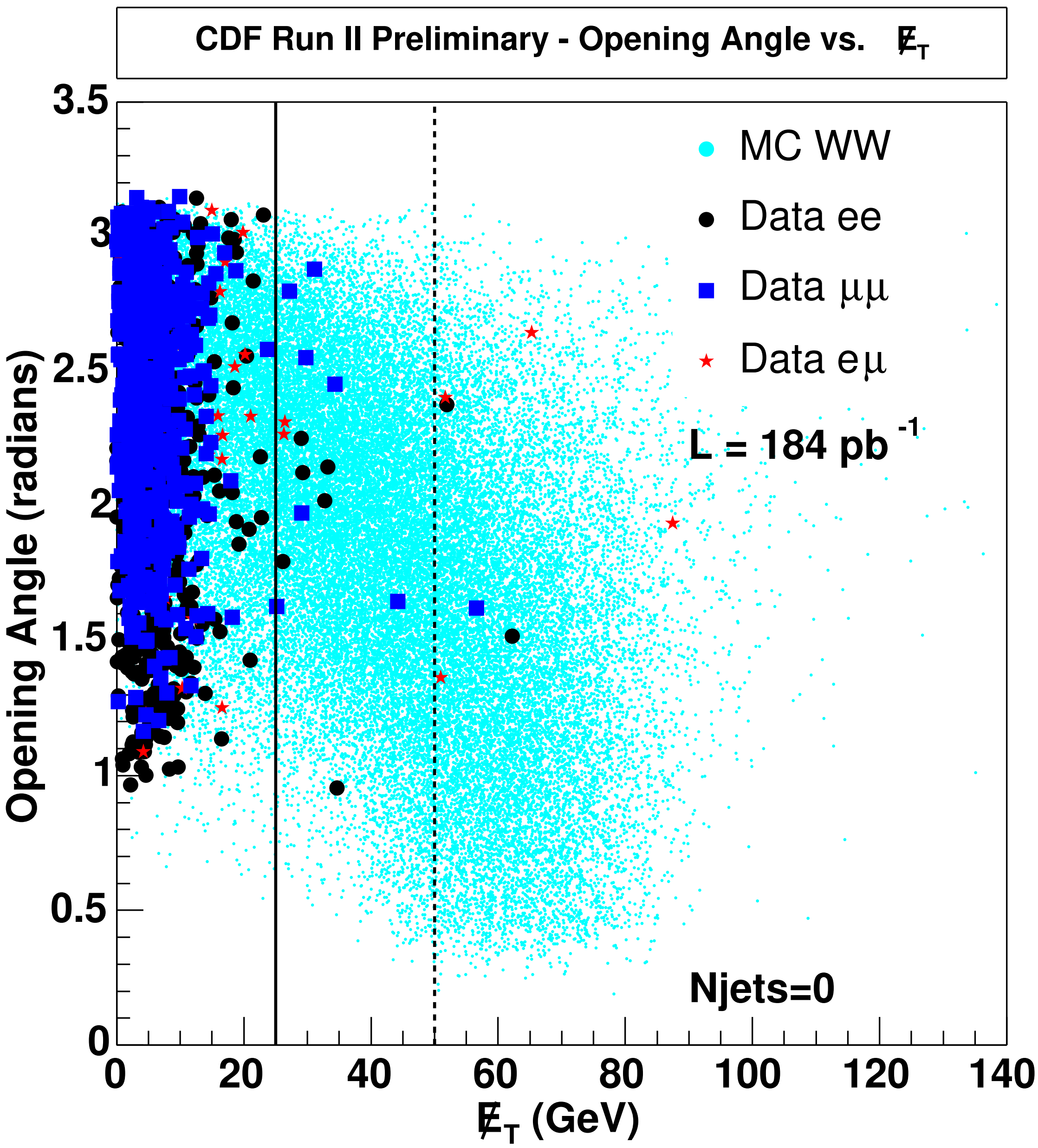

Figure 33: The opening angle of the two leptons versus the $\not\!\!E_T$. The data is overlayed on the $WW \to l^+l^-\nu\bar{\nu}$ Monte Carlo expectation after all cuts except $\not\!\!E_T > 25$, $\Delta\phi(\not\!\!E_T$, nearest l or j) $> 20°$ if $\not\!\!E_T < 50$ GeV and opposite sign requirement.

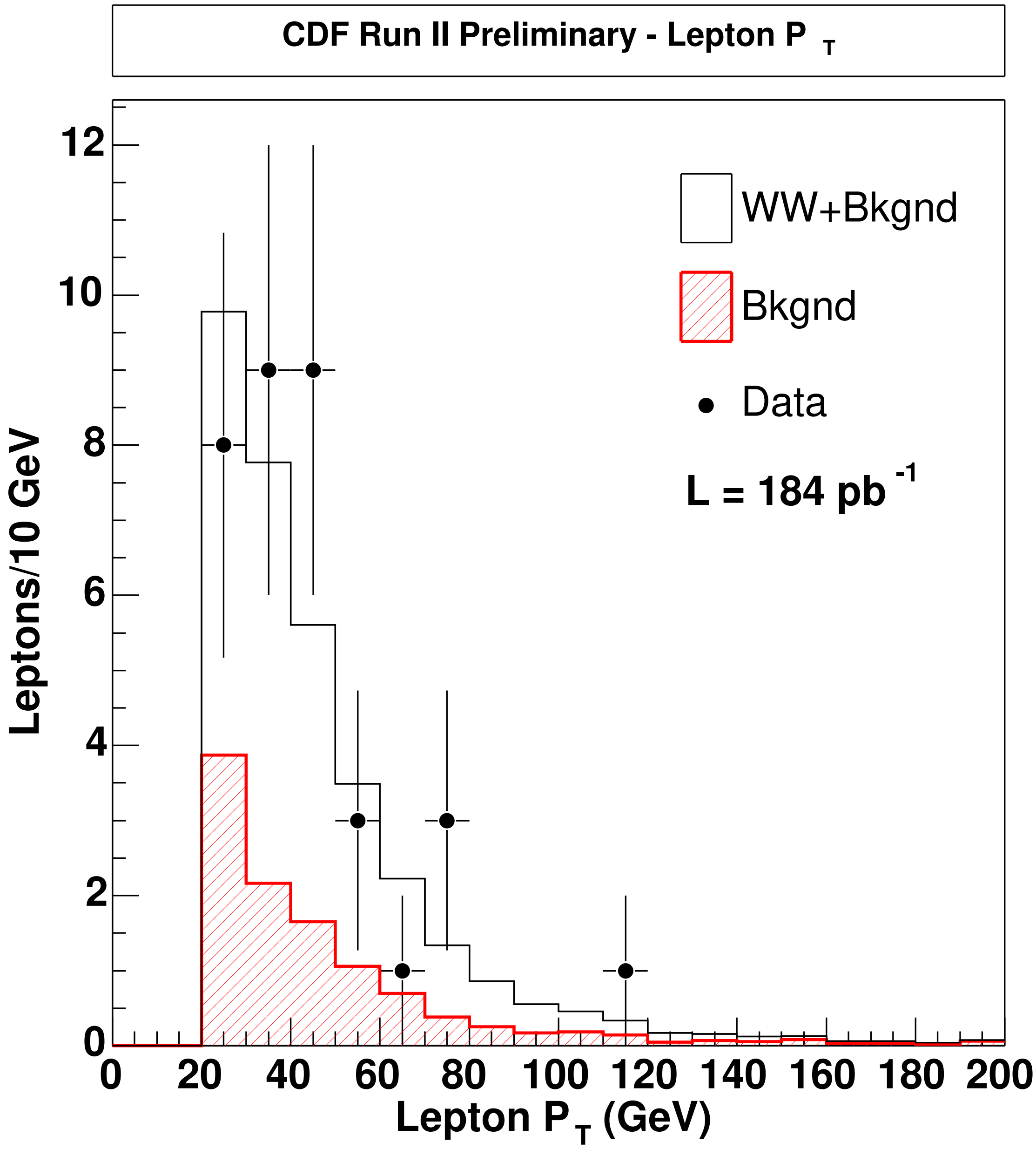

Figure 34: The transverse momentum of each lepton. The data is overlayed on the WW plus all backgrounds Monte Carlo expectation after all cuts(black line histogram). The solid histogram is backgrounds only.

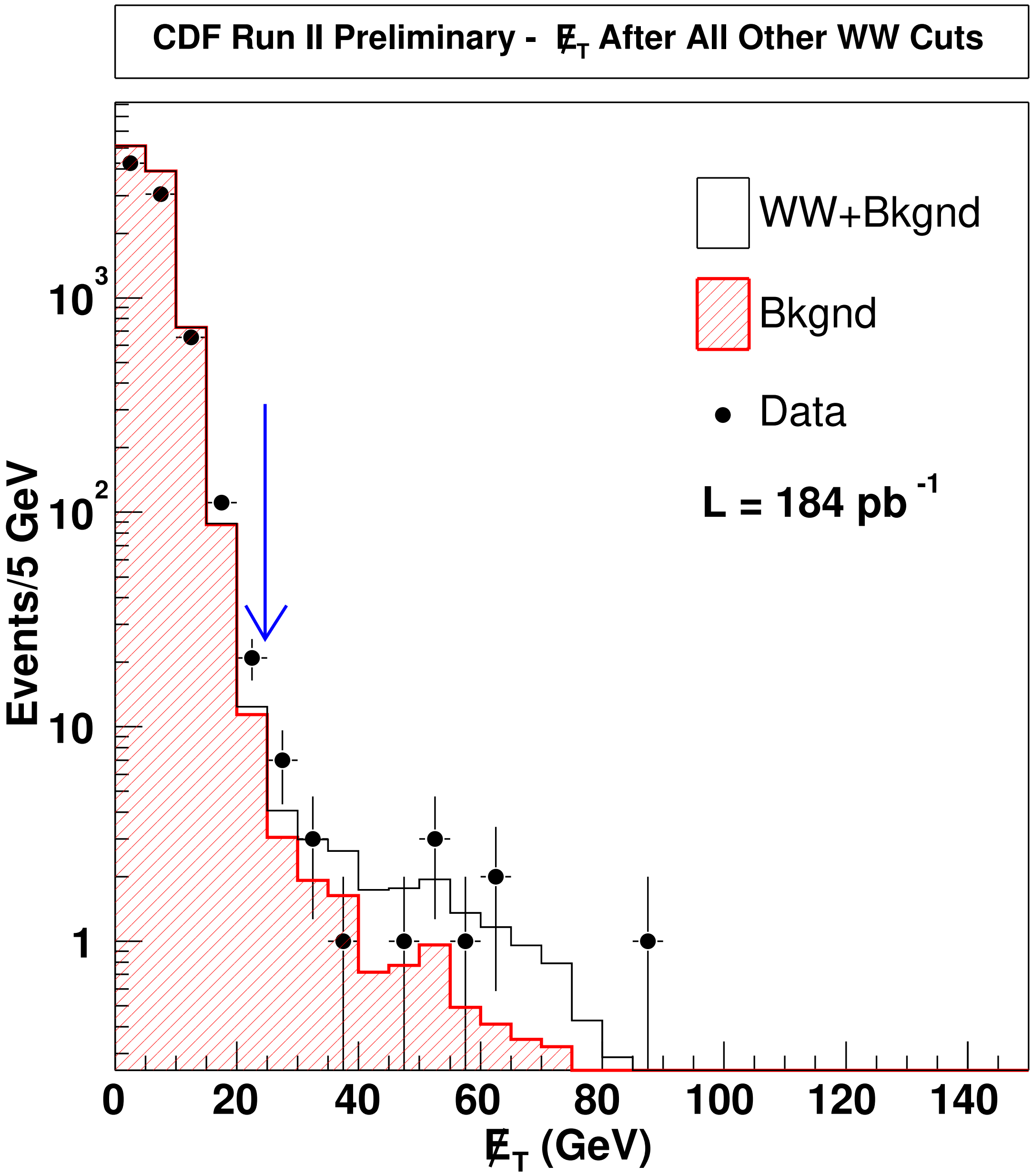

Figure 35: The missing transverse energy before $\not\!\!E_T$ and $\not\!\!E_T^{sig}$ cuts. The data is overlayed on the WW plus all backgrounds Monte Carlo expectation(black line histogram). The solid histogram is backgrounds only. All other WW cuts are applied.

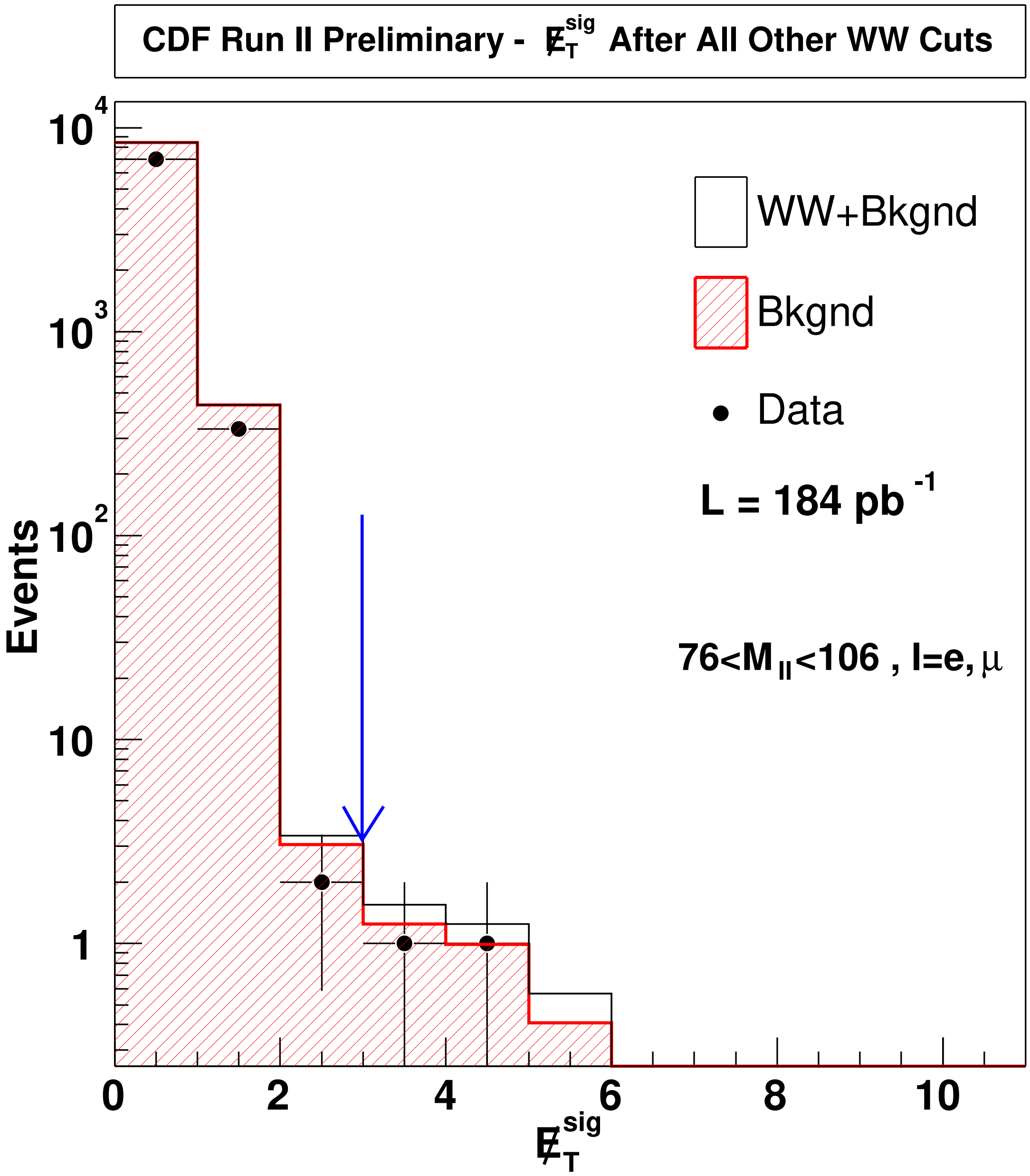

Figure 36: The missing transverse energy significance before the $\not{E}_T$ and $\not{E}_T^{sig}$ cuts. The data is overlayed on the WW plus all backgrounds Monte Carlo expectation (black line histogram). The solid histogram is backgrounds only. All other WW cuts are applied. Recall we only make the $\not{E}_T^{sig}$ cut to same flavor dilepton events in the Z window. We have 2 such events passing this cut.

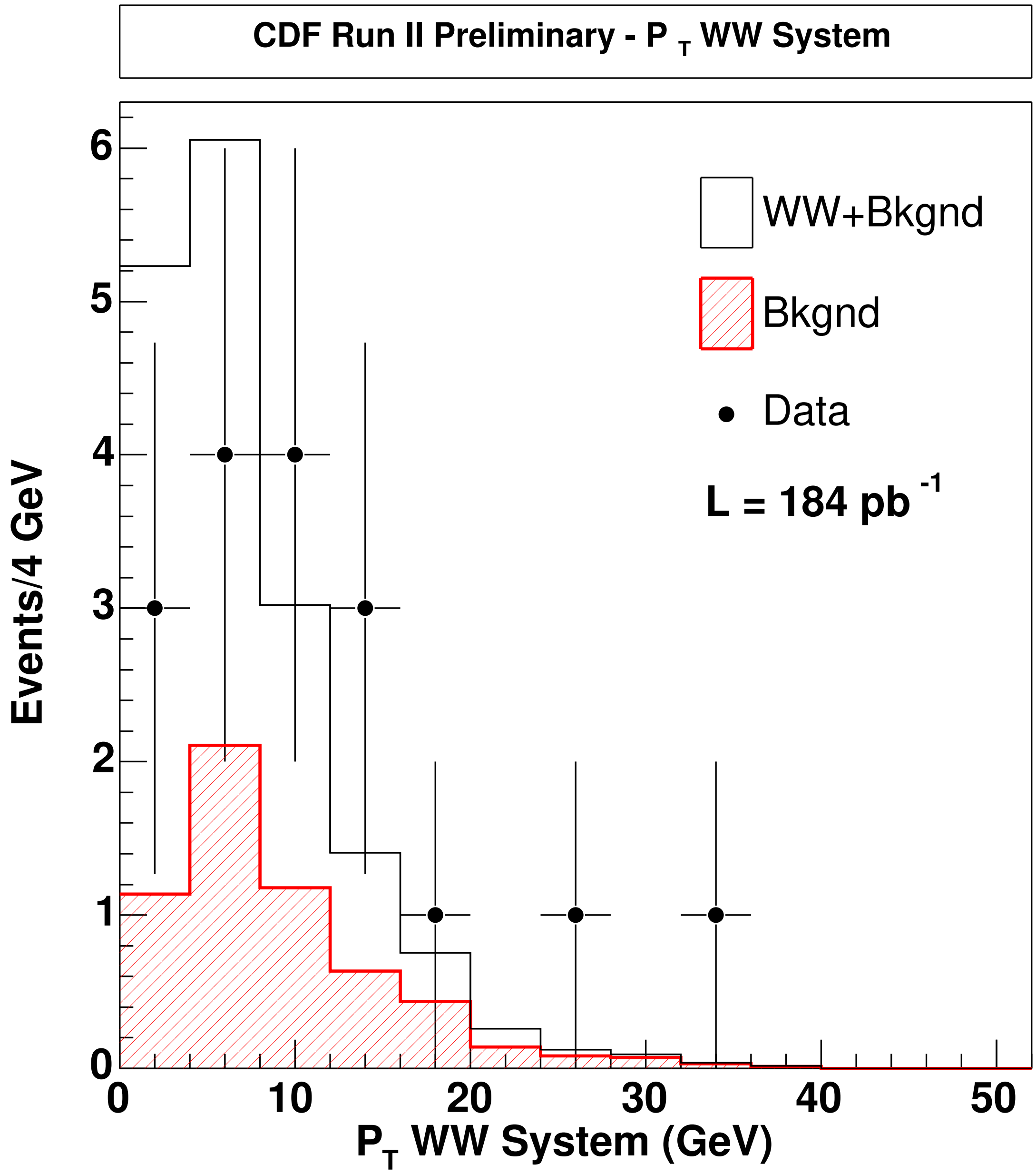

Figure 37: The transverse momentum of the WW system. The data is overlayed on the WW plus all backgrounds Monte Carlo expectation after all cuts(black line histogram). The solid histogram is backgrounds only.

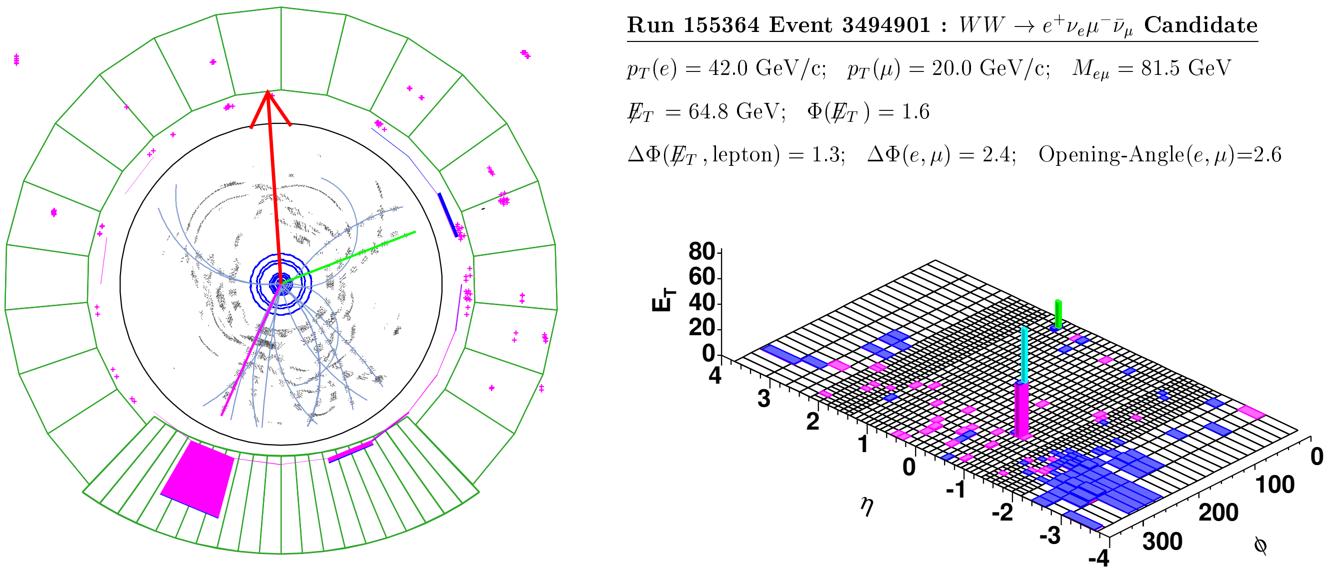

Figure 38: r-ϕ and lego views of the $WW \rightarrow e\mu$ candidate: Run, Event = 155364, 3494901.

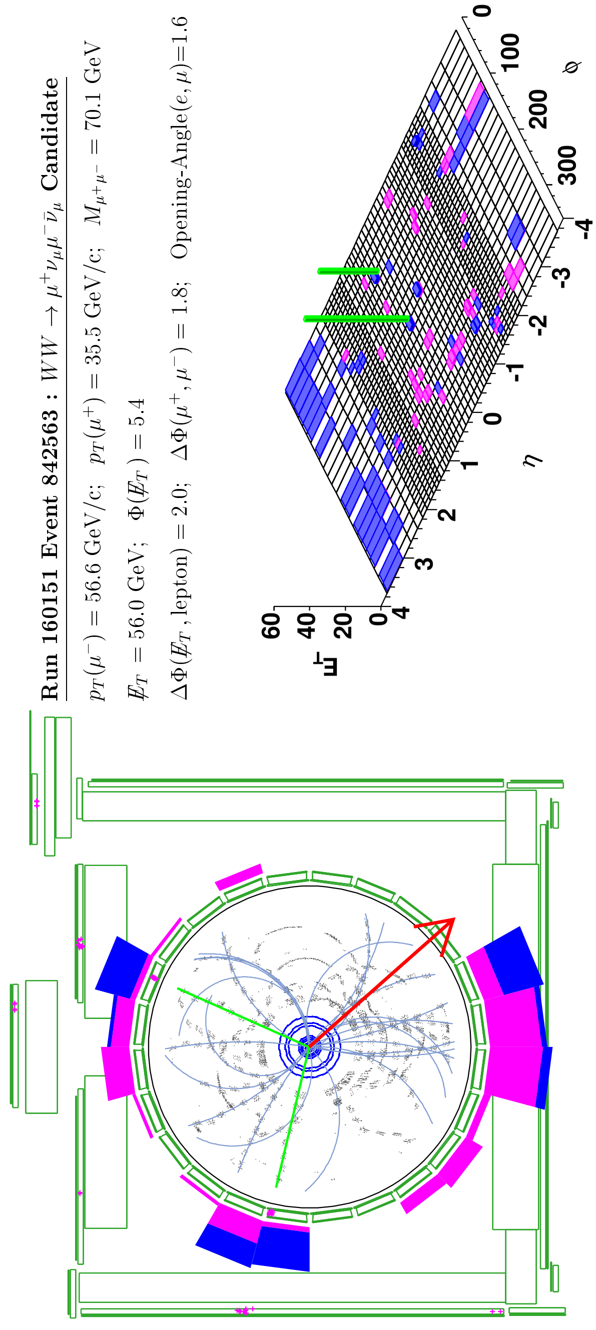

Figure 39: r-ϕ and lego views of the $WW \to \mu\mu$ candidate: Run, Event $= 160151, 842563$.

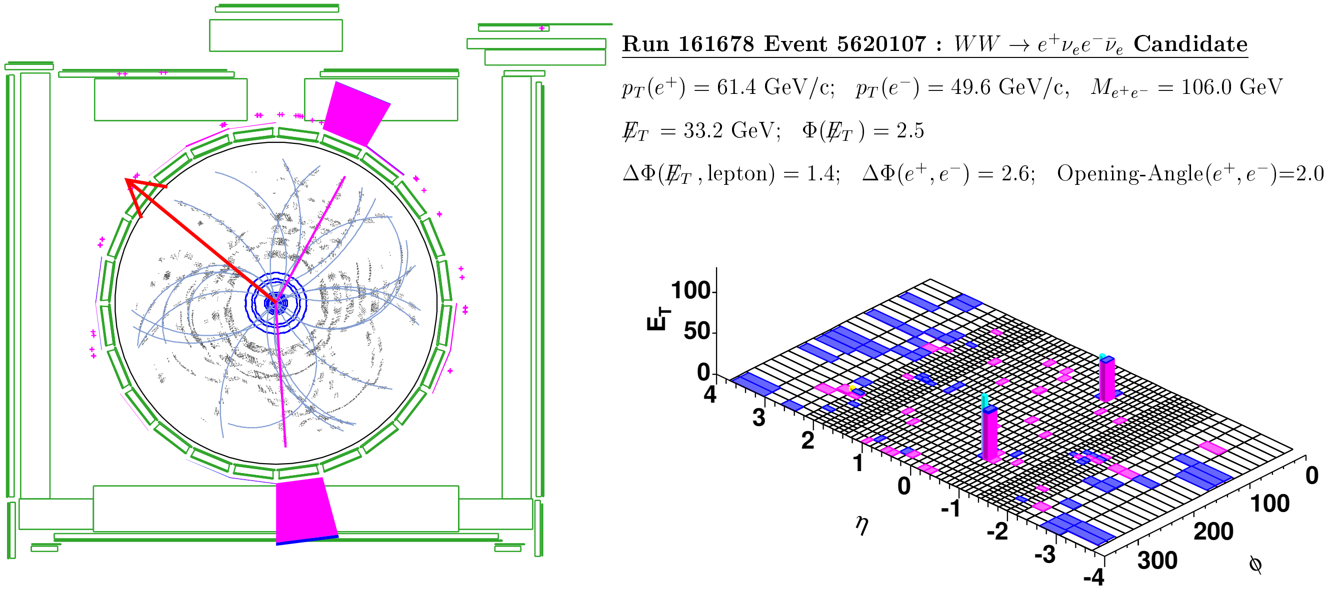

Figure 40: r-ϕ and lego views of the $WW \to ee$ candidate: Run, Event = 161678,5620107.

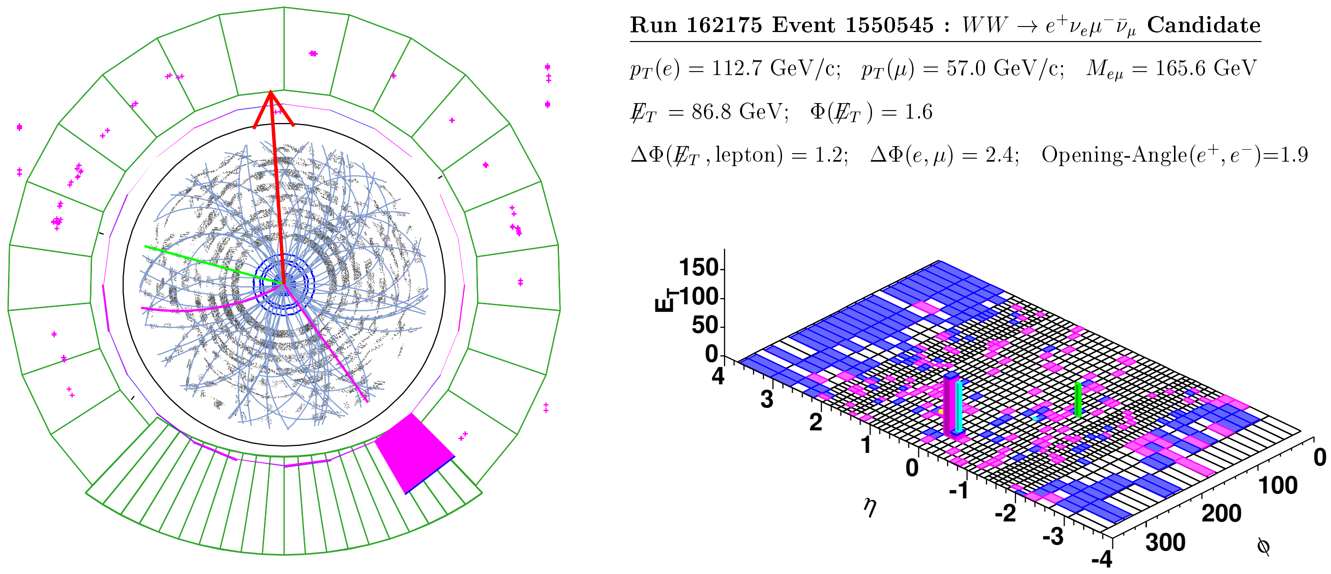

Figure 41: r-ϕ and lego views of the $WW \rightarrow e\mu$ candidate: Run, Event = 162175, 1550545.

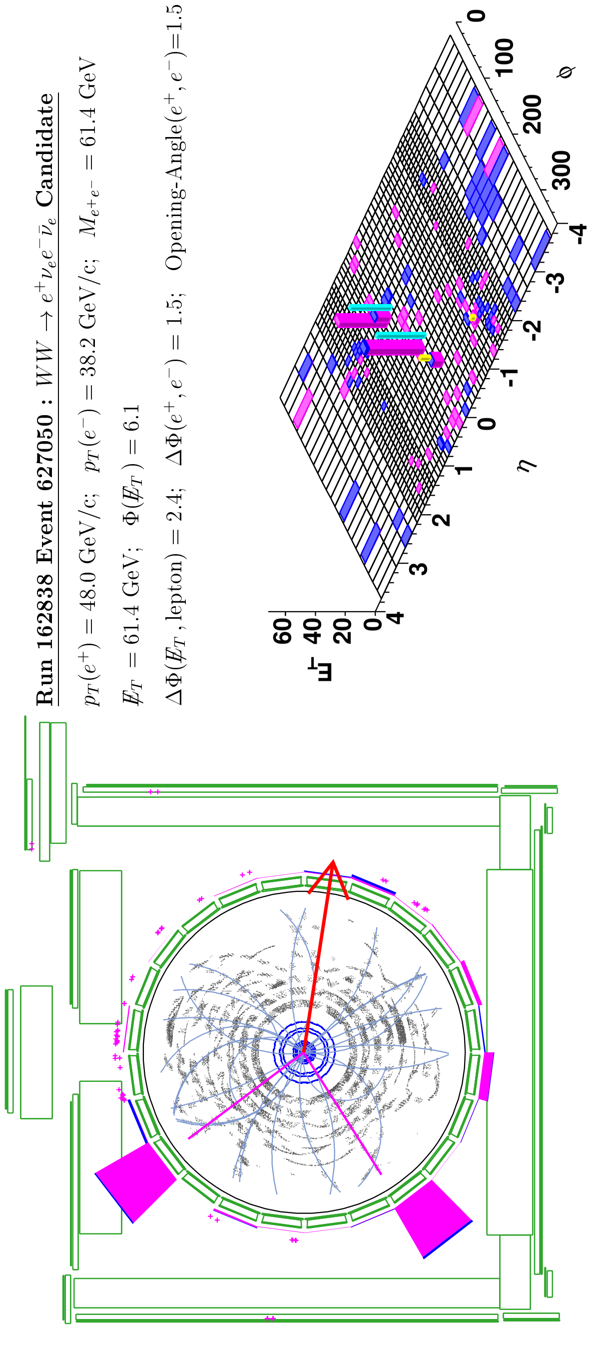

Figure 42: r-ϕ and lego views of the $WW \rightarrow ee$ candidate: Run, Event = 162838, 627050.

12 God-parents requests and answers

From the first god-parent meeting on Jan 8 2004, several questions and requests were raised which we here summarize and address. Note that a more comprehensive and constantly updated list of questions and answers is maintained here :

```
http://www-cdf.fnal.gov/internal/physics/WW/
      ww_dilepton_q_and_a/gp_q_and_a.html
```

12.1 Cross check of $\sigma \cdot B(p\bar{p} \to W \to \ell\nu)$ and $\sigma \cdot B(p\bar{p} \to Z \to \ell\ell)$

We have checked the selection of baseline electrons and muons for our WW analysis, by measuring $\sigma(p\bar{p} \to W) \cdot B(W \to \ell\nu)$ and $\sigma(p\bar{p} \to Z) \cdot B(Z \to \ell\ell)$ for our lepton and dilepton categories. We find results to be consistent with other CDF W/Z cross-section measurements, as well as the Standard Model predictions.

12.1.1 Data

The data collections and triggers we used for the W/Z cross-section measurements are the same as for WW analysis. The good run lists applied for each W/Z channel are shown in table 49.

12.1.2 MC Samples

We used MC samples from the cdfptop book of the Data File Catalog (DFC). We processed the on-tape files into Duke Ntuples in 4.11.1 and ran the same kinematic cuts on them as on data.

All the MC samples we used were generated using PYTHIA 6.2, with Rick Field's Tune A for underlying events. The CDF detector material configuration for them were default for cdfsoft2 version 4.9.1.

12.1.3 Cuts and Corrections

We selected $W^\pm \to \ell^\pm\nu$ and $Z \to \ell^+\ell^-$ events using exactly the same cuts as for WW analysis except that second Zee central electrons were loosely selected to improve statistics under the premise of not introducing significant backgrounds. One may refer to the tables of baseline lepton cuts in previous sections of this note or check the tables in this section for comparison of tight and loose lepton cuts and for the few additional cut(s) signifying W/Z event features.

We intended to do inclusive W/Z cross-check analyses, so did not apply the 0-jet requirement. Hence we corrected $\not\!\!E_T$ not for jets but only for muons and plug electrons.

For $W \to \ell\nu$, we required $\not\!\!E_T$ to be above the same value as E_T to reflect the fact that ℓ and ν should fly back-to-back in the rest-frame of W with almost equal fraction of transverse energy.

W/Z Channel	Good Run Condition	Luminosity $\pm$ Error (1/pb)
$W \to e\nu$ PHX	$e \cap \mu$ Good Silicon	161.8 ± 1.0
$W \to e\nu$ TCE	$e \cap \mu$ No Silicon	195.3 ± 1.2
$W \to \mu\nu$ CMUP		
$Z \to ee$ TCE-LCE		
$Z \to ee$ TCE-PHX		
$Z \to \mu\mu$ CMUP		
$Z \to \mu\mu$ CMX	$e \cap \mu$ CMX, No Si	175.3 ± 1.1
$W \to \mu\nu$ CMX		

Table 49: Integrated offline luminosities (after 1.019 correction) for each W/Z channel.

Channel		Dataset ID	Simulated Process
$W \to e\nu$	TCE and PHX	`wtop0e`	inclusive $W \to e\nu$
$W \to \mu\nu$	CMUP and CMX	`wtop0m`	inclusive $W \to \mu\nu$
$Z \to ee$	TCE LCE and TCE PHX	`ztop0e`	inclusive Drell-Yan $Z \to ee$
$Z \to \mu\mu$	CMUPmuon and CMXmuon	`ztop0m`	inclusive Drell-Yan $Z \to \mu\mu$

Table 50: Monte Carlo samples we used for W/Z cross-check.

$W \to e\nu$ Tight Central	$Z \to ee$ 2nd Central
detector region == CEM	detector region == CEM
$E_T > 20$ GeV	$E_T > 20$ GeV
$p_t > 10$ GeV	$p_t > 10$ GeV
$E_{had}/E_{em} < 0.055 + 0.00045E$	$E_{had}/E_{em} < 0.055 + 0.00045E$
$p_t > 50$ GeV $\|\|$ $E/p < 2.0$	
$L_{shr} < 0.2$	$L_{shr} < 0.2$
$-3.0 < Q\Delta x < 1.5$ cm	$-3.0 < Q\Delta x < 1.5$ cm
$\|\Delta z\| < 3.0$ cm	$\|\Delta z\| < 3.0$ cm
$\chi^2_{\mathrm{strip}} < 10$	
fidEle == 1	fidEleShrMax == 1
$\|z_0\| < 60.0$ cm	$\|z_0\| < 60.0$ cm
$N_{\text{st s.l. hits}} \geq 7$ and $N_{\text{ax s.l. hits}} \geq 7$ and $N_{\text{super layer}} \geq 3$ for each	$N_{\text{st s.l. hits}} \geq 7$ and $N_{\text{ax s.l. hits}} \geq 7$ and $N_{\text{super layer}} \geq 3$ for each
non-conversion	non-conversion
$\mathrm{Isolation}_{\Delta R=0.4} < 0.1$	$\mathrm{Isolation}_{\Delta R=0.4} < 0.1$
$\not{E}_T > 20$ GeV	
	opposite sign of charge
	$66 < M_{ee} < 116$ GeV

Table 51: Cuts for tight and loose central electrons.

For $W \to \mu\nu$ we removed one-legged $Z \to \mu\mu$ events in the following way. If in one event we found any additional tracks with $p_t > 10$ GeV, $E_{em} < \max(3, 3 + .014(p - 100))$ GeV and $E_{had} < \max(6, 6 + .042(p - 100))$ GeV, we vetoed the event.

We did not apply any cut on the transverse mass of reconstructed W.

For $Z \to \ell\ell$, we additionally required (a) the two lepton candidates to be of opposite charge signs and same flavors and (b) the reconstructed dilepton invariant mass to sit within a window of $66 < M_Z < 116$.

For $Z \to \mu\mu$ we additionally required $|\Delta z_0| < 4$ cm between the two muons; we cut negligible fraction of candidates with this cut though.

12.1.4 Backgrounds

We referred to the W/Z cross-section group's notes for thorough W/Z background studies. The major backgrounds to $W \to \ell\nu$ considered were QCD fakes, $Z/\gamma^* \to \ell\ell$ mis-measurement (one-legged) and $W \to \tau\nu \to \ell\nu\nu\nu$. The major backgrounds to $Z \to \ell\ell$ considered were QCD fakes, $Z/\gamma^* \to \tau\tau \to \ell\ell\nu\nu\nu\nu$ and $W \to \ell\nu$ mis-measurement. We adopted their W/Z background fractions for our cross-check $\sigma \cdot B(p\bar{p} \to W \to \ell\nu)$ and $\sigma \cdot B(p\bar{p} \to Z \to \ell\ell)$ with reference to [25], [27], [18], [26], [28] and [29].

12.1.5 Trigger Efficiencies

The standard trigger efficiencies were used. Please refer to table 8.

12.1.6 Acceptance $\times$ ID efficiencies

We ran about 0.36M MC events for each process through the same kinematic cuts as for data to get acceptance $\times$ ID efficiencies, $A\epsilon_{\mathrm{ID}}$. We applied data/MC scale factors, as shown in table 8, to adjust the acceptance $\times$ ID efficiencies.

For the Z acceptance $\times$ ID efficiencies, we only considered the events with $66 < {M_Z}^{\mathrm{true}} < 116$ from the Drell-Yan Z MC samples as input. We applied a factor of 1.004 ± 0.001 [19] to the number of input MC Z events to account for the fraction of events with $66 < {M_Z}^{\mathrm{true}} < 116$ in true Z events.

12.1.7 Results

The formula we used to calculate the W/Z cross-section $\times$ branching ratio is given below

$$\sigma \cdot B \quad = \quad \frac{N_{\mathrm{signal}}(1 - p_{\mathrm{bg}})}{\mathcal{L}_{\mathrm{int}} \cdot \epsilon_{\mathrm{trigger}} \cdot f_{\mathrm{data/MC}} \cdot \mathcal{A}\epsilon_{\mathrm{ID}}}$$

Our results on $\sigma(p\bar{p} \to W) \cdot B(W \to \ell\nu)$ and $\sigma(p\bar{p} \to Z) \cdot B(Z \to \ell\ell)$ are listed in table 54 and 55.

Figures 43 and 44 show that the W and Z cross-sections are reasonably constant with integrated luminosity. Figures 45 and 46 show the same data but with smaller bin sizes.

Figures 47 and 48 show the yield of W's and Z's versus time with the same binning as reference [29] for comparison.

For $W^{\pm} \to \ell^{\pm}\nu$ distributions of the lepton track η and lepton E_T of the candidates are shown in figure 49 and figure 50 respectively.

For $Z \to \ell^{+}\ell^{-}$ the invariant mass $M_{\ell\ell}$ distribution of the candidates is shown in figure 51. In figure 52 we present the same-sign $M_{\ell\ell}$ distribution and the η distribution of the Phoenix electron tracks from "$Z \to \ell^{\pm}\ell^{\pm}$ ".

12.1.8 Conclusion from W and Z cross-section checks

We compare our results to the W/Z cross-section group's latest blessed results at $\sqrt{s} =$ 1.96 TeV, quoted from [27], [18], [26] and [28]:

$$
\begin{aligned}
\sigma \cdot B_{\mathrm{TCE}}(p\bar{p} \to W \to e\nu) &= 2.753 \pm 0.015_{\mathrm{stat}} \pm 0.084_{\mathrm{syst}} \pm 0.165_{\mathrm{lumi}}\ \mathrm{nb} \\
\sigma \cdot B_{\mathrm{plug}}(p\bar{p} \to W \to e\nu) &= 2.874 \pm 0.034_{\mathrm{stat}} \pm 0.167_{\mathrm{syst}} \pm 0.172_{\mathrm{lumi}}\ \mathrm{nb} \\
\sigma \cdot B_{\mathrm{CMUP}}(p\bar{p} \to W \to \mu\nu) &= 2.781 \pm 0.019_{\mathrm{stat}} \pm 0.102_{\mathrm{syst}} \pm 0.166_{\mathrm{lumi}}\ \mathrm{nb} \\
\sigma \cdot B_{\mathrm{CMX}}(p\bar{p} \to W \to \mu\nu) &= 2.755 \pm 0.028_{\mathrm{stat}} \pm 0.076_{\mathrm{syst}} \pm 0.165_{\mathrm{lumi}}\ \mathrm{nb} \\
\sigma \cdot B_{\mathrm{TCE\text{-}LCE}}(p\bar{p} \to Z \to ee) &= 0.2609 \pm 0.0063_{\mathrm{stat}} \pm 0.0067_{\mathrm{syst}} \pm 0.0157_{\mathrm{lumi}}\ \mathrm{nb} \\
\sigma \cdot B_{\mathrm{TCE\text{-}PEM}}(p\bar{p} \to Z \to ee) &= 0.2484 \pm 0.0051_{\mathrm{stat}} \pm 0.0078_{\mathrm{syst}} \pm 0.0148_{\mathrm{lumi}}\ \mathrm{nb} \\
\sigma \cdot B_{\mathrm{CMUP}}(p\bar{p} \to Z \to \mu\mu) &= 0.251 \pm 0.007_{\mathrm{stat}} \pm 0.009_{\mathrm{syst}} \pm 0.015_{\mathrm{lumi}}\ \mathrm{nb} \\
\sigma \cdot B_{\mathrm{CMX}}(p\bar{p} \to Z \to \mu\mu) &= 0.261 \pm 0.010_{\mathrm{stat}} \pm 0.010_{\mathrm{syst}} \pm 0.016_{\mathrm{lumi}}\ \mathrm{nb}
\end{aligned}
$$

We find good overall consistency.

Our results also compare well to the Standard Model predictions at $\sqrt{s} = 1.96$ TeV:

$$
\begin{aligned}
\sigma \cdot B_{\mathrm{SM}}(p\bar{p} \to W \to \ell\nu) = 2.731\ \mathrm{nb} \\
\sigma \cdot B_{\mathrm{SM}}(p\bar{p} \to Z \to \ell\ell) = 0.2505\ \mathrm{nb}
\end{aligned}
$$

We thus conclude that the baseline electron and muon selection methods for our WW analysis are valid, yielding consistent results of inclusive $\sigma \cdot B(p\bar{p} \to W \to \ell\nu)$ and $\sigma \cdot B(p\bar{p} \to Z \to \ell\ell)$ with other CDF measurements.

12.2 Data cross check of Drell-Yan background estimate

We included this cross check in section 5.4, and added a systematic to the DY estimate accordingly. This is all explained in that section.

12.3 Data cross check of Jet Veto systematic

We have now included this cross check in section 8.1, by applying the WW Monte Carlo, the ratio of 0-jet fractions in Drell-Yan MC to data. See that section for details.

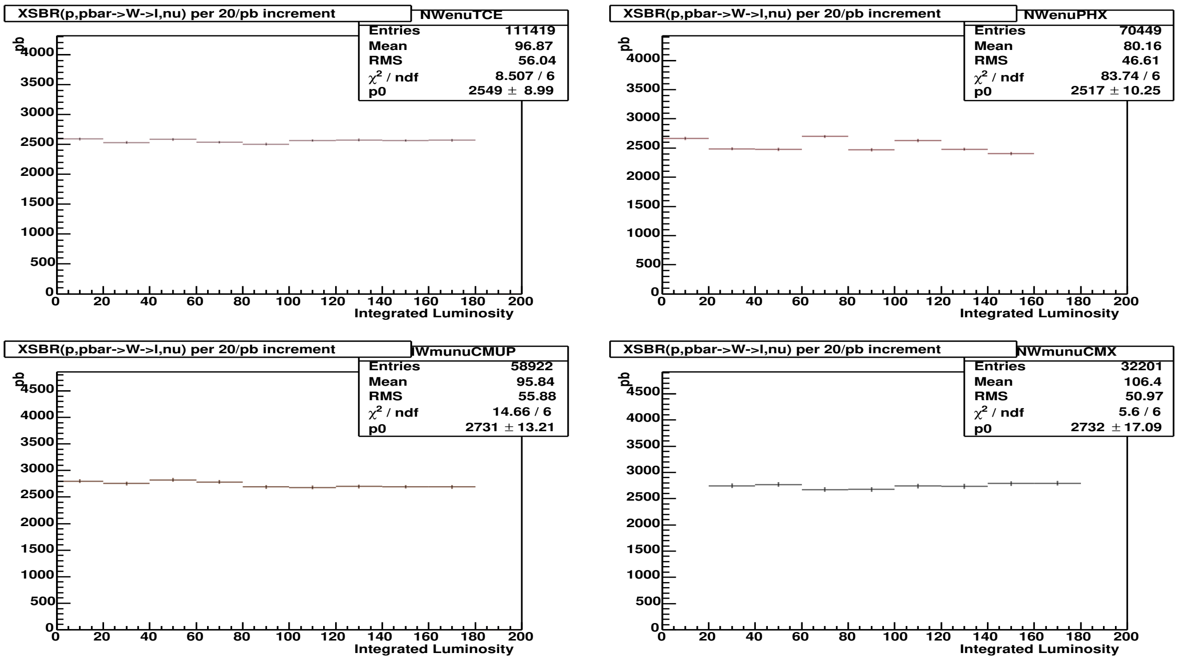

Figure 43: W cross-section measured per 20 pb^{-1} as a function of integrated luminosity, scale factors not applied.

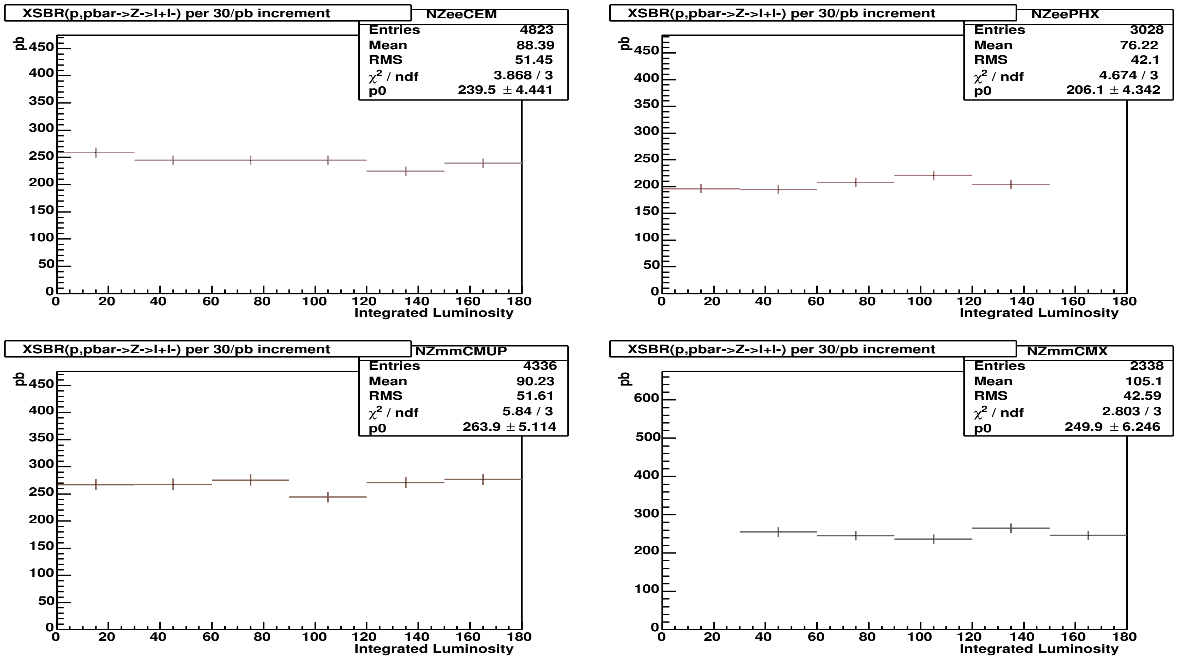

Figure 44: Z cross-section measured per 30 pb^{-1} as a function of integrated luminosity, scale factors not applied.

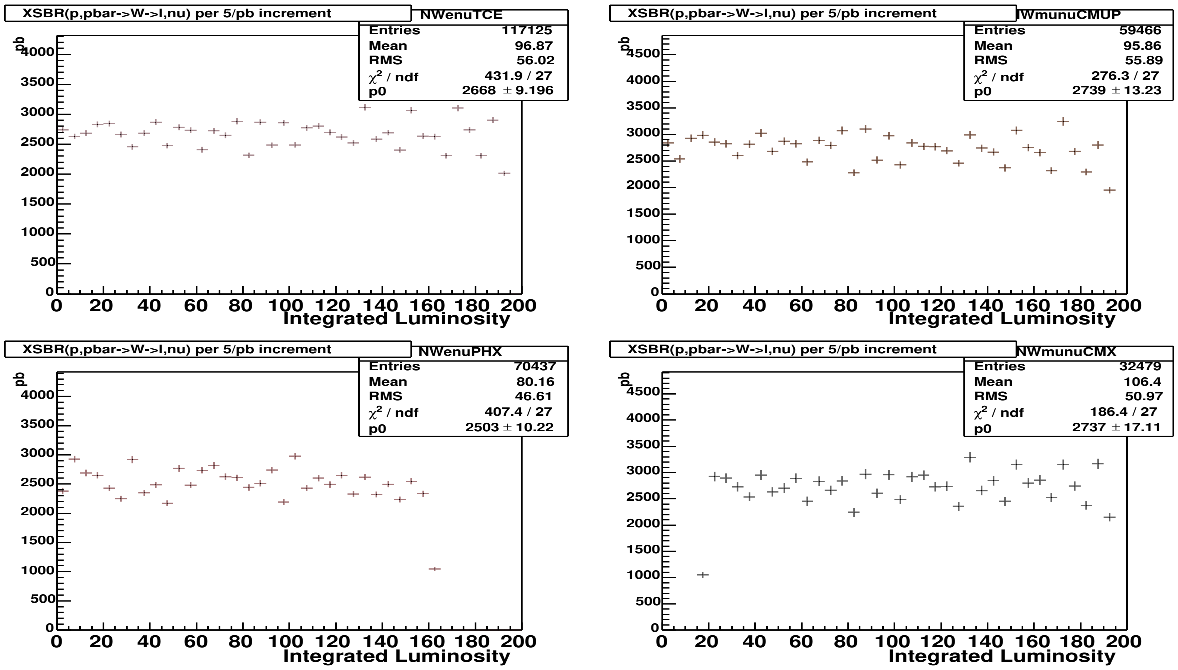

Figure 45: W cross-section measured per 5 pb^{-1} as a function of integrated luminosity, scale factors not applied.

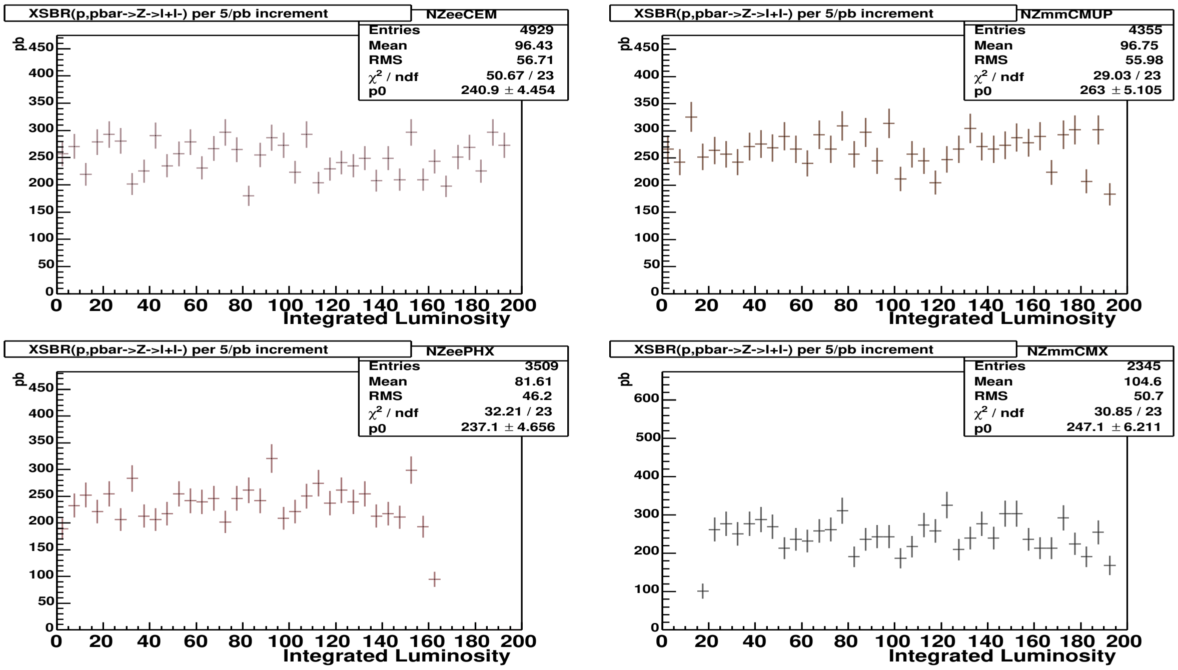

Figure 46: Z cross-section measured per 5 pb^{-1} as a function of integrated luminosity, scale factors not applied.

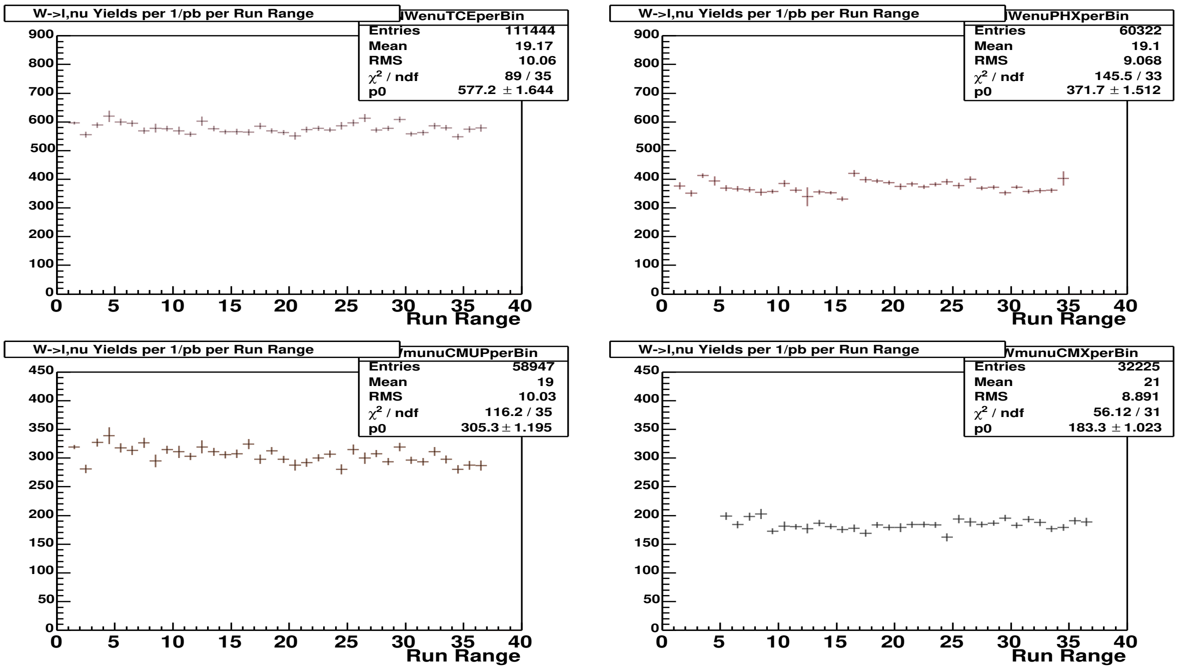

Figure 47: The yield of the $W \to \ell\nu$ candidates per pb^{-1} as a function of time.

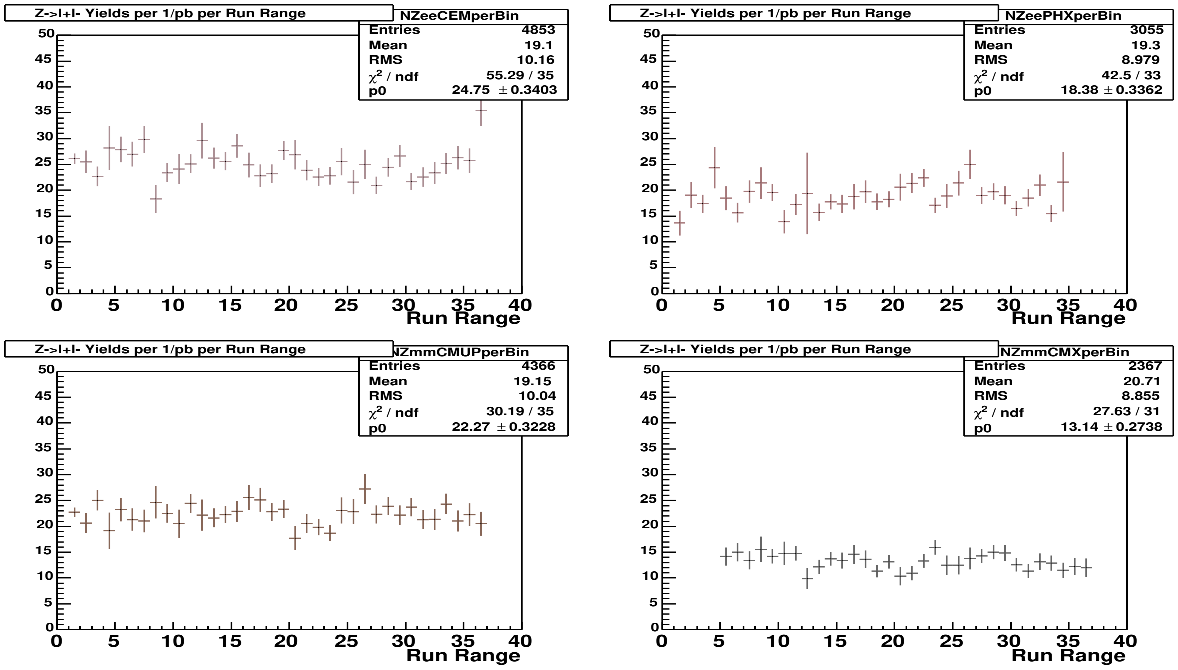

Figure 48: The yield of the $Z \to \ell\ell$ candidates per pb^{-1} as a function of time.

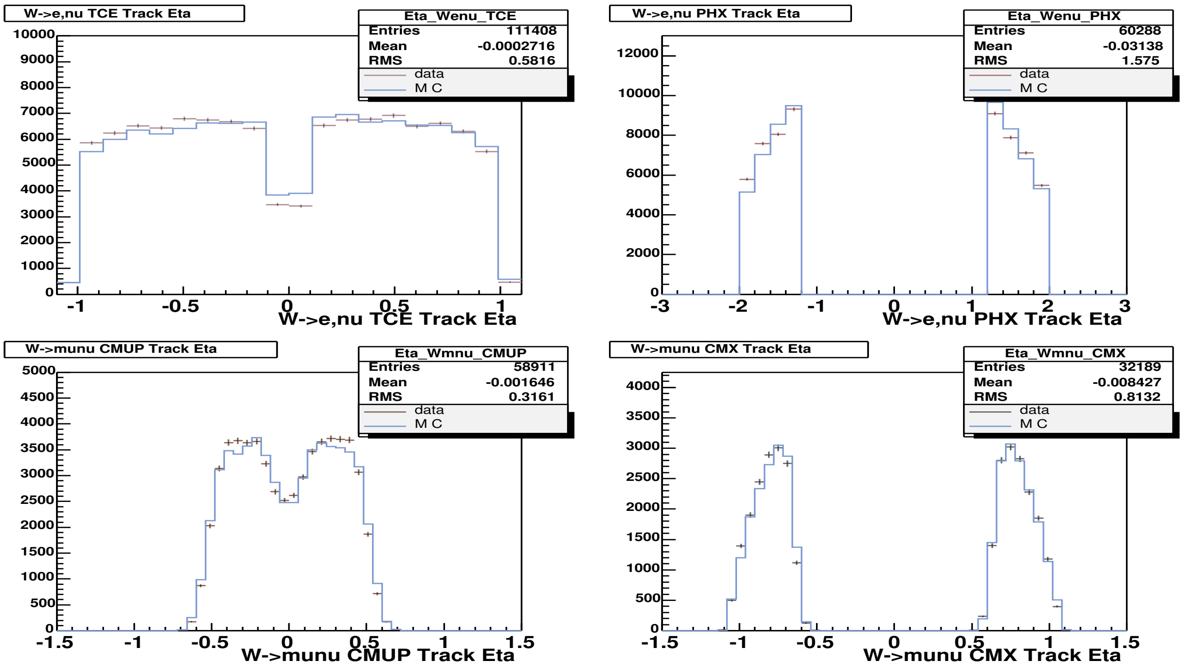

Figure 49: The η distribution of the $W \to \ell\nu$ candidate lepton tracks.

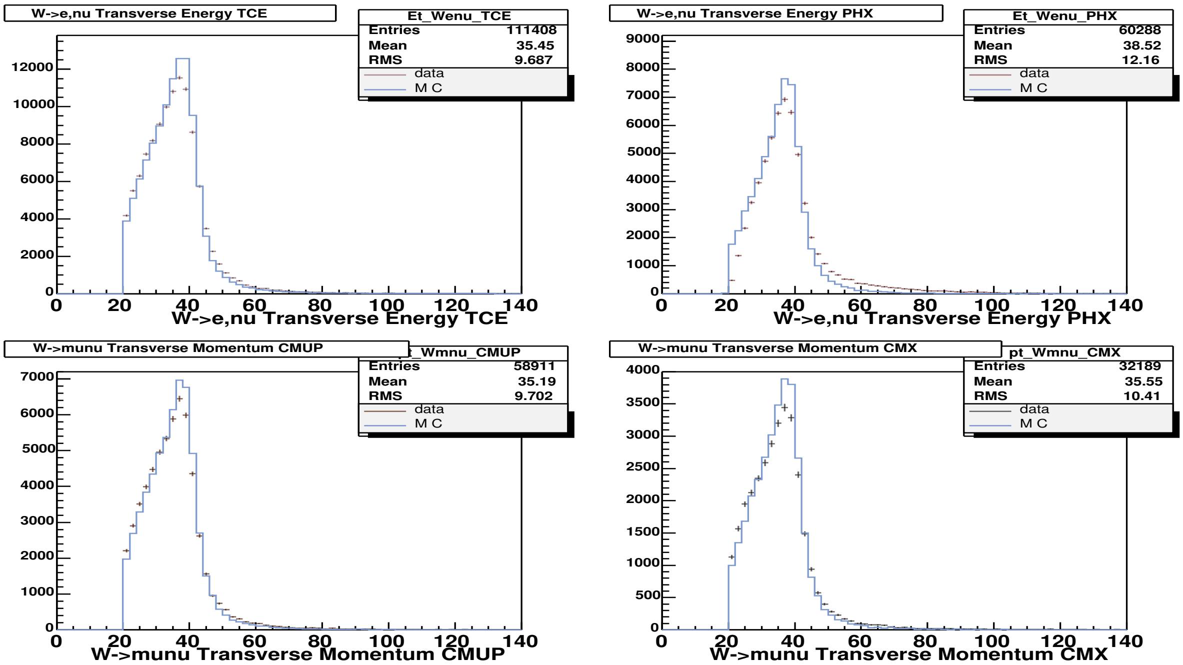

Figure 50: The E_T distribution of the $W \to \ell\nu$ candidate leptons.

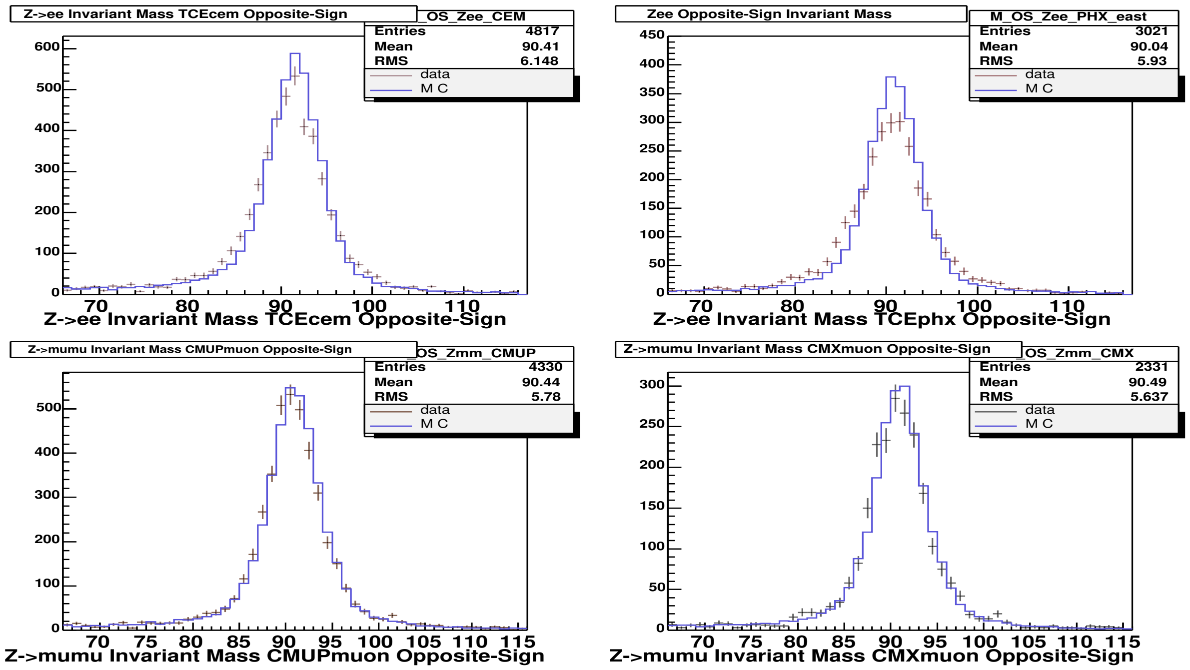

Figure 51: The invariant mass $M_{\ell\ell}$ distribution of the $Z \to \ell^+\ell^-$ candidates.

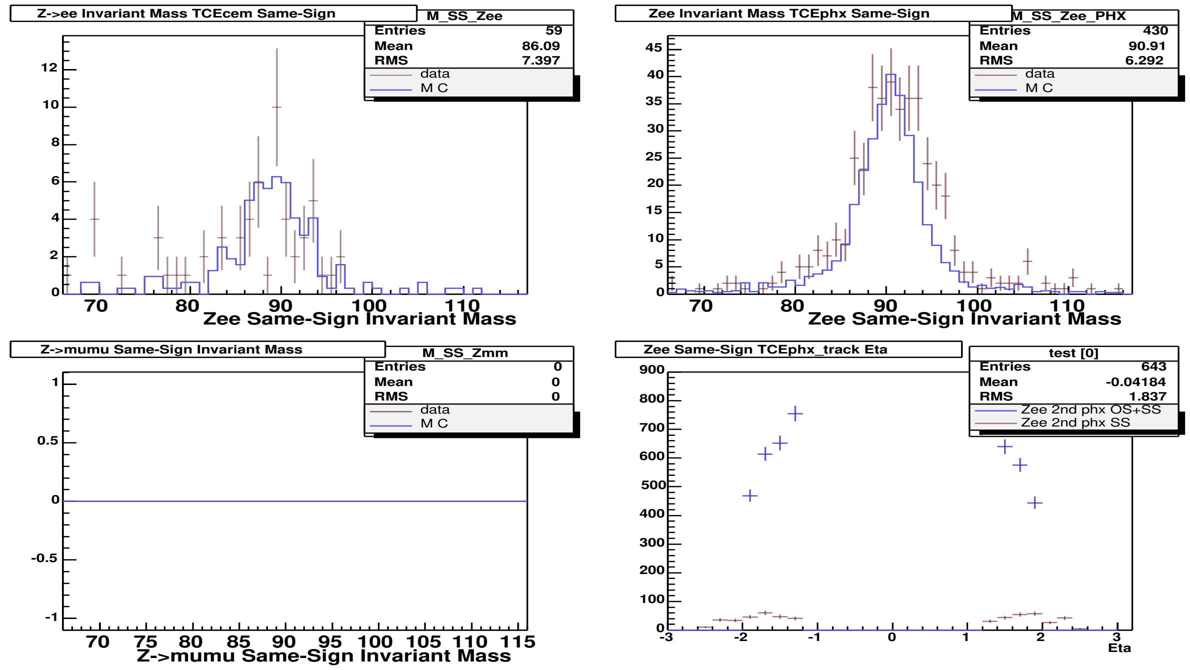

Figure 52: The invariant mass $M_{\ell\ell}$ distribution of the same-sign $Z \to \ell^\pm\ell^\pm$ candidates and the η distribution of the PHX electrons as $Z \to ee$ 2nd legs. There was an abnormal excess of $Z \to e^\pm e^\pm$ in the TCE-PHX channel, demonstrating the ambiguity of plug electron charge information in high η region.

12.4 Generator systematic

We have first quantified the contributions of the different WW decay modes to the acceptance in the dilepton channels ee, $e\mu$ and $\mu\mu$ using PYTHIA (table 56) and HERWIG (table 57). Table 58 provides a summary of the total acceptance numbers. The difference in the acceptance for each WW decay mode is shown in table 59. The difference in the total acceptance is 6.3%. However this number could contain not only differences due to the modeling of the events by the two generators, but also differences in the values for BR($W \to \ell\nu$) $\ell : e, \mu, \tau$ used by the two generators.

The generator level content of both MC samples is analyzed at parton level without any analysis cuts in tables 60 and 61. The relative content in the different dilepton decay channels found in wtop0f indicates that PYTHIA is using the same BR($W \to \ell\nu$) for e, μ and τ. On the other hand, the relative content found in atop0x indicates that HERWIG is using different BR($W \to \ell\nu$) for e, μ and τ, and those are different from PYTHIA. We need to correct for these differences in order to arrive at a systematic error due to the QCD and event modeling differences between the two generators.

In tables 62 and 63 we redefine the acceptances A' by normalizing to individual dilepton decay channels. The differences between these ratios when comparing both samples are independent of potential BR($W \to \ell\nu$) differences (see table 64). Averaging these differences over the PYTHIA acceptances listed in table 56 results in an overall shift of 4% in the total acceptance between PYTHIA and HERWIG. Note that there is a significant cancellation between higher ee and $\mu\mu$ efficiencies in PYTHIA and a higher $e\mu$ efficiency in HERWIG. Nevertheless we are primarily interested in the difference in the total acceptance, so we use 4% as our generator systematic uncertainty for this analysis.

References

[1] Observation of W^+W^- production in $\bar{p}p$ collisions at $\sqrt{s} = 1.8$ TeV, Phys. Rev. Lett.**78**(1997)4536-4540.

[2] Susana Cabrera *et al.*, "WW Production Cross-Section in the Dilepton Channel at CDF in Run II", CDF-6323.

[3] J. M. Campbell and R. K. Ellis, *Phys. Rev.* **D60**, 113006 (1999).

[4] M. Coca *et al.*, "Central Electron Identification Efficiencies for Summer 2003 Conferences", CDF-6580.
M. Coca, E. Halkiadakis, "Central Electron Identification Efficiencies for Winter 2003 conferences", CDF-6262.
http://www-cdf.fnal.gov/internal/physics/ewk/hipt_lepton_baseline_cuts.html

[5] C. Issever *et al.*, " Measurement of $W \to e\nu$ Charge Asymmetry in Run 2 with Calorimeter-Seeded Silicon Tracks ", CDF-6282

[6] K. Bloom *et al.*, “Muon Efficiencies”, CDF-6293;
ID efficiencies for CMU and CMP muons can be found in the blessing talk by A. Hocker : http://www-cdf.fnal.gov/internal/physics/top/topmtg/top013003/index.html

[7] D. McGivern *et al.*, “Drell-Yan background rejection in WW dilepton production”, CDF-Note 6834

[8] G. Manca, Y.-K. Kim, “$Z \to e^+e^-$ Cross-Section Measurement with Run II Data”, CDF-6202

[9] S. Cabrera *et al.*, “Measurement of ZZ+ZW cross section using Run II data”, CDF-6920.

[10] S. Frixione and B. R. Webber, “Matching NLO QCD Computations and Parton Shower Simulations”, hep-ph/0204244.

[11] Y.-K. Kim, J. Nielsen, L. Tompkins, G. Veramendi, “Trigger Efficiencies for High-E_T Electrons”, CDF-6234.

[12] V. Martin, L. Cerrito, “Muon Cuts and Efficiencies for 4.11 Analyses”, CDF-6825.

[13] M. Coca, E. Halkiadakis, “Central Electron Identification Efficiencies for the 200 pb^{-1} Run 2 Dataset”, CDF-6580.

[14] C. Issever *et al.*, “Plug Electron Baseline Cuts and Efficiencies for Summer 2003”, CDF-6789.

[15] M. Tecchio, “Adding CMIO muons to the top dilepton cross-section measurement”, CDF-6517.

[16] W. K. Sakumoto and A. Hocker, “Event $|Z_{vtx}| \leq 60$ cm Cut Efficiency for Run II”, CDF-6331.

[17] G. Chiarelli, I. Fedorko, A. Sidoti, “Trigger Efficiencies for Plug Electrons for $W \to e\nu$ identification”, CDF-6864.

[18] G. Chiarelli, R. Dell, I. Fedorko, S. Leone, A. Sidoti, “Measurement of the $\sigma(p\bar{p} \to W) \times BF(W \to e\nu)$ in the Plug Region Using Combined Calorimetric and Forward Tracking Information”, CDF-6535.

[19] D. Goldstein *et al.*, “A Measurement of the $t\bar{t}$ Cross-Section using Dileptons”, CDF-6830.

[20] M. Coca *et al.*, “A Second Determination of the Fake Lepton Background for the Summer 1003 Top Dilepton Analysis”, CDF-6742.

[21] D. Benjamin *et al.*, “Measurement of $W\gamma$ and $Z\gamma$ Production at CDF in Run 2”, CDF-6601.

[22] J. M. Campbell *et al.*, "MCFM v3.4.3 Users Guide", http://mcfm.fnal.gov/

[23] "The LHAPDF Interface", http://vircol.fnal.gov/

[24] D. Stump *et al.*, " Inclusive Jet Production, Parton Distributions, and the Search for New Physics", hep-ph/0303013
M. Blackston *et al*, "PDF studies using LHAPDF and the Hessian Method", CDF-6630

[25] M. Coca, E. Halkiadakis, A. Hocker, Y.-K. Kim, G. Manca, W. Sakumoto, G. Veramendi, "$W \to e\nu$ Cross-Section Analysis with Run II Data", CDF-6300.

[26] A. Robson, G. Manca, P. Renton, G. Veramendi, Y.-K. Kim, "A Measurement of $\sigma \cdot B(Z \to ee)$ Using Run 2 Central and Plug Electrons, Winter 2003", CDF-6642.

[27] D. Amidei *et al.*,"Measurements of $\sigma \cdot B(W \to e\nu)$, $\sigma \cdot B(Z \to ee)$ and $R \equiv \frac{\sigma \cdot B(W \to e\nu)}{\sigma \cdot B(Z \to ee)}$ using CDF Run II Data", CDF-6681.

[28] D. Amidei *et al.*, "Measurements of $\sigma \cdot B(W \to \mu\nu)$, $\sigma \cdot B(Z \to \mu\mu)$ and $R \equiv \frac{\sigma \cdot B(W \to \mu\nu)}{\sigma \cdot B(Z \to \mu\mu)}$ using CDF Run II Data", CDF-6711.

[29] A. Goshaw, H. Hayward, B. Heinemann, M. Kirby, N. Tanimoto, "Inclusive W and Z selection in the Run II $W/Z + \gamma$ analysis", CDF-6841.

[30] N. Tanimoto, D. Benjamin, A. Goshaw, M. Kirby, B. Heinemann, H. Hayward, "Photon ID Efficiencies for W+gamma analysis in Run II", CDF-6857.

[31] G. J. Feldman and R. D. Cousins, "A Unified Approach to the Classical Statistical Analysis of Small Signals", Phys. Rev. **D57**(1998)3873-3889.

<table>
<tr><th>$W \rightarrow e\nu$ Phoenix</th><th>$Z \rightarrow ee$ 2nd Phoenix</th></tr>
<tr><td colspan="2">$1.2 < |\eta| < 2.0$</td></tr>
<tr><td colspan="2">energy scaling, factors in table 11</td></tr>
<tr><td colspan="2">$E_T > 20$ GeV</td></tr>
<tr><td colspan="2">$E_{had}/E_{em} < 0.05$ GeV for $E \leq 100$ GeV
$< 0.05 + 0.026 \ln(E/100)$ GeV for $E > 100$ GeV</td></tr>
<tr><td colspan="2">PES 5×9 U-ratio > 0.65
PES 5×9 V-ratio > 0.65</td></tr>
<tr><td colspan="2">PEM 3×3 $\chi^2 < 10.$</td></tr>
<tr><td colspan="2">$N_{\text{silicon hits}} > 2$</td></tr>
<tr><td colspan="2">$|z_0| < 60.0$ cm</td></tr>
<tr><td colspan="2">$\Delta R_{\text{PES, COT track}} < 3.0$ cm</td></tr>
<tr><td colspan="2">$\text{Isolation}_{\Delta R=0.4} < 0.1$</td></tr>
<tr><td>$\not\!\!E_T > 20$ GeV</td><td></td></tr>
<tr><td></td><td>opposite sign of charge</td></tr>
<tr><td></td><td>$66 < M_{ee} < 116$ GeV</td></tr>
</table>

Table 52: Phoenix electron cuts for W/Z cross-section × branching ratios.

<table>
<tr><th>$W \to \mu\nu$ High-p_t Muon</th><th>$Z \to \mu\mu$ 2nd Muon</th></tr>
<tr><td>CMUP || CMX</td><td>CMUP || CMU || CMP || CMX || STUBLESS
$E_{em} + E_{had} > 0.1$ GeV for CMU, CMP & STUBLESS</td></tr>
<tr><td colspan="2">$p_t > 20$ GeV</td></tr>
<tr><td colspan="2">$E_{em} < 2 + \max(0, .0115(p - 100))$ GeV</td></tr>
<tr><td colspan="2">$E_{had} < 6 + \max(0, .0280(p - 100))$ GeV</td></tr>
<tr><td colspan="2">corrected $|d_0^{\mathrm{COT}}| < 0.2$ cm; $|d_0^{\mathrm{SVX}}| < 0.02$ cm</td></tr>
<tr><td colspan="2">$|z_0| < 60.0$ cm</td></tr>
<tr><td colspan="2">$\rho_{\mathrm{COT}} < 140.0$ cm for CMX</td></tr>
<tr><td colspan="2">$\Delta x_{\mathrm{CMU}} < 3.0$ cm
$\Delta x_{\mathrm{CMP}} < 5.0$ cm
$\Delta x_{\mathrm{CMX}} < 6.0$ cm</td></tr>
<tr><td colspan="2">$N_{\mathrm{st\ s.l.\ hits}} \geq 7$ and $N_{\mathrm{ax\ s.l.\ hits}} \geq 7$ and $N_{\mathrm{super\ layer}} \geq 3$ for each</td></tr>
<tr><td colspan="2">MuonFiducialTool</td></tr>
<tr><td colspan="2">non-cosmic</td></tr>
<tr><td colspan="2">$\mathrm{Isolation}_{\Delta R=0.4} < 0.1$</td></tr>
<tr><td>no additional muon tracks with
$p_t > 10$ GeV   not Z-vetoed
$E_{em} < \max(3, 3 + .014(p - 100))$ GeV
$E_{had} < \max(6, 6 + .042(p - 100))$ GeV</td><td></td></tr>
<tr><td>$\not\!\!E_T > 20$ GeV</td><td></td></tr>
<tr><td></td><td>opposite sign of charge</td></tr>
<tr><td></td><td>$|\Delta z_0| < 4.0$ cm</td></tr>
<tr><td></td><td>$66 < M_{\mu\mu} < 116$ GeV</td></tr>
</table>

Table 53: Muon cuts for W/Z cross-section $\times$ branching ratios.

process	ℓ_{det} type	N_{signal}	$p_{\mathrm{bg}}(\%)$	$\mathcal{L}_{\mathrm{int}}(/\mathrm{pb})$	$\epsilon_{\mathrm{trigger}}$	$f_{\mathrm{data/MC}}$	$A \cdot \epsilon_{\mathrm{ID}}$	$\sigma{\cdot}B \pm \mathrm{stat} \pm \mathrm{lumi}$ (nb)
$W \to e\nu$	TCE	117123	0.035	193.525	0.962	0.948	0.2344	$2.732 \pm 0.008 \pm 0.164$
	PHX	60288	0.03	161.804	0.958	0.895	0.1526	$2.764 \pm 0.012 \pm 0.166$
$W \to \mu\nu$	CMUP	59466	0.0943	193.525	0.887	0.872	0.1286	$2.799 \pm 0.013 \pm 0.168$
	CMX	32479	0.0921	175.302	0.954	0.990	0.0632	$2.820 \pm 0.017 \pm 0.169$
$Z \to ee$	TCELCE	4929	0.0026	193.525	0.999	0.948	0.1072	$0.2505 \pm 0.0036 \pm 0.0150$
	TCEPHX	3812	0.0015	161.804	0.921	0.879	0.0996	$0.2435 \pm 0.0043 \pm 0.0146$
$Z \to \mu\mu$	CMUPmuon	4355	0.0000	193.525	0.929	0.872	0.1063	$0.2615 \pm 0.0040 \pm 0.0157$
	CMXmuon	2345	0.0000	175.302	0.974	0.990	0.0554	$0.2501 \pm 0.0052 \pm 0.0150$

Table 54: Number of candidates found, background fraction, integrated luminosity, trigger efficiency, data/MC scale factor, acceptance $\times$ ID efficiency, W/Z cross-section $\times$ branching ratio $\pm$ statistical error $\pm$ luminosity error per process type we checked.

process	ℓ_{det} type	N_{signal}	$p_{\mathrm{bg}}(\%)$	$\mathcal{L}_{\mathrm{int}}(/\mathrm{pb})$	$\epsilon_{\mathrm{trigger}}$	$f_{\mathrm{data/MC}}$	$A \cdot \epsilon_{\mathrm{ID}}$	$\sigma \cdot B \pm \mathrm{stat} \pm \mathrm{lumi}$ (nb)
$W \to e\nu$	TCE	111396	0.035	193.525	0.962	0.948	0.2276	2.680 ± 0.008 ± 0.161
	PHX	60288	0.03	161.804	0.958	0.895	0.1526	2.764 ± 0.012 ± 0.166
$W \to \mu\nu$	CMUP	58909	0.0943	193.525	0.887	0.872	0.1275	2.797 ± 0.013 ± 0.168
	CMX	32189	0.0921	175.302	0.954	0.990	0.0626	2.820 ± 0.017 ± 0.169
$Z \to ee$	TCELCE	4817	0.0026	193.525	0.999	0.948	0.1058	0.2477±0.0036±0.0149
	TCEPHX	3021	0.0015	161.804	0.921	0.879	0.0967	0.2383±0.0043±0.0143
$Z \to \mu\mu$	CMUPmuon	4330	0.0000	193.525	0.929	0.872	0.1017	0.2716±0.0041±0.0163
	CMXmuon	2331	0.0000	175.302	0.974	0.990	0.0532	0.2593±0.0054±0.0156

Table 55: Number of candidates found, background fraction, integrated luminosity, trigger efficiency, data/MC scale factor, acceptance × ID efficiency, W/Z cross-section × branching ratio ± statistical error ± luminosity error per process type we checked. **Track isolation < 0.1 was required for TCE, CMUP and CMX leptons for the above table**.

PYTHIA WW wtop0f $N_{analyzed} = 828000$ $N_{tot} = N_{analyzed}/Br(W\to\ell\nu)^2 = 7544208.50$			
$N[WW\to\ell\nu\ell\nu]$	ee	$\mu\mu$	$e\mu$
$N[WW\to ee\nu\nu]$	9572	0	21
$N[WW\to e\mu\nu\nu]$	13	217	19710
$N[WW\to\mu\mu\nu\nu]$	0	9495	25
$N[WW\to e\tau\nu\nu]$	1123	16	1201
$N[WW\to e\tau(\tau\to e\nu\nu)\nu\nu]$	1102	0	2
$N[WW\to e\tau(\tau\to\mu\nu\nu)\nu\nu]$	0	16	1194
$N[WW\to e\tau(\tau\to had)\nu\nu]$	21	0	5
$N[WW\to\mu\tau\nu\nu]$	0	1162	1109
$N[WW\to\mu\tau(\tau\to e\nu\nu)\nu\nu]$	0	18	1080
$N[WW\to\mu\tau(\tau\to\mu\nu\nu)\nu\nu]$	0	1134	4
$N[WW\to\mu\tau(\tau\to had)\nu\nu]$	0	10	25
$N[WW\to\tau\tau\nu\nu]$	38	40	56
$N[WW\to anythingelse]$	0	0	0
$A[WW\to\ell\nu\ell\nu]$ (%)	$A[ee]$ (%)	$A[\mu\mu]$ (%)	$A[e\mu]$ (%)
$A[WW\to ee\nu\nu]$	0.127 ± 0.001	0.000 ± 0.000	0.000 ± 0.000
$A[WW\to e\mu\nu\nu]$	0.000 ± 0.000	0.003 ± 0.000	0.261 ± 0.002
$A[WW\to\mu\mu\nu\nu]$	0.000 ± 0.000	0.126 ± 0.001	0.000 ± 0.000
$A[WW\to e\tau\nu\nu]$	0.015 ± 0.000	0.000 ± 0.000	0.016 ± 0.000
$A[WW\to e\tau(\tau\to e\nu\nu)\nu\nu]$	0.015 ± 0.000	0.000 ± 0.000	0.000 ± 0.000
$A[WW\to e\tau(\tau\to\mu\nu\nu)\nu\nu]$	0.000 ± 0.000	0.000 ± 0.000	0.016 ± 0.000
$A[WW\to e\tau(\tau\to had)\nu\nu]$	0.000 ± 0.000	0.000 ± 0.000	0.000 ± 0.000
$A[WW\to\mu\tau\nu\nu]$	0.000 ± 0.000	0.015 ± 0.000	0.015 ± 0.000
$A[WW\to\mu\tau(\tau\to e\nu\nu)\nu\nu]$	0.000 ± 0.000	0.000 ± 0.000	0.014 ± 0.000
$A[WW\to\mu\tau(\tau\to\mu\nu\nu)\nu\nu]$	0.000 ± 0.000	0.015 ± 0.000	0.000 ± 0.000
$A[WW\to\mu\tau(\tau\to had)\nu\nu]$	0.000 ± 0.000	0.000 ± 0.000	0.000 ± 0.000
$A[WW\to\tau\tau\nu\nu]$	0.001 ± 0.001	0.001 ± 0.001	0.001 ± 0.001
$A[WW\to anythingelse]$	0.000 ± 0.000	0.000 ± 0.000	0.000 ± 0.000
$A[WW\to everything]$	0.142 ± 0.001	0.145 ± 0.001	0.293 ± 0.002

Table 56: Contributions of the different WW decay modes in PYTHIA WW MC (dataset wtop0f) to the total acceptance.

ALPGEN+HERWIG WW atop4x $N_{analyzed} = 500000$ $N_{tot} = N_{analyzed}/Br(W\to\ell\nu) = 1509251.75$			
$N[WW\to\ell\nu\ell\nu]$	ee	$\mu\mu$	$e\mu$
$N[WW\to ee\nu\nu]$	1800	0	0
$N[WW\to e\mu\nu\nu]$	0	0	4400
$N[WW\to\mu\mu\nu\nu]$	0	1400	0
$N[WW\to e\tau\nu\nu]$	200	0	200
$N[WW\to e\tau(\tau\to e\nu\nu)\nu\nu]$	200	0	0
$N[WW\to e\tau(\tau\to\mu\nu\nu)\nu\nu]$	0	0	200
$N[WW\to e\tau(\tau\to had)\nu\nu]$	0	0	0
$N[WW\to\mu\tau\nu\nu]$	0	0	200
$N[WW\to\mu\tau(\tau\to e\nu\nu)\nu\nu]$	0	0	200
$N[WW\to\mu\tau(\tau\to\mu\nu\nu)\nu\nu]$	0	0	0
$N[WW\to\mu\tau(\tau\to had)\nu\nu]$	0	0	0
$N[WW\to\tau\tau\nu\nu]$	0	0	0
$N[WW\to anythingelse]$	0	0	0
$A[WW\to\ell\nu\ell\nu]$ (%)	$A[ee]$ (%)	$A[\mu\mu]$ (%)	$A[e\mu]$ (%)
$A[WW\to ee\nu\nu]$	0.119 ± 0.003	0.000 ± 0.000	0.000 ± 0.000
$A[WW\to e\mu\nu\nu]$	0.000 ± 0.000	0.000 ± 0.000	0.292 ± 0.004
$A[WW\to\mu\mu\nu\nu]$	0.000 ± 0.000	0.093 ± 0.002	0.000 ± 0.000
$A[WW\to e\tau\nu\nu]$	0.013 ± 0.001	0.000 ± 0.000	0.013 ± 0.001
$A[WW\to e\tau(\tau\to e\nu\nu)\nu\nu]$	0.013 ± 0.001	0.000 ± 0.000	0.000 ± 0.000
$A[WW\to e\tau(\tau\to\mu\nu\nu)\nu\nu]$	0.000 ± 0.000	0.000 ± 0.000	0.013 ± 0.001
$A[WW\to e\tau(\tau\to had)\nu\nu]$	0.000 ± 0.000	0.000 ± 0.000	0.000 ± 0.000
$A[WW\to\mu\tau\nu\nu]$	0.000 ± 0.000	0.000 ± 0.000	0.013 ± 0.001
$A[WW\to\mu\tau(\tau\to e\nu\nu)\nu\nu]$	0.000 ± 0.000	0.000 ± 0.000	0.013 ± 0.001
$A[WW\to\mu\tau(\tau\to\mu\nu\nu)\nu\nu]$	0.000 ± 0.000	0.000 ± 0.000	0.000 ± 0.000
$A[WW\to\mu\tau(\tau\to had)\nu\nu]$	0.000 ± 0.000	0.000 ± 0.000	0.000 ± 0.000
$A[WW\to\tau\tau\nu\nu]$	0.000 ± 0.000	0.000 ± 0.000	0.000 ± 0.000
$A[WW\to anythingelse]$	0.000 ± 0.000	0.000 ± 0.000	0.000 ± 0.000
$A[WW\to everything]$	0.133 ± 0.003	0.093 ± 0.002	0.318 ± 0.005

Table 57: Contributions of the different WW decay modes in ALPGEN+HERWIG $W(l\nu)W + 0p$ MC (dataset atop4x) to the total acceptance.

wtop0f	A_{ee}	$A_{\mu\mu}$	$A_{e\mu}$	$A_{ee+\mu\mu+e\mu}$
A_{abs}	(0.137 ± 0.001) %	(0.145 ± 0.001) %	(0.288 ± 0.002) %	(0.570 ± 0.003) %
A_{rel}	24.0 %	25.4 %	50.5 %	100.0 %
atop4x	A_{ee}	$A_{\mu\mu}$	$A_{e\mu}$	$A_{ee+\mu\mu+e\mu}$
A_{abs}	(0.126 ± 0.003) %	(0.093 ± 0.002) %	(0.313 ± 0.005) %	(0.532 ± 0.006) %
A_{rel}	23.8 %	17.4 %	58.8 %	100.0 %

Table 58: Acceptance summary for PYTHIA WW (wtop0f, top) and ALPGEN+HERWIG $WW + 0p$ (atop4x, bottom) Monte Carlo samples. No scale factors have been applied.

Relative differences in acceptance			
$\Delta A[WW \to \ell\nu\ell\nu]$	ee	$\mu\mu$	$e\mu$
$\Delta A[WW \to ee\nu\nu]$	6.299	0.000	0.000
$\Delta A[WW \to e\mu\nu\nu]$	0.000	100.000	-11.877
$\Delta A[WW \to \mu\mu\nu\nu]$	0.000	26.190	0.000
$\Delta A[WW \to e\tau\nu\nu]$	13.333	0.000	18.750
$\Delta A[WW \to e\tau(\tau \to e\nu\nu)\nu\nu]$	13.333	0.000	0.000
$\Delta A[WW \to e\tau(\tau \to \mu\nu\nu)\nu\nu]$	0.000	0.000	18.750
$\Delta A[WW \to e\tau(\tau \to had)\nu\nu]$	0.000	0.000	0.000
$\Delta A[WW \to \mu\tau\nu\nu]$	0.000	100.000	13.333
$\Delta A[WW \to \mu\tau(\tau \to e\nu\nu)\nu\nu]$	0.000	0.000	0.000
$\Delta A[WW \to \mu\tau(\tau \to \mu\nu\nu)\nu\nu]$	0.000	0.000	0.000
$\Delta A[WW \to \mu\tau(\tau \to had)\nu\nu]$	0.000	0.000	0.000
$\Delta A[WW \to \tau\tau\nu\nu]$	100.000	100.000	100.000
$\Delta A[WW \to anythingelse]$	0.000	0.000	0.000
$\Delta A[WW \to everything]$	6.338	35.862	-8.532
$\Delta A[WW \to everything]$	Total 6.3%		

Table 59: Differences in the acceptance between wtop0f (PYTHIA WW) and atop4x (ALPGEN+HERWIG $WW + 0p$) for the different WW decay modes.

PYTHIA WW wtop0f $N_{analyzed} = 828000$ $W \to \ell\nu W \to \ell\nu$			
$N[WW \to \ell\nu\ell\nu]$	N_{tot}	%	$\Delta(wtop0f - atop4x)\%$
$N[WW \to ee\nu\nu]$	91966	11.107 ± 0.077	2.25
$N[WW \to e\mu\nu\nu]$	183569	22.170 ± 0.102	0.97
$N[WW \to \mu\mu\nu\nu]$	91913	11.101 ± 0.077	9.8
$N[WW \to e\tau\nu\nu]$	184242	22.251 ± 0.102	-0.8
$N[WW \to e\tau(\tau \to e\nu\nu)\nu\nu]$	32790	3.960 ± 0.048	-15.7
$N[WW \to e\tau(\tau \to \mu\nu\nu)\nu\nu]$	31736	3.833 ± 0.047	-13.3
$N[WW \to e\tau(\tau \to had)\nu\nu]$	119729	14.460 ± 0.086	6.5
$N[WW \to \mu\tau\nu\nu]$	184304	22.259 ± 0.102	-4.5
$N[WW \to \mu\tau(\tau \to e\nu\nu)\nu\nu]$	32507	3.926 ± 0.048	-1.3
$N[WW \to \mu\tau(\tau \to \mu\nu\nu)\nu\nu]$	31850	3.847 ± 0.047	-34.8
$N[WW \to \mu\tau(\tau \to had)\nu\nu]$	119963	14.488 ± 0.086	2.58
$N[WW \to \tau\tau\nu\nu]$	92006	11.112 ± 0.077	-3.1

Table 60: Generator level content of the WW PYTHIA MC sample. No analysis cuts have been applied.

ALPGEN+HERWIG WW atop4x $N_{analyzed} = 500000$ $W \to \ell\nu W \to hadrons$			
$N[WW \to \ell\nu\ell\nu]$	N_{tot}	%	% 500000-334200
$N[WW \to ee\nu\nu]$	18000	3.600 ± 0.026	10.856 ± 0.076
$N[WW \to e\mu\nu\nu]$	36400	7.280 ± 0.037	21.954 ± 0.102
$N[WW \to \mu\mu\nu\nu]$	16600	3.320 ± 0.025	10.012 ± 0.074
$N[WW \to e\tau\nu\nu]$	37200	7.440 ± 0.037	22.437 ± 0.102
$N[WW \to e\tau(\tau \to e\nu\nu)\nu\nu]$	7600	1.520 ± 0.017	4.584 ± 0.051
$N[WW \to e\tau(\tau \to \mu\nu\nu)\nu\nu]$	7200	1.440 ± 0.017	4.343 ± 0.050
$N[WW \to e\tau(\tau \to had)\nu\nu]$	22400	4.480 ± 0.029	13.510 ± 0.084
$N[WW \to \mu\tau\nu\nu]$	38600	7.720 ± 0.038	23.281 ± 0.104
$N[WW \to \mu\tau(\tau \to e\nu\nu)\nu\nu]$	6600	1.320 ± 0.000	3.981 ± 0.048
$N[WW \to \mu\tau(\tau \to \mu\nu\nu)\nu\nu]$	8600	1.720 ± 0.000	5.187 ± 0.054
$N[WW \to \mu\tau(\tau \to had)\nu\nu]$	23400	4.680 ± 0.000	14.113 ± 0.086
$N[WW \to \tau\tau\nu\nu]$	19000	3.800 ± 3.800	11.460 ± 0.078
$N[WW \to anythingelse]$	334200	66.840 ± 0.067	

Table 61: Generator level content of the $WW + 0p$ ALPGEN+HERWIG MC sample. No analysis cuts have been applied.

PYTHIA WW wtop0f $N_{analyzed} = 828000$ $N_{tot} = N_{analyzed}/Br(W\to\ell\nu)^2 = 7544208.50$				
$N[WW\to\ell\nu\ell\nu]$	828000	ee	$\mu\mu$	$e\mu$
$N[WW\to ee\nu\nu]$	91966	9572	0	21
$N[WW\to e\mu\nu\nu]$	183569	13	217	19710
$N[WW\to\mu\mu\nu\nu]$	91913	0	9495	25
$N[WW\to e\tau\nu\nu]$	184242	1123	16	1201
$N[WW\to\mu\tau\nu\nu]$	184304	0	1162	1109
$N[WW\to\tau\tau\nu\nu]$	119963	38	40	56
$A'[WW\to\ell\nu\ell\nu]$ (%)		$A[ee]$ (%)	$A[\mu\mu]$ (%)	$A[e\mu]$ (%)
$A'[WW\to ee\nu\nu]$		10.4082 ± 0.1007	0.0000 ± 0.0000	0.0228 ± 0.0050
$A'[WW\to e\mu\nu\nu]$		0.0071 ± 0.0020	0.1182 ± 0.0080	10.7371 ± 0.0723
$A'[WW\to\mu\mu\nu\nu]$		0.0000 ± 0.0000	10.3304 ± 0.1004	0.0272 ± 0.0054
$A'[WW\to e\tau\nu\nu]$		0.6095 ± 0.0181	0.0087 ± 0.0022	0.6519 ± 0.0187
$A'[WW\to\mu\tau\nu\nu]$		0.0000 ± 0.0000	0.6305 ± 0.0184	0.6017 ± 0.0180
$A'[WW\to\tau\tau\nu\nu]$		0.0413 ± 0.0067	0.0435 ± 0.0069	0.0609 ± 0.0081

Table 62: Contributions of the different WW decay modes in PYTHIA $W(l\nu)W(l\nu)$ MC (wtop0f) and acceptance redefinition.

ALPGEN+HERWIG WW atop4x $N_{analyzed} = 500000$ $N_{tot} = N_{analyzed}/Br(W\to\ell\nu) = 1509251.75$				
$N[WW\to\ell\nu\ell\nu]$	500000-334200	ee	$\mu\mu$	$e\mu$
$N[WW\to ee\nu\nu]$	18000	1800	0	0
$N[WW\to e\mu\nu\nu]$	36400	0	0	4400
$N[WW\to\mu\mu\nu\nu]$	16600	0	1400	0
$N[WW\to e\tau\nu\nu]$	37200	200	0	200
$N[WW\to\mu\tau\nu\nu]$	38600	0	0	200
$N[WW\to\tau\tau\nu\nu]$	19000	0	0	0
$A'[WW\to\ell\nu\ell\nu]$ (%)		$A'[ee]$ (%)	$A'[\mu\mu]$ (%)	$A'[e\mu]$ (%)
$A'[WW\to ee\nu\nu]$		10.0000 ± 0.2236	0.0000 ± 0.0000	0.0000 ± 0.0000
$A'[WW\to e\mu\nu\nu]$		0.0000 ± 0.0000	0.0000 ± 0.0000	12.0879 ± 0.1709
$A'[WW\to\mu\mu\nu\nu]$		0.0000 ± 0.0000	8.4337 ± 0.2157	0.0000 ± 0.0000
$A'[WW\to e\tau\nu\nu]$		0.5376 ± 0.0379	0.0000 ± 0.0000	0.5376 ± 0.0379
$A'[WW\to\mu\tau\nu\nu]$		0.0000 ± 0.0000	0.0000 ± 0.0000	0.5181 ± 0.0365
$A'[WW\to\tau\tau\nu\nu]$		0.0000 ± 0.0000	0.0000 ± 0.0000	0.0000 ± 0.0000

Table 63: Contributions of the different WW decay modes in ALPGEN+HERWIG $W(l\nu)W + 0p$ MC (atop4x) and acceptance redefinition.

$\Delta A'$	ee	$\mu\mu$	$e\mu$
$\Delta A'[WW\to ee\nu\nu]$	3.9219	0.0000	100.0000
$\Delta A'[WW\to e\mu\nu\nu]$	100.0000	100.0000	-12.5807
$\Delta A'[WW\to \mu\mu\nu\nu]$	0.0000	18.3602	100.0000
$\Delta A'[WW\to e\tau\nu\nu]$	11.7944	100.0000	17.5230
$\Delta A'[WW\to \mu\tau\nu\nu]$	0.0000	100.0000	13.8915
$\Delta A'[WW\to \tau\tau\nu\nu]$	100.0000	100.0000	100.0000
$\sum_i \Delta A'_i \times A_i[wtop0f] / \sum_i A_i[wtop0f] \sim 4\%$			

Table 64: Relative differences between wtop0f and atop4x acceptances, for different decay and detection channels.